

# Coupling of Quantum Dot Systems to Microwave Cavities

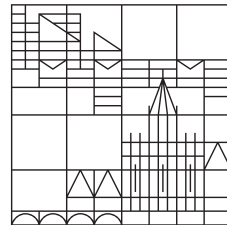
## Masterarbeit

by

**Felicitas Hellbach**

at the

Universität  
Konstanz



Mathematisch-Naturwissenschaftlichen Sektion  
Fachbereich Physik

Supervisor: Dr. Gianluca Rastelli  
Jun.-Prof. Dr. Fabian Pauly  
Prof. Dr. Wolfgang Belzig

1. Evaluated by Jun.-Prof. Dr. Fabian Pauly  
2. Evaluated by Prof. Dr. Wolfgang Belzig

Konstanz, 2017



---

## Acknowledgment

I would like to thank Jun.-Prof. Dr Fabian Pauly for the opportunity to write my master thesis in his group and supporting my desire to write an analytical thesis.

I would also like to thank Prof. Wolfgang Belzig for being the second referee of this theses and furthermore for participating in productive discussion.

Especially I want to thank my supervisors Dr. Gianluca Rastelli and Jun.-Prof. Dr Fabian Pauly for the great support in many discussions during the last year and the development of a really interesting topic for the thesis. Both introduced me well to the topics and gave me the opportunity to educate myself at the Heraeus-Seminar or the DPG meeting in Dresden.

This thesis would not have been possible unless Dr. Gianluca Rastelli who supported me with his patience and knowledge in many discussions lasting for hours, great ideas and input in complicated situations and he has always an open door to listen to my questions.

Finally I would like to thank my parents who enabled me this studies and supported me, even in stressful phases, with much patience throughout the whole time. Furthermore I would like to thank my boyfriend who took load off me so that I could completely focus on my thesis.



---

## Abstract

Since the realization of high quality superconducting microwave cavities[20], the so-called circuit quantum electrodynamics enables the possibility to investigate the coherent interaction of light and matter. Artificial atoms can be realized with quantum dots, and experiments have already proved strong coupling between a quantum dot and a microwave cavity[22, 23]. We study two parallel quantum dots arranged in the geometry of an Aharonov-Bohm interferometer (ABI)[18, 19]. Each dot is capacitively coupled to a microwave cavity. We explore how quantum correlation between the two cavity fields is generated by the coherent transport of a single electron traveling in two different paths of the ABI. We want to calculate the covariance of the two cavity fields by use of a diagrammatic perturbative expansion (Keldysh Greens functions) to the fourth order in the dot-cavity coupling constant. Thus we develop an analytic formula ready-made for a numerical evaluation to test the covariance for varying magnetic flux.



---

## Deutsche Zusammenfassung

Motiviert von unterschiedlichen Experimenten ein System aus Quantenpunkten und Kavitäten zu untersuchen, betrachten wir ein System, in dem zwei Quantenpunkte in ein Aharonov-Bohm Interferometer (ABI) eingebettet sind, wobei jeder Quantenpunkt kapazitiv an eine Mikrowellenkavität gekoppelt wurde.

Unser Ziel ist es die Korrelation oder Quantenverschränkung der beiden Kavitäten zu untersuchen, verursacht durch den kohärenten Transport eines einzelnen Elektrons, das sich in zwei verschiedenen Armen des ABI bewegt.

In dieser Thesis haben wir uns zunächst auf die Korrelation beschränkt. Dazu berechnen wir die Kovarianz der beiden Mikrowellenkavitäten. Dafür haben wir einen äquivalenten aber vollständig zeitgeordneten Ausdruck definiert. Diesen entwickeln wir nun in einer diagrammatischen Störungsentwicklung bis zur vierten Ordnung der Kopplungskonstanten von Quantenpunkt und Kavität. Dazu nutzen wir die Keldysh Green'schen Funktionen. Um die Terme der Störungsrechnung zu berechnen verwenden wir das Wick'sche Theorem. Dieses führt zu einer Summe mehrerer Multiplikationen Green'scher Funktionen, die man auch durch Feynman Diagramme darstellen kann. Wir können zeigen, dass sich die Kovarianz auf sieben Diagramme reduziert.

Um diese Green'schen Funktionen zu berechnen greifen wir sowohl für die freie retardierte und avancierte als auch für die Keldysh Green'schen Funktionen auf die Dyson Gleichung zurück. Um die sieben Diagramme zu berechnen identifizieren wir zunächst drei verschiedene Diagrammtypen. Jeden dieser Typen haben wir von Konturzeiten zu Realzeiten transformiert. Dazu wurde die Keldysh Kontur parametrisiert. Normalerweise führt dies zu einer großen Anzahl von Termen, da jede Konturzeit auf zwei verschiedenen Zweigen der Keldysh Kontur liegen könnte. Da wir den Grenzfall einer Temperatur von Null Kelvin betrachten reduzieren sich alle Variationsmöglichkeiten auf eine einzige.

Im nächsten Schritt haben wir die Fouriertransformationen der Green'schen Funktionen eingesetzt und über die Zeiten integriert. Übrig blieb eine Integration von vier freien bosonischen und vier fermionischen Green'schen Funktionen, integriert über vier unterschiedliche Frequenzen.

Mit einer Partialbruchzerlegung konnten wir die Integration über zwei Frequenzen durchführen. Wir haben also eine analytische Formel erhalten, in der nur noch zwei Integrationen über die Frequenzen enthält.

Zusammengefasst haben wir eine analytische Formel für die Kovarianz hergeleitet, die nun numerisch berechnet werden kann. Der nächste Schritt ist diese numerische Implementierung, die es uns ermöglicht über die zwei übrigen Frequenzen zu integrieren und das Verhalten des Systems, abhängig von Größen wie dem magnetischen Fluss oder die Bias Spannung, zu untersuchen.

Anschließend werden wir untersuchen ob die Zustände der Kavitäten nicht nur korreliert sondern sogar quantenverschränkt sind. Dazu berechnen wir die Kohärenzfunktion zweiter Ordnung und testen die Cauchy-Schwarz Ungleichung, indem wir erneut die diagrammatische Störungsentwicklung benutzen, ähnlich wie bereits in dieser Thesis gezeigt.





# Contents

<b>Acknowledgment</b>	<b>3</b>
<b>Abstract</b>	<b>5</b>
<b>Deutsche Zusammenfassung</b>	<b>7</b>
<b>1 Introduction and Theoretical background</b>	<b>15</b>
1.1 Electronic Transport . . . . .	16
1.2 Double-Dot Aharonov-Bohm Interferometer . . . . .	19
1.3 Single Quantum Dot Coupled to a Microwave Cavity . . . . .	20
1.4 Inequalities in Quantum Coherence Theory . . . . .	22
1.5 Parallel Double-Dot Coupled to Microwave Cavities . . . . .	24
1.6 Proceeding and Structure of the Work . . . . .	26
<b>2 Green's Functions and Perturbation Theory</b>	<b>27</b>
2.1 Real Time Green's Functions of Double-Dot Aharonov-Bohm Interferometer . . . . .	27
2.2 Formalism of the Keldysh Green's Functions and Perturbation Theory . . . . .	29
2.3 Keldysh Green's Functions of Double-Dot Aharonov-Bohm Interferometer . . . . .	35
2.3.1 Unperturbed Greater and Lesser Green's Functions . . . . .	35
2.3.2 Dyson Equation and Full Green's Functions . . . . .	38
2.4 Bosonic Green's Functions of a Single Microwave Cavity . . . . .	41
<b>3 Diagrammatic Perturbative Expansion of the Covariance</b>	<b>44</b>
3.1 Derivation of the Covariance From the Time-Ordered Expression . . . . .	44
3.2 Color Code and Legend of the Green's Functions and Feynman Diagrams . . . . .	45
3.3 Perturbative Expansion of the Single Cavities . . . . .	45
3.4 Perturbative Expansion of the Combined Cavities A and B . . . . .	50
3.5 Neglect of Tadpole Diagrams . . . . .	54
3.6 Perturbative Expansion represented as Feynman Diagrams . . . . .	56
3.7 Specification of the Covariance in Terms of the Perturbative Expansion . . . . .	58
<b>4 Results: Analytic Formula for the Covariance</b>	<b>61</b>
4.1 Real Time and Frequency Representation . . . . .	61
4.1.1 Transformation of the Bubble Diagram . . . . .	62
4.1.2 Transformation of a Square-shaped Diagram . . . . .	63
4.1.3 Transformation of a Twisted-shaped Diagram . . . . .	64
4.2 Integration at the Example of a Square-Shaped Diagram . . . . .	68
4.2.1 Integral Containing Two Principal Values . . . . .	68
4.2.2 Integration of Components Containing Delta Functions . . . . .	72
4.2.3 Full Analytical Integral . . . . .	73
4.3 Extension of the Integration to the Remaining Diagrams . . . . .	75
<b>5 Conclusion</b>	<b>78</b>

## List of Symbols and Abbreviations

- $\alpha_i(t)$  Coherent state
- A Vector potential
- $A_c$  cross-sectional area
- ABI Aharonov-Bohm interferometer
- $a^{(\dagger)}$  Bosonic creation (annihilation) operator of cavity a
- $b^{(\dagger)}$  Bosonic creation (annihilation) operator of cavity a
- $\beta$   $1/kT$  with the Boltzman constant and the Temperature
- B Magnetic field
- C Covariance
- $c_{k\alpha}^{(\dagger)}$  Creation (annihilation) operators of the contacts
- $d_i^{(\dagger)}$  Creation (annihilation) operators of the dots
- $D_i$  Coherent displacement operator and
- $D_{a,b}$  Unperturbed Bosonic Green's function of resonator a,b
- $\varepsilon_{k\alpha}$  Energy levels of the contacts
- $\varepsilon_i$  Energy levels of the dots
- e Elementary charge
- $E$  Energy of the system
- $E^{r,a}$  Retarded and advanced energy, shifted by  $\pm i\eta$
- F Green's function with operators  $A = ab$
- $f(E)$  Fermi function
- $\varphi$  Phase shift of an electron traveling in the Aharonov-Bohm structure with  $\varphi = \frac{2\pi\Phi}{\Phi_0}$
- $\Delta\varphi_{AB}$  Aharonov-Bohm Phase
- $\Phi$  Magnetic flux
- $\Phi_0$  Magnetic flux quanta
- $\phi$  Bosonic operators
- g General dot-cavity coupling strength
- G Conductance
- $G_0$  Quantum of conductance
- $g^{r,a,\pm\mp}$  Unperturbed retarded, advanced, lesser and greater fermionic Green's function
- $G^{r,a}$  Retarded and advanced Green's function
- $G^{\pm\mp}$  Time-ordered, lesser, greater and anti-time ordered Keldysh Green's function
- $\hat{G}$  Keldysh Green's functions in matrix notation
- $\Gamma$  Scattering rate of the leads
- $|GS\rangle_{1,2}$  Ground state of resonator 1,2, respectively a,b
- h Plank constant

- H Hamiltonian of the complete systems
- $H_0$  Unperturbed Hamiltonian
- $H^{(i)}$  Interaction Hamiltonian
- $H_C$  Hamiltonian of the contacts in the noninteracting resonant-level model
- $H_{cen}$  Hamiltonian of the central region in the noninteracting resonant-level model
- $H_T$  Tunnel-Hamiltonian in the noninteracting resonant-level model
- I Current
- $k_F$  Fermi-wave vector
- $\kappa$  Common denominator of  $G^r \cdot G^a$
- L Length of the conductor
- $L_\varphi$  phase-relaxation length
- $L_m$  mean free path
- $\lambda_F$  Fermi-wavelength
- $\lambda_{a,b}$  Dot-cavity coupling strength of dot 1 and cavity a or dot 2 and cavity b
- $\mu_{L,R}$  Chemical potential of the left, right lead
- $|\psi_e\rangle$  initial electronic state
- $|\Psi_{sys}\rangle_{in}$  initial state of the complete system
- $\Psi_H$  field operator in the Heisenberg picture with respect to Hamiltonian H
- $\psi$  Fermionic operators
- $\rho$  Density matrix
- $\rho_i(E)$  Local density of states at energy E
- $\sigma$  electrical conductivity
- $\Sigma$  Total self energy
- $\Sigma_{L,R}$  Tunneling self energy from a left, right lead
- $\Sigma_{int}$  Self energy from interaction inside the central region
- $T_n$  Transmission of mode n
- $\tau_m$  mean free time
- T Time ordering operator
- $T_C$  Contour-time ordering operator
- $t_{r,i}$  Tunneling coupling between the lead  $r$  and dot  $i$
- $U(t, t')$  Time evolution operator
- U Voltage
- $v_F$  Fermi velocity
- V Perturbation in terms of the tunneling
- $V_{k\alpha,i}$  Tunneling coupling between the lead  $\alpha$  and dot  $i$
- $\omega_{a,b}$  Resonance frequency of cavity  $a, b$
- $\Omega_\alpha^\pm$  Shift of the frequency  $\omega_\alpha$  with  $\alpha = v, x, y, z, \omega_\alpha \pm \omega_b$
- $\zeta_P$  number of transpositions of operators



## List of Figures

1	a) Classical diffusive transport regime. b) Quantum transport regime an weak localization. c) Ballistic transport regime. From [7]. . . . .	16
2	Double-dot Aharonov Bohm Interferometer. . . . .	19
3	Experimental results of A. Holleitner et al. for weak and intermediate coupling of two quantum dots in an ABI . . . . .	20
4	Schematic representation of a quantum dot, considerable as a two level system, coupled to a microwave cavity with coupling strength $g$ and the decay rate $\kappa$ of the photon field. Picture adapted from [21]. . . . .	21
5	Color scale plot of the differential conductance of one quantum dot. a) Both Coulomb diamonds and the the Kondo ridge at zero bias can be seen by sweeping the source-drain and gate voltages of the dot[21]. b) Energy level splitting depending on the input power of the microwave cavity for a quantum dot in Coulomb blockade regime[21]. . . . .	21
6	Color scale plot of the differential conductance of one quantum dot. a) Both Coulomb diamonds and the the Kondo ridge at zero bias can be seen by sweeping the source-drain and gate voltages of the dot[21]. b) Energy level splitting depending on the input power of the microwave cavity for a quantum dot in Coulomb blockade regime[21]. . . . .	22
7	Parallel quantum dots coupled to microwave cavities. . . . .	24
8	Sketch of the idea of entangled cavities via a quantum double-dot. . . . .	25
9	Tadpole diagram of order of $\lambda$ as integrand of the first order perturbative expansion of $\langle b \rangle$ . . . . .	54
10	Integrand of the perturbative expansion of $\langle b \rangle$ up to third order . . . . .	55
11	Feynman diagrams of the zeroth order perturbative expansion . . . . .	56
12	Feynman diagrams of the second order perturbative expansion. . . . .	56
13	Feynman diagrams of the perturbative expansion of the fourth order of the single cavities . . . . .	56
14	Feynman diagrams of the fourth order perturbative expansion of the combined cavities - part 2 . . . . .	57
15	Feynman diagrams of the Covariance . . . . .	59
16	Three different types of diagrams that are contained in the covariance. . . . .	61
17	Basic diagram of the bubble diagram. . . . .	62
18	Basic diagram of the square-shaped diagrams. . . . .	63
19	Basic diagram of the twisted-shaped diagrams. . . . .	64
20	All diagrams for the calculation of the covariance . . . . .	66



---

# 1 Introduction and Theoretical background

In recent years, the development and fabrication of devices of nanoscaled length is well advanced. Also the theoretical interest increased and the field of mesoscopic physics is getting larger. The transport properties of electronic nanostructures is a large research area. Phase coherent transport enables the possibility for interference experiments. A well studied mesoscopic system is the Aharonov-Bohm interferometer (ABI)[11].

Important and well studied systems are quantum dots. Quantum dots consist of a small amount of localized electrons, confined in all three spatial dimensions with discretized energy levels. The investigation of quantum dots revealed interesting properties and phenomena like the resonant tunneling[24], Coulomb blockade[25, 26] and the Kondo effect[27].

The cavity quantum electrodynamics deals with the interaction of light and matter at the most elementary form. For instance a single atom can interact with few photons of a single-mode cavity[20, 38]. The dipole interaction with the photon field induces a controllable entanglement by modification of the photon field[21].

The so-called circuit quantum electrodynamics investigates similar systems as the cavity quantum electrodynamics but the photon is stored in a one-dimensional on-chip resonator[39]. The atom can be replaced with a quantum dot with two levels which acts like an artificial atom[38]. Several experiments have already proven a strong coupling between quantum dots and microwave cavities[22]. Since this can also be used as a qubit and the qubit could be readout through the cavity the circuit quantum electrodynamics is an interesting field of quantum computation.

In this thesis we combine several of these aspects. We developed a system of two parallel quantum dots, whereby each dot is embedded in one path of an ABI. Both dots are independently coupled to two separate microwave cavities. Due to the coherent transport of an electron through the two branches of the ABI, i.e. through the dots that are coupled to the cavities, we expect a quantum correlation or entanglement of the two photonic fields. We explore this correlation using a diagrammatic perturbative expansion, in particular the Keldysh Green's functions, and derive an analytic formula ready for a numerical evaluation.

## 1.1 Electronic Transport

It is well known that we can describe the current in macroscopic systems by Ohm's law  $I = G \cdot U$ , which says that the current is proportional to the applied voltage. The constant of proportionality is the conductance  $G = \sigma A_c / L$ . The current increases linear with the cross-sectional area  $A_c$  and decreases due to the length of the sample  $L$ . Here the constant of proportionality is the electrical conductivity  $\sigma$  which depends on the material[4].

Since it became possible to produce much smaller devices one could ask what changes, regarding this behavior, when the dimensions of the system are reduced. The answer is, that Ohm's law is no longer valid. To describe this so-called mesoscopic regime, which is still larger than the atomic scale, we have to compare the dimensions of the conductor with some characteristic length scales[1].

The first length scale is the Fermi-wavelength  $\lambda_F = 2\pi/k_F$  corresponding to the de-Broglie wavelength of an electron at the Fermi level. Since we consider the system at low temperatures the current is mainly determined by electrons near the Fermi level. The second length scale is the mean free path  $L_m = v_F \cdot \tau_m$  corresponding the distance an electron could travel without being scattered whereby  $v_F$  is the Fermi velocity and  $\tau_m$  is the corresponding traveling-time. Finally we have the phase-relaxation length  $L_\varphi$  "[...] the distance that an electron travels before its initial phase is destroyed"[1]. For this we imagine that an electron splits its path into two and recombine them later. If these paths are equal there should be a perfect constructive interference at the end. Elastic scattering at static defects doesn't affect this process in contrast to inelastic scattering like electron-electron and electron-phonon scattering or scattering on impurities with an internal degree of freedom like magnetic impurities[1]. Since these length scales depend on several external influences, like the temperature or the magnetic field, they can vary from only a few nanometers to hundreds of micrometers [1].

We have mesoscopic regime if the length scale  $L$  of the system is smaller than the phase-relaxation length  $L_\varphi$ . In this case a coherent propagation of the electron through the conductor is possible whereas the mean free path  $L_m$  still determines the amount of scattering events on spatial potential fluctuations inside the conductor.

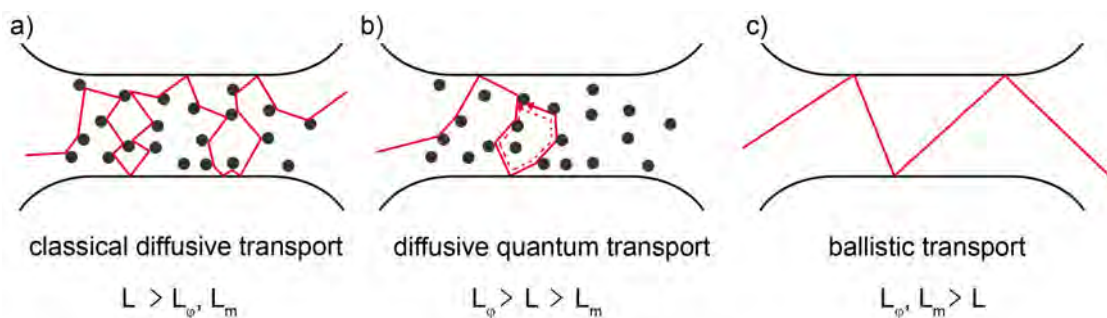


Figure 1: a) Classical diffusive transport regime. b) Quantum transport regime an weak localization. c) Ballistic transport regime. From [7].

In the well known macroscopic regime, where Ohm's law is valid, the length of the system is much larger than the mean free path  $L_m \ll L$  and the phase-relaxation length. Here we have



diffusive classical transport, depicted in Fig.(1) (a), and the conductivity is described by the Drude model. If  $L$  is smaller than  $L_\varphi$  but larger than  $L_m$ ,  $L_\varphi > L > L_m$ , we have diffusive quantum transport in a mesoscopic regime. The Drude model doesn't hold in this case. The electron is scattered several times inside the sample. It is possible that it is backscattered on exactly the same path as we can see in Fig. (1) (b). If  $L_\varphi$  is now larger than  $L_m$  this results in an destructive interference and we have a kind of weak localization. This deconstructive interference leads to a negative logarithmic correction to the Drude Model[7]. If the length scale of the system is much smaller than the mean free path and the phase-relaxation length,  $L \ll L_m, L_\varphi$  we are in the ballistic regime and the scattering with electrons or the boundaries of the sample dominates, see Fig. (1) (c).

If the length is comparable to the Fermi wavelength  $\lambda_F$  this means that the electron cannot propagate in this direction. Therefore the system is completely confined in this dimension. If we split the length scale  $L$  of the system in the lengths of the three spatial dimensions  $L_{x,y,z}$  we obtain, depending on the number of complete confinements, different geometries in the mesoscopic regime. We abbreviate the Fermi wavelength, mean free path and phase-relaxation length with  $L_0$ [6].

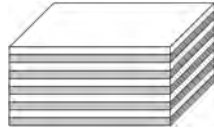
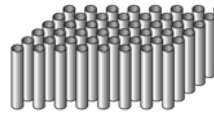
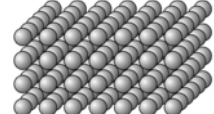
$L_{x,y} > L_0 > L_z$	Two dimensional nanostructure	Quantum Wells	
$L_x > L_0 > L_{y,z}$	One dimensional nanostructure	Quantum Wires	
$L_0 > L_{x,y,z}$	Zero dimensional nanostructure	Quantum Dots	

Table 1: Nanostructures in different dimensions compare [6].

A description of the conductance in this regime was developed by Landauer in the end of the 1950s[8]. His theory is also called Landauer or scattering approach. He proposed "[...]that if one can ignore inelastic interactions, a transport problem can always be viewed as a scattering problem"[4]. Therefore the electrical conductance can be expressed in terms of the transmission probability. This relation is the so-called Landauer formula

$$G = \frac{2e^2}{h} \sum_{n=1}^N T_n .$$

The main idea is to determine the transmission values of all modes that contribute to the current. These individual transmission have to be summed up whereby a perfect transmission would give exactly one quantum of conductance  $G_0 = 2e^2/h$ . Therefore the current depends not directly on the length and cross-sectional area of the conductor but indirectly. A larger contact leads to a different amount of modes that give an contribution to the conductance[4].

A very common used two dimensional device is a GaAs-AlGaAs-heterostructure. GaAs and Al-GaAs have different conduction, valence and Fermi energies and if they are connected electrons

travel towards the GaAs with the lower Fermi level and create positively charged donors in the AlGaAs. This leads to an electrostatic potential which affects the conduction and valence band. An area appears where a sharp peak and dip of the conduction band creates a small area under the constant Fermi energy and confines the electrons in one dimension. This is the so-called two dimensional electron gas (2-DEG), a thin conduction layer[1].

This heterostructure can be used to generate a zero dimensional nanostructure - a quantum dot. For this one evaporates gold electrodes on top of the GaAs-AlGaAs-heterostructure and applies a gate voltage. Due to the field effect of the electrodes the two dimensional electron gas is depleted and one could define a small quasi-zero dimensional area, the quantum dot. A similar procedure can be applied to carbon nanotubes instead of the 2DEG[37].

These quantum dots are similar to atoms: strong localized electrons with a discretization of the energy levels. Therefore quantum dots can be used as artificial atoms. The advantage is that one can control the properties of the dots easily in contrast to normal atoms[19].

To study such more complex phenomena(i.e. interactions) we have to introduce a new method because the Landauer approach is not able to describe transport situations with inelastic interactions[4]. One theoretical method is the Keldysh Greens functions technique that is able to describe the quantum transport in a mesoscopic conductor beyond the linear regime (nonequilibrium regime) and in presence of interaction in the quantum dots. The only condition is that we know the Hamiltonian of the system.

### Noninteracting Resonant-Level Model

In this thesis we consider systems that contain quantum dots which are coupled via tunneling to the leads. So we start by discussing mesoscopic tunneling structures in the noninteracting resonant-level model. Then the Hamiltonian of a mesoscopic tunneling model can be divided in three parts[2]

$$H = H_C + H_{cen} + H_T .$$

$$H_C = \sum_{k\alpha \in L,R} \varepsilon_{k\alpha} c_{k\alpha}^\dagger c_{k\alpha}$$

Hamiltonian of the noninteracting contacts(i.e. Fermi gas).

$$H_{cen} = \sum_i \varepsilon_i d_i^\dagger d_i$$

Hamiltonian of the central region. For the noninteracting resonant-level model the Hamiltonian includes only the non-interacting creation and annihilation operator of an electron in state  $i$ .

$$H_T = \sum_{k\alpha \in L,R} V_{k\alpha,i} c_{k\alpha}^\dagger d_i + \text{h.c.}$$

Tunneling coupling of the leads and the central region with the resonant levels.

$$\Sigma = \Sigma_L + \Sigma_R$$

The self energy of the system is given by the contributions of the tunneling.

$$\Sigma_{\alpha,mn}(\varepsilon) = \sum_k V_{k\alpha,m}^* g_{k\alpha} V_{k\alpha,n}$$

Tunneling self-energy.

$\varepsilon_{k\alpha}$ ,  $\varepsilon_i$  are the energy levels of the contacts or dots.  $c_{k\alpha}^\dagger$ ,  $c_{k\alpha}$  are the creation and annihilation operators of the contacts and  $d_i^\dagger$ ,  $d_i$  those of the dots.  $V_{k\alpha,i}$  is the tunneling coupling between the lead  $\alpha$  and dot  $i$ .  $g_{k\alpha}$  is an unperturbed Green's function of the system.

## 1.2 Double-Dot Aharonov-Bohm Interferometer

As a first example of the noninteracting resonant-level model we consider the case of two resonant levels: A parallel double quantum dot coupled to a left and right lead. As an additional controlling field we apply a magnetic flux. The system is depicted in Fig. (2). The magnetic flux leads to a phase shift of the electrons. Since this symmetric phase shift occurs when the electron travels between a lead  $r$  and a dot  $i$  we include it in the tunneling parameter  $t_{ri} = te^{\pm i\frac{\varphi}{4}}$  whereby the sign depends on the traveling direction of the electron. The Hamiltonian reads

$$H = \sum_{k,r=L,R} \varepsilon_{kr} c_{kr}^\dagger c_{kr} + \sum_{i=1,2} \varepsilon_i d_i^\dagger d_i + \sum_{\substack{i=1,2 \\ k,r=L,R}} \left( t_{ri} c_{kr}^\dagger d_i + h.c. \right)$$

The operators are defined for the noninteracting resonant-level model.

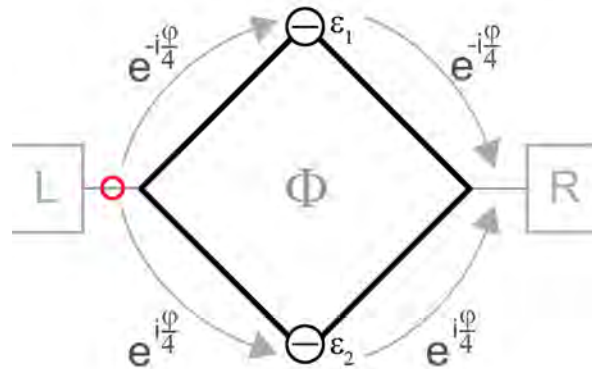


Figure 2: Double-dot Aharonov Bohm Interferometer. Two parallel quantum dots are coupled to a left and right lead. A magnetic flux is applied in the loop.

This geometry plays an important role in experimental physics. In general the measured quantity in experiments is the current. The Aharonov Bohm interferometer (ABI) offers the possibility to perform interference experiments with mesoscopic nanostructures, to use the information provided in the phase. The geometry is like the one in Fig.(2) except for the two quantum dots. A magnetic field  $B$  is applied in such a way that it is confined inside the area enclosed by the loop but vanishes along the loop and beyond. The electron travels along these paths and its phase depends on the vector potential  $A$  caused by the magnetic field,  $B = \nabla \times A$ . If an electron takes on turn through the complete ring it acquires the Aharonov-Bohm-phase:  $\Delta\varphi_{AB} = -|e|/\hbar \oint A ds = -|e|/\hbar \phi = -2\pi\phi/\phi_0$ [11].

In a transport experiment an electron can travel through the upper or lower branch which leads to an effective phaseshift of  $\Delta\varphi_{AB}$ . Due to this an interference periodic in the magnetic field,

with periodicity  $\Delta B = h/eS$  occurs in the measured current by sweeping the magnetic field, while  $S$  is the area of the loop[7].

Studying transport through quantum dots, like resonant tunneling, Coulomb blockade, and the Kondo effect the common measured quantity is the current which provides no information whether the transport is coherent or not. This information can be obtained by embedding a quantum dot in an ABI[12].

Transport through quantum dots that are arranged in an ABI are theoretically well investigated, both with one or two dots, taking into account electron-electron Coulomb interaction or spin[12, 13, 14]. There have also been several experiments placing one quantum dot in an ABI and considering coherent transport[15, 16] or the Kondo-effect[17]. An experiment with two quantum dots, each one in another branch and depicted in Fig. (3), was done by A. Holleitner et al.[18]. They were able to tune the coupling between the dots and demonstrate for a weak coupling Aharonov-Bohm oscillation on the Coulomb diamonds, see Fig.(3) (c). For intermediate coupling the showed a coherent coupling of the two dots and that the tunnel splitting depends on the magnetic field, see Fig.(3) (d).

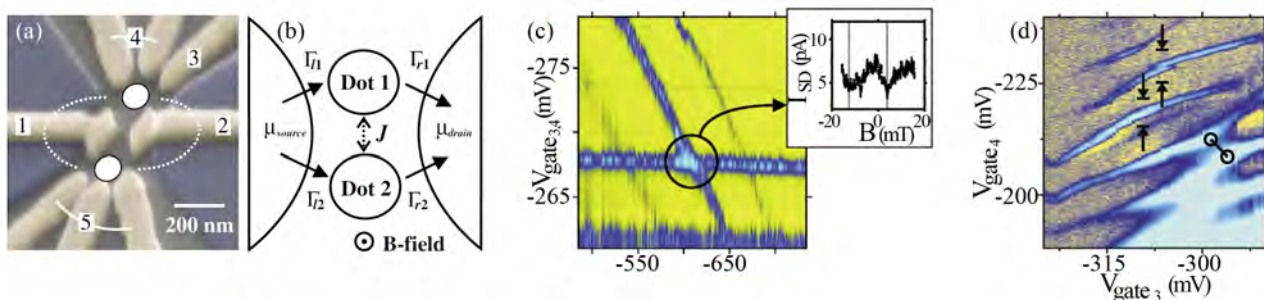


Figure 3: Experimental results of A. Holleitner et al.[18] for weak and intermediate coupling of two quantum dots in an ABI. a) and b): Setup of the device. Two parallel quantum dots coupled to a left and right gate 1,2 and the gates 3-4 for the measurement. c) Weak coupling: Coulomb blockade resonances of the double dot, through detuning of the gates 3-5, and Aharonov-Bohm interferences in the current amplitude by varying the magnetic field as shown in the inset. d) Intermediate coupling: Charging diagram spanned by voltage of gate 3 and 4. The two connected circles denote the coherent coupling of the two quantum dots. Two arrows pointing at each other show two regions that indicates coherent coupling. Ref. [18].

### 1.3 Single Quantum Dot Coupled to a Microwave Cavity

Another interesting application in mesoscopic physics of the quantum dots is in the "circuit quantum electrodynamic". Since the realization of high quality superconducting microwave cavities[20], circuit quantum electrodynamics enables the possibility to investigate the coherent interaction of light and matter. This can be reached using a quantum dot that represents some kind of an artificial atom and placed in a high quality superconducting microwave cavity[20, 22, 23]. The schematic representation in Fig.(4) shows the quantum dot, that can be considered as a two level system coupled to a cavity with coupling strength  $g$ .

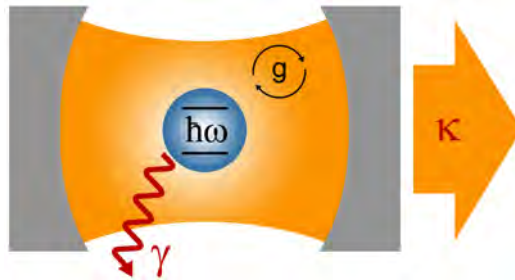


Figure 4: Schematic representation of a quantum dot, considerable as a two level system, coupled to a microwave cavity with coupling strength  $g$  and the decay rate  $\kappa$  of the photon field. Picture adapted from [21].

Delbecq et al. studied the case of one[22] or two[23] quantum dots coupled to a cavity. There are two possibilities for the readout. In the first case the state of the quantum dot affect the electromagnetic mode which can be observed by detecting the outgoing field. The second opportunity is the detection of the state of the quantum dot so that one can gain information regarding the photon state[21]. In the case of the single quantum dot coupled to a microwave cavity they were able to detect the strong electronic interactions of the quantum dot as Coulomb diamonds and the Kondo effect as depicted in Fig.(5) (a), whereby the red line is a cut at zero bias that we will not discuss here. By tuning the input power of the microwave cavity one can observe the funnel shaped splitting of the energy levels of the quantum dot depicted in Fig.(5) (b). This could be due to a direct coupling of the quantum dot levels with the cavity mode[21].

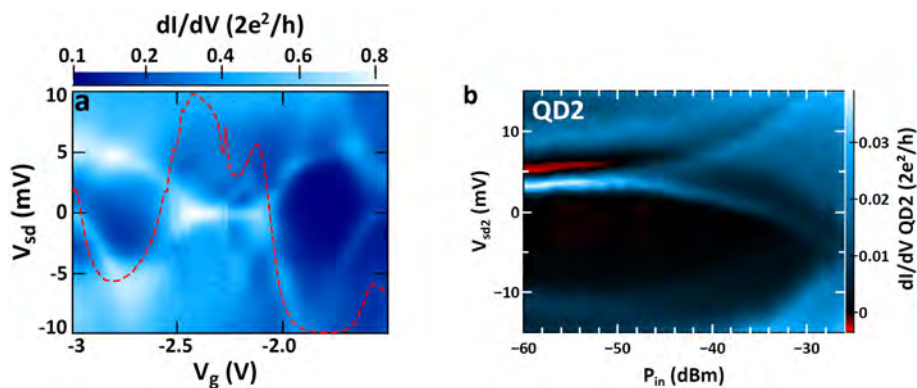


Figure 5: Color scale plot of the differential conductance of one quantum dot. a) Both Coulomb diamonds and the the Kondo ridge at zero bias can be seen by sweeping the source-drain and gate voltages of the dot[21]. b) Energy level splitting depending on the input power of the microwave cavity for a quantum dot in Coulomb blockade regime[21].

They also investigated two separated quantum dots that are both coupled to the same cavity. They drove the gate voltages of each quantum dot and readout the differential conductance of one quantum dot. As depicted in Fig.(6) (a) they were able to detect a crossing and anticrossing. Fig.(6) (b) is a close up of an anticrossing region. This indicates some kind of correlation between the displaced dots since a normal superposition should lead to an equal behavior of the energy levels of the dot[21].

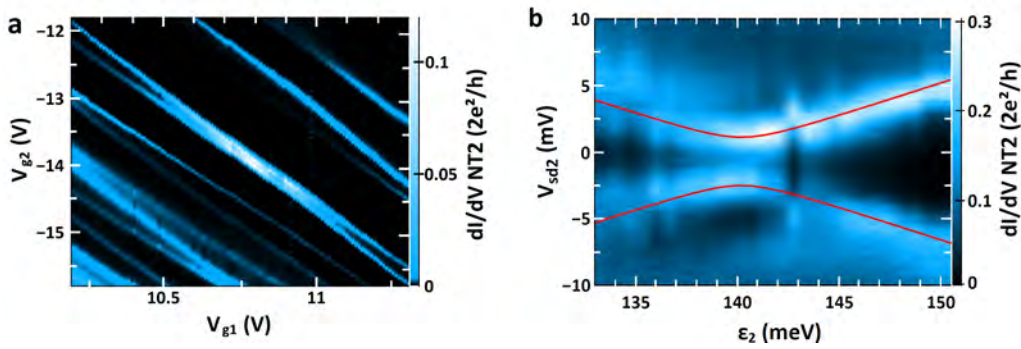


Figure 6: Color scale plot of the differential conductance of one quantum dot. a) Both Coulomb diamonds and the the Kondo ridge at zero bias can be seen by sweeping the source-drain and gate voltages of the dot[21]. b) Energy level splitting depending on the input power of the microwave cavity for a quantum dot in Coulomb blockade regime[21].

## 1.4 Inequalities in Quantum Coherence Theory

We have seen so far that there are several possibilities to investigate a single or several quantum dots. In the case of several quantum dots, like the two separated quantum dots in the microwave cavity, it is of high interest if the states of the dots are correlated or even entangled. Entanglement is one of the most important things to differ between classical and the quantum physics. One can derive several inequalities to proof a correlation or entanglement.

We can describe the quantum mechanical state of a system via its density matrix,  $\rho$ . If we measure an observable we determine actually the expectation value that is a trace of the density matrix and the related operator. We consider a bipartite system, containing two subsystems (1) and (2), for example two quantum dots, two cavities or a dot and a cavity, with commuting operators. The system is defined as separable or uncorrelated if the density matrix  $\rho$  of the combined system is a direct product of the two sub-system density matrices  $\rho^{(1)}$  and  $\rho^{(2)}$ , so  $\rho = \rho^{(1)} \otimes \rho^{(2)}$ [28].

In this separable case the measurement result of any value  $A^{(1)}$  of the first subsystem is completely independent of the measurement result of any value  $B^{(2)}$  of the second one. This means  $\langle A^{(1)} B^{(2)} \rangle = \langle A^{(1)} \rangle \langle B^{(2)} \rangle$  for any A and B. If the system is not separable and the density matrix cannot be factorized, so  $\rho \neq \rho^{(1)} \otimes \rho^{(2)}$ , this equality is violated and concerning this matter we can define the covariance

$$C := \text{cov}(A^{(1)} B^{(2)}) = \langle A^{(1)} B^{(2)} \rangle - \langle A^{(1)} \rangle \langle B^{(2)} \rangle .$$

The covariance is nonzero in the case of a correlation between the two subsystems[28].

To prove if the system is not simply correlated but entangled (i.e. quantum correlation) we need different equalities. The most known inequality that is violated in the case of quantum entanglement is the Bell's inequality. It contradicts the theory of Einstein, Podolsky, and Rosen that the quantum theory can be explained with hidden variables[30]. But there are several more where the general separability criterion is used[31, 32, 33, 34, 35]. Furthermore it exists a class of inequalities which are applications of the Cauchy-Schwarz inequality. For instance, Ref. [36] analyses entanglement criteria based on the Cauchy-Schwarz inequality  $|\langle x, y \rangle|^2 \leq \langle x, x \rangle \langle y, y \rangle$

and the properties of separable states. We focus on bipartite systems with the expectation value  $\langle A_1 A_2 B_1 B_2 \rangle$ , whereby  $A_i$  and  $B_j$  belong to the two subsystems, and use it to detect entanglement.

The inequality

$$\left| \langle A_1 A_2 B_1 B_2 \rangle_{sep} \right|^2 \leq \langle A_1 A_1^\dagger B_2^\dagger B_2 \rangle_{sep} \langle A_2^\dagger A_2 B_1 B_1^\dagger \rangle_{sep}$$

is valid for separable states and can only be violated by entangled states, which depends on the choice of the operators  $A$  and  $B$ .

If  $A_2 = B_1 = 1$ ,  $A_1 = A^\dagger = (a^m)^\dagger$  and  $B_2 = B = b^n$ , whereby  $a, b$  are the annihilation and  $a^\dagger, b^\dagger$  the creation operators of system A,B, we obtain the criterion

$$\left| \langle a^m (b^\dagger)^n \rangle_{sep} \right|^2 \leq \langle (a^\dagger)^m a^m (b^\dagger)^n b^n \rangle_{sep} .$$

If  $A_1 = B_1 = 1$ ,  $A_2 = (a^m)^\dagger$  and  $B_2 = B = b^n$  we obtain the criterion

$$\left| \langle a^m b^n \rangle_{sep} \right|^2 \leq \langle (a^\dagger)^m a^m \rangle_{sep} \langle (b^\dagger)^n b^n \rangle_{sep} .$$

These two criterion where also discussed by Hillery and Zubairy[31].

### 1.5 Parallel Double-Dot Coupled to Microwave Cavities

We consider two parallel quantum dots with energy levels  $\varepsilon_{1,2}$ , that are arranged in the geometry of an Aharonov-Bohm interferometer. The applied flux creates a phase shift to the electrons, depending on their traveling direction. Each dot is capacitively coupled to a microwave cavity with different resonance frequencies  $\omega_{a,b}$  and to a common left and right lead.

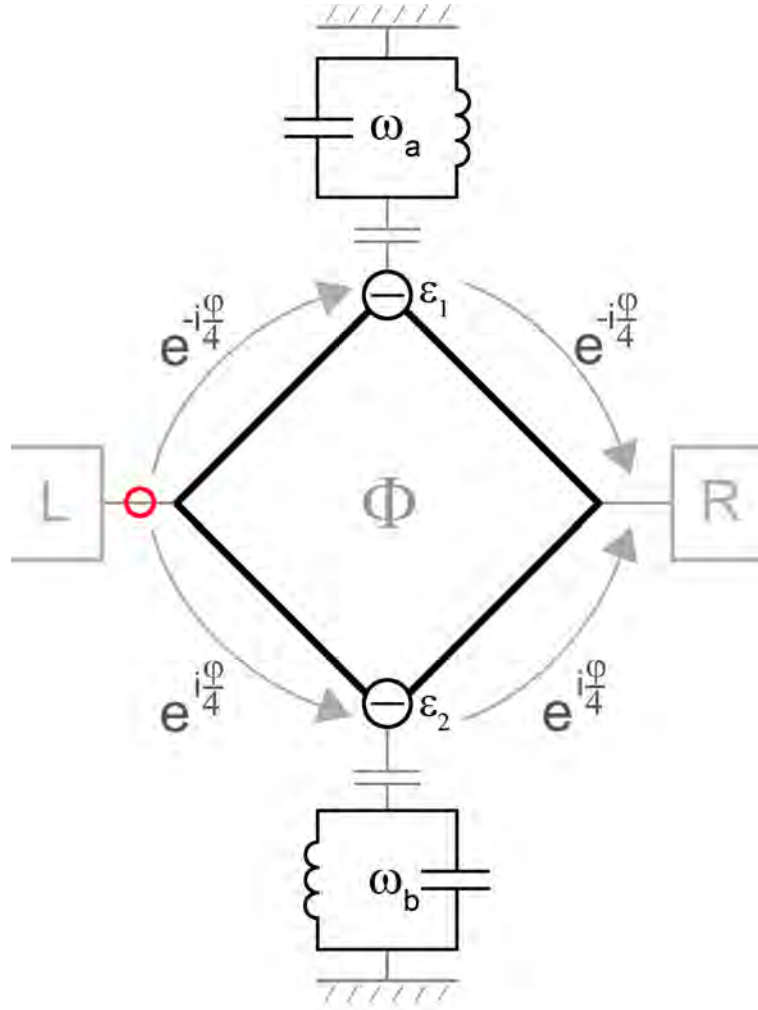


Figure 7: System of two parallel quantum dots, each one coupled to a microwave cavity and to a common left and right lead.

The system is described through a modified Anderson-Holstein Hamiltonian that includes the fermion-photon interaction.

$$\begin{aligned}
 H = & \sum_{k,r=L,R} \varepsilon_{kr} c_{kr}^\dagger c_{kr} + \sum_{i=1,2} \varepsilon_i d_i^\dagger d_i + \sum_{\substack{i=1,2 \\ k,r=L,R}} \left( t_{ri} c_{kr}^\dagger d_i + h.c. \right) \\
 & + \sum_{\alpha=a,b} \hbar \omega_\alpha \alpha^\dagger \alpha + \lambda_a (a + a^\dagger) d_1^\dagger d_1 + \lambda_b (b + b^\dagger) d_2^\dagger d_2 .
 \end{aligned} \tag{1.1}$$



Here  $c_{kr}^\dagger$  and  $c_{kr}$  with  $r = L, R$  are the creation and annihilation operator of the electrons in the left and right lead.  $d_i^\dagger$  and  $d_i$  with  $i = 1, 2$  are the creation and annihilation operator of the electrons in the two quantum dots and  $a, b$  and  $a^\dagger, b^\dagger$  are the creation and annihilation operator of the photons with frequency  $\omega_{a,b}$  in cavity  $a, b$ . The coupling element  $t_{ri} = te^{\pm i\frac{\varphi}{4}}$  describes, just like it was explained in section (1.2), the hopping of an electron from lead  $r$  to dot  $i$  and vice versa including a phase shift  $\pm\varphi = \pm 2\pi\Phi/\Phi_0$  whereby the sign depends on the traveling direction of the electron.

### Quantum Correlation and Entanglement - A Heuristic Argument

We want to explore how quantum correlation and entanglement between the two cavity fields is generated by the coherent transport of a single electron traveling in two different paths of the ABI.

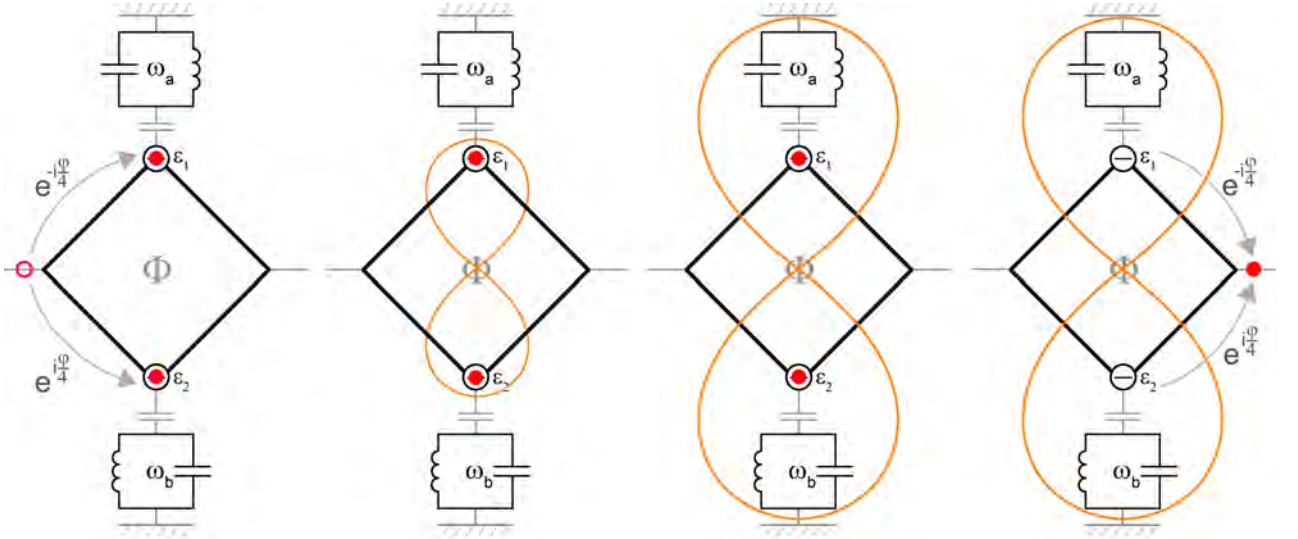


Figure 8: Sketch of the main idea regarding an entanglement of two microwave cavities via a coupled parallel quantum double-dot with an additional applied magnetic flux. The electron "splits" because of the possibility to travel trough both branches. Therefore the state of the electron is a coherent superposition of the states of the two dots. The correlation is extended to the two cavities even when the electron leaves the system.

When one electron travels in the system it "splits" in the sense that it can travel in the upper or in the lower branch. Depending on the traveling direction a positive or negative phase shift occurs. We assume that the state of the electron is a coherent superposition between the state in dot  $n_1$  and the state in dot  $n_2$ ,

$$|\psi_e\rangle = \frac{1}{\sqrt{2}} (|n_1=1\rangle + |n_2=1\rangle) .$$

Therefore the initial state of the system is determined by the electronic state  $|\psi_e\rangle$  and the ground state of the two cavities  $|GS\rangle_{1,2}$ ,

$$|\Psi_{sys}\rangle_{initial} = |\Psi_e\rangle |GS\rangle_1 |GS\rangle_2 = \frac{1}{\sqrt{2}} (|n_1=1, n_2=0\rangle + |n_1=0, n_2=1\rangle) |GS\rangle_1 |GS\rangle_2 .$$

To determine the time evolution operator of  $|\Psi_{sys}\rangle_{initial}$  we consider the Schrödinger equation with a reduce Hamiltonian

$$i\hbar \frac{\partial |\Psi_{sys}\rangle}{\partial t} = H_{red} |\Psi_{sys}\rangle .$$

Neglecting the interaction with the leads, the new Hamiltonian contains only the dots, cavities and dot-cavity coupling. The time evolution operator becomes

$$U(t) = D_1[n_1\alpha_1(t)] \times D_2[n_2\alpha_2(t)] ,$$

whereby  $D_i[n_i\alpha_i(t)]$  is the coherent displacement operator and  $\alpha_i(t)$  is a coherent state. Now we are able to consider the time evolution of the initial state of the system.

$$|\Psi_{sys}(t)\rangle = U(t) |\Psi_{sys}\rangle_{initial} = \frac{1}{\sqrt{2}} ( |n_1=1, n_2=0\rangle \underline{|\alpha_1(t)\rangle} \underline{|GS\rangle_2} + |n_1=0, n_2=1\rangle \underline{|GS\rangle_1} \underline{|\alpha_2(t)\rangle_2} )$$

The correlation of the two dots, due to the possibility of the electron to travel through both branches, is extended to the two cavities. This result indicates the possibility of an entangled state of the two cavities. This entangled state can remain even when the electron leaves the system.

## 1.6 Proceeding and Structure of the Work

We would like to investigate correlation in the system of two parallel quantum dots coupled to two microwave cavities. To achieve this we calculate the covariance of the two cavities a and b,

$$C = \langle n_a n_b \rangle - \langle n_a \rangle \langle n_b \rangle .$$

If this quantity is non-zero we can conclude that the two cavities are correlated.

We proceed as follows: We use the Keldysh Greens functions techniques and carry out the perturbative expansion of the system up to fourth order by choosing the dot-cavity coupling as perturbation.

The covariance contain photon creation and annihilation operators at equal times for instance  $\langle n_a \rangle = \langle a^\dagger(t)a(t) \rangle$ . Since we consider a full time-ordered expression to do the perturbative expansion, it is necessary to reach the quantity  $n_a = \langle a^\dagger(t)a(t) \rangle$  from the expression  $\langle T_c (a^\dagger(t)a(t')) \rangle$ . This quantity correspond to the so called lesser Greens function in the diagrammatic language.

This lesser function contains, due to the application of Wick's theroem, the unperturbed bosonic Green's functions of the two cavities and the fermionic Green's functions of the noninteracting tunneling model which are integrated over contour times. We determine the fermionic Green's functions using the Dyson equation and consider the dot-lead coupling as perturbation.

In the next step we transform the integration back to real time space and subsequently to the frequency space. We perform the integration analytically up to a certain point where the method should be changed to a numerical integration. So in the end we have developed an expression that is the starting point for a numerical integration and analysis.

---

## 2 Green's Functions and Perturbation Theory

In a first step we introduce a method to determine easily the energy dependent retarded and advanced Green's functions of the dot-lead system. Since the dot-cavity system is more complicated we introduce time-ordered Green's functions and consider them in an equilibrium and non-equilibrium system. We introduce a closed time path, which is also denoted as contour, and show that the transformation to the interaction picture is equal for Green's functions defined by field operators depending on real times or contour times. We develop the perturbative theory on this contour and introduce the so called Wick theorem, to handle the terms of the perturbative expansion easier.

### 2.1 Real Time Green's Functions of Double-Dot Aharonov-Bohm Interferometer

One common used Green's function approach is the definition of the Green's function as the inverse of a differential operator[4]. It is possible to apply this approach to the Schrödinger equation, since it is a second order differential equation. To keep it simple we start with an electron in a one-dimensional problem. The Schrödinger equation and the corresponding electron Green's function read

$$H(x)\Psi(x) = E\Psi(x), \text{ and } [E - H(x)]G(x, x') = \delta(x - x') .$$

To distinguish the retarded Green's function, that corresponds to the propagation of an electron forward in time, and the advanced Green's function, that corresponds to the propagation of an electron backwards in time, we insert an infinitesimal imaginary part  $\pm i\eta$  in the energy, whereby the  $\pm$  corresponds to the retarded or advanced Green's function. The definition of the Green's function, according to a Hamiltonian  $H = H_0 + V$ , becomes

$$G^{r,a}(E) = \lim_{\eta \rightarrow 0} [(E \pm i\eta)\mathbb{1} - H_0 - V]^{-1} . \quad (2.1)$$

In the considered system of the two quantum dots within the Aharonov-Bohm structure we are dealing with a Hamiltonian containing the two dots, the two leads and the tunneling. The unperturbed Hamiltonian contains only the dots and leads.

#### Unperturbed Retarded and Advanced Green's Functions

The unperturbed retarded and advanced Green's function now can be calculated with

$$g^{r,a}(E) = \lim_{\eta \rightarrow 0} [(E \pm i\eta)\mathbb{1} - H_0]^{-1} . \quad (2.2)$$

We include the infinitesimal imaginary part in a retarded and advanced energy as  $E^{r,a} = E \pm i\eta$ . The unperturbed Hamiltonian of the fermionic system is

$$H_0 = \begin{pmatrix} \varepsilon_1 & 0 & 0 & 0 \\ 0 & \varepsilon_2 & 0 & 0 \\ 0 & 0 & \varepsilon_{kL} & 0 \\ 0 & 0 & 0 & \varepsilon_{kR} \end{pmatrix}$$

and therefore the unperturbed retarded and advanced Green's functions read

$$g^{r,a}(E) = \begin{pmatrix} (E^{r,a} - \varepsilon_1)^{-1} & 0 & 0 & 0 \\ 0 & (E^{r,a} - \varepsilon_2)^{-1} & 0 & 0 \\ 0 & 0 & (E^{r,a} - \varepsilon_{kL})^{-1} & 0 \\ 0 & 0 & 0 & (E^{r,a} - \varepsilon_{kR})^{-1} \end{pmatrix}. \quad (2.3)$$

### Full Retarded and Advanced Green's Function

To determine the retarded and advanced Green's function of the complete system that is described by the Hamiltonian  $H = H_0 + V$  we resort to Dyson's equation. This equation can be obtained if we transform Eq.(2.1) and insert Eq.(2.2) [4].

$$G^{r,a}(E) = g^{r,a}(E) + g^{r,a}(E)V G^{r,a}(E)$$

The perturbation  $V$  which describes the dot-lead coupling reads

$$V = \begin{pmatrix} 0 & 0 & t_{1L} & t_{1R} \\ 0 & 0 & t_{2L} & t_{2R} \\ t_{L1} & t_{L2} & 0 & 0 \\ t_{R1} & t_{R2} & 0 & 0 \end{pmatrix}. \quad (2.4)$$

The different components of the Green's function can be calculated using

$$G_{ij}^{r,a}(E) = g_{ij}^{r,a}(E) + \sum_{lm} g_{il}^{r,a}(E) V_{lm} G_{mj}^{r,a}(E) \quad (2.5)$$

whereby  $l, m = 1, 2, L, R$ . Since  $g^{r,a}$  is diagonal, the first addend of Eq.(2.5) vanishes for all off-diagonal elements  $i \neq j$ . The sum over  $l, m = 1, 2, L, R$  can be reduced to only two terms. Again, due to the diagonal form of the unperturbed Green's function,  $g_{il}^{r,a}$  is zero if  $l \neq i$  and in this case the complete sum vanishes. Therefore  $l$  is determined through the initial index  $i$  and the sum reduces to a summation over  $m$ . The perturbation, or tunneling,  $V_{lm}$  gives only then a contribution if one of its indices corresponds to a dot and the other to a lead, compare Eq.(2.4). Since the first index  $l$  is already fixed with a dot- or lead-index  $i$  we get only two terms. We sum over  $m = L, R$  if  $i \in 1, 2$  or  $m = 1, 2$  if  $i \in L, R$ . This leads to eight interdependent equations for the dots,  $i, j \in 1, 2$  and dot-leads,  $i \in L, R$  and  $j \in 1, 2$ . We eliminate the dot-lead Green's functions by inserting their equations inside the equations of the dots. We summarize first after the factors  $g_{LL}^{r,a}$  and  $g_{RR}^{r,a}$  and then after the different Green's functions. Next, we insert the expression of  $t_{ij}$ .

$$G_{11}^{r,a} = g_{11}^{r,a} + g_{11}^{r,a} (g_{LL}^{r,a} \cdot t^2 + g_{RR}^{r,a} \cdot t^2) G_{11}^{r,a} + g_{11}^{r,a} (g_{LL}^{r,a} \cdot t^2 e^{i\frac{\varphi}{2}} + g_{RR}^{r,a} \cdot t^2 e^{-i\frac{\varphi}{2}}) G_{21}^{r,a} \quad (2.6)$$

$$G_{22}^{r,a} = g_{22}^{r,a} + g_{22}^{r,a} (g_{LL}^{r,a} \cdot t^2 + g_{RR}^{r,a} \cdot t^2) G_{22}^{r,a} + g_{22}^{r,a} (g_{LL}^{r,a} \cdot t^2 e^{-i\frac{\varphi}{2}} + g_{RR}^{r,a} \cdot t^2 e^{i\frac{\varphi}{2}}) G_{12}^{r,a} \quad (2.7)$$

$$G_{12}^{r,a} = g_{11}^{r,a} (g_{LL}^{r,a} \cdot t^2 + g_{RR}^{r,a} \cdot t^2) G_{12}^{r,a} + g_{11}^{r,a} (g_{LL}^{r,a} \cdot t^2 e^{i\frac{\varphi}{2}} + g_{RR}^{r,a} \cdot t^2 e^{-i\frac{\varphi}{2}}) G_{22}^{r,a} \quad (2.8)$$

$$G_{21}^{r,a} = g_{22}^{r,a} (g_{LL}^{r,a} \cdot t^2 + g_{RR}^{r,a} \cdot t^2) G_{21}^{r,a} + g_{22}^{r,a} (g_{LL}^{r,a} \cdot t^2 e^{-i\frac{\varphi}{2}} + g_{RR}^{r,a} \cdot t^2 e^{i\frac{\varphi}{2}}) G_{11}^{r,a} \quad (2.9)$$

We define that  $\Gamma_R = \Gamma_L = \frac{\Gamma}{2}$  and use the wideband approximation for the leads so that  $g_{ii}^{r,a} t_i^2 = \mp i\Gamma_i$  with  $i = L, R$  [4]. Consequently  $g_{LL}^{r,a} t^2 + g_{RR}^{r,a} t^2 = \mp i\Gamma_L \mp i\Gamma_R = \mp i\Gamma$ . Then we sort the equations according  $G_{ij}^{r,a}$  with  $i, j = 1, 2$ .

$$G_{11}^{r,a} (E^{R,A} - \varepsilon_1 \pm i\Gamma) = 1 \mp i\Gamma \cdot \cos \frac{\varphi}{2} G_{21}^{r,a} \quad (2.10)$$

$$G_{22}^{r,a} (E^{R,A} - \varepsilon_2 \pm i\Gamma) = 1 \mp i\Gamma \cdot \cos \frac{\varphi}{2} G_{12}^{r,a} \quad (2.11)$$

$$G_{12}^{r,a} (E^{R,A} - \varepsilon_1 \pm i\Gamma) = \mp i\Gamma \cdot \cos \frac{\varphi}{2} \cdot G_{22}^{r,a} \quad (2.12)$$

$$G_{21}^{r,a} (E^{R,A} - \varepsilon_2 \pm i\Gamma) = \mp i\Gamma \cdot \cos \frac{\varphi}{2} \cdot G_{11}^{r,a} \quad (2.13)$$

Since the diagonal Green's functions depend on an off-diagonal and vice versa, we insert them into each other and obtain the final expression of the retarded and advanced Green's functions.

$$G_{11}^{r,a} = \frac{E^{r,a} - \varepsilon_2 \pm i\Gamma}{(E^{r,a} - \varepsilon_1 \pm i\Gamma)(E^{r,a} - \varepsilon_2 \pm i\Gamma) + \Gamma^2 \cos^2 \frac{\varphi}{2}} \quad (2.14)$$

$$G_{21}^{r,a} = \frac{\mp i\Gamma \cdot \cos \frac{\varphi}{2}}{(E^{r,a} - \varepsilon_1 \pm i\Gamma)(E^{r,a} - \varepsilon_2 \pm i\Gamma) + \Gamma^2 \cos^2 \frac{\varphi}{2}} \quad (2.15)$$

$$G_{22}^{r,a} = \frac{E^{r,a} - \varepsilon_1 \pm i\Gamma}{(E^{r,a} - \varepsilon_2 \pm i\Gamma)(E^{r,a} - \varepsilon_1 \pm i\Gamma) + \Gamma^2 \cos^2 \frac{\varphi}{2}} \quad (2.16)$$

$$G_{12}^{r,a} = \frac{\mp i\Gamma \cdot \cos \frac{\varphi}{2}}{(E^{r,a} - \varepsilon_2 \pm i\Gamma)(E^{r,a} - \varepsilon_1 \pm i\Gamma) + \Gamma^2 \cos^2 \frac{\varphi}{2}} \quad (2.17)$$

## 2.2 Formalism of the Keldysh Green's Functions and Perturbation Theory

The retarded and advanced Green's function that we have calculated for the double-dot Aharonov-Bohm interferometer depends on the energy  $E$ . To develop the perturbation formalism we define the Green's functions in time domain. We replace the real-time axis by a closed time contour and transform the Green's functions from real-time arguments to contour-times. Then we develop the perturbative expansion of the contour-ordered Green's functions and introduce Wick's theorem, which simplifies the calculation of a string of field operators. The energy dependent Green's functions can be obtained by a Fourier transformation of the time-dependent Green's functions. The following sections are close to sec. 3.3 to 4.3.3 of [3].

The Hamiltonian of our system is composed by an noninteracting part  $H_0$  and an interacting part  $H^{(i)}$

$$H = H_0 + H^{(i)} .$$

We use the second quantization formalism to represent the time-ordered Green's function, whereby the time arguments correspond to the general real-time axis

$$G(x, t, x', t') = -i \left\langle T \Psi_H(x, t) \Psi_H^\dagger(x', t') \right\rangle . \quad (2.18)$$

The expectation value is evaluated for an arbitrary state described by the statistical operator  $\rho$  and the notation means  $\langle \dots \rangle = \text{Tr}(\rho \dots)$ . The field operators  $\psi_H(x, t)$  are defined in the

Heisenberg picture with respect to Hamiltonian  $H$ .  $T$  is the time ordering operator and orders the creation and annihilation operators according to their argument. The operator with the larger argument is placed to the left. In the case that it's known which time argument is larger or smaller we can define the corresponding greater and lesser Green's function.

$$G(x, t, x', t') = \begin{cases} G^<(x, t, x', t') = -i \langle \Psi_H(x, t) \Psi_H^\dagger(x', t') \rangle & t' > t \\ G^>(x, t, x', t') = \pm i \langle \Psi_H^\dagger(x', t') \Psi_H(x, t) \rangle & t' < t \end{cases}$$

whereby the upper sign of  $G^>$  corresponds to Fermions and the lower one to Bosons. To complete the different Green's functions we introduce the anti-time-ordered Green's function

$$\tilde{G}(x, t, x', t') = \langle \tilde{T} \Psi_H(x, t) \Psi_H^\dagger(x', t') \rangle$$

whereby  $\tilde{T}$  orders the arguments reverse to  $T$ .

### Green's Functions of a System in Equilibrium

At the beginning we consider the case of a system in thermal equilibrium. The statistical operator  $\rho$  becomes the Boltzman statistical operator  $\rho = e^{-H_0/kT} / \text{Tr}(e^{-H_0/kT})$  and the Green's functions become

$$G(x, t, x', t') = -i \langle T \Psi_{H_0}(x, t) \Psi_{H_0}^\dagger(x', t') \rangle = \text{Tr} \left( \frac{e^{-H_0/kT} \Psi_{H_0}(x, t) \Psi_{H_0}^\dagger(x', t')}{\text{Tr}(e^{-H_0/kT})} \right) .$$

The Green's functions depend only on the difference of the time arguments  $t - t'$ . As it was said before we can perform a Fourier transformation to pass from the time domain to the energy space with

$$G(x, t, x', t') = \int \frac{dp}{(2\pi)^3} \int \frac{dE}{2\pi} e^{i(p(x-x') - E(t-t'))} G(p, E) .$$

### Extension of the System to the Non-Equilibrium

Now we extend the system to the non-equilibrium. First we consider a system that is completely described by the Hamiltonian  $H_0$ . To characterize the non-equilibrium state we assume that the system was at a time  $t < t_0$  in equilibrium at temperature  $T$ . The state of the system at time  $t_0$  is therefore described through

$$\rho(H_0) = \frac{e^{-H_0/kT}}{\text{Tr}(e^{-H_0/kT})} . \tag{2.19}$$

At time  $t > t_0$  an additional perturbation  $H^i$  is applied to the system. The Hamiltonian that describes the system changes to

$$H = H_0 + H^i .$$

Using the time evolution operator  $U(t, t_0) = T e^{-i \int_{t_0}^t d\bar{t} H(\bar{t})}$  we are able to develop the new state of the system  $\rho(t) = U(t, t_0) \rho(H_0) U^\dagger(t, t_0)$ .

### Green's Functions of a System in the Ground State and Transformation to the Interaction Picture

To introduce the closed time contour and the perturbation theory for zero temperature we consider the system in the ground state  $|G\rangle$ . The Green's function reads in detail

$$G(x, t, x', t') = -i \left\langle T \Psi_H(x, t) \Psi_H^\dagger(x', t') \right\rangle = -i \langle G | T \Psi_H(x, t) \Psi_H^\dagger(x', t') | G \rangle . \quad (2.20)$$

The field operators  $\Psi_H(x, t)$  are now in the Heisenberg picture with respect to  $H$ . We transform the field operators to the Heisenberg picture with respect to  $H_0$  which is called the interaction picture.

$$\text{The field operators can be represented as } \psi_H(x, t) = U^\dagger(t, t_r) \psi_{H_0}(x, t) U(t, t_r) \quad (2.21)$$

$$\text{with } \psi_{H_0}(x, t) = e^{iH_0(t-t_r)} \psi_{H_0}(x) e^{-iH_0(t-t_r)} \text{ and } U(t, t_r) = T e^{-i \int_{t_r}^t d\bar{t} H_{H_0}^{(i)}(\bar{t})}$$

$$\text{whereby } H_{H_0}^{(i)}(t) = e^{iH_0(t-t_r)} H^{(i)} e^{-iH_0(t-t_r)} .$$

We replace the field operators in Eq.(2.20) with the representation of Eq.(2.21). Using several properties of the evolution operator and choose the reference time, where the operators in the Heisenberg and Schrödinger pictures coincide, to infinity we obtain

$$G(x, t, x', t') = -i \left\langle U^\dagger(\infty, -\infty) T(\psi_{H_0}(x, t) \psi_{H_0}^\dagger(x', t') U(\infty, -\infty)) \right\rangle$$

whereby the average is evaluated in the ground state. We assume that the interaction is turned on and off adiabatically. This can be reached by replace  $H_{H_0}^{(i)}(t)$  with  $e^{\epsilon|t|} H_{H_0}^{(i)}(t)$ . In the limit  $\lim_{\epsilon \rightarrow 0}$  the ground state transforms to  $|G\rangle_\epsilon = U_\epsilon(0, \infty) |G_0\rangle = e^{i\Phi} |G_0\rangle$  with  $e^{i\Phi} \langle G_0 | U_\epsilon(\infty, -\infty) | G_0 \rangle$ . Therefore the time-ordered Green's functions reads

$$G(x, t, x', t') = -i \frac{\langle G_0 | T(\psi_{H_0}(x, t) \psi_{H_0}^\dagger(x', t') U(\infty, -\infty)) | G_0 \rangle}{\langle G_0 | U_\epsilon(\infty, -\infty) | G_0 \rangle} .$$

### Approach of a Closed Time Contour

Another way is to calculate on a closed time contour. We perform again the unitary transformations of an operator between the Heisenberg picture with respect to  $H$  and the Heisenberg picture with respect to  $H_0$  with the equations

$$O_H(t) = V^\dagger(t, t_0) O_{H_0}(t) V(t, t_0) \text{ with } V(t, t_0) = T e^{-i \int_{t_0}^t d\bar{t} H_i(\bar{t})} \quad (2.22)$$

$$\text{and } H_{H_0}^i(t) = U_{H_0}^\dagger(t, t_0) H_i U_{H_0}(t, t_0) \text{ with } U_{H_0}(t, t_0) = e^{-iH_0(t-t_0)} .$$

If we compare this transformation with those from the Schrödinger picture

$$O_H(t) = U_H^\dagger(t, t_0) U_{H_0}(t, t_0) O_{H_0}(t) U_{H_0}^\dagger(t, t_0) U_H(t, t_0) \text{ with } U_H(t, t_0) = T e^{-i \int_{t_0}^t d\bar{t} H(\bar{t})}$$

we can identify the equality

$$V(t, t_0) = U_{H_0}^\dagger(t, t_0) U_H(t, t_0) \text{ which reads in detail } T e^{-i \int_{t_0}^t d\bar{t} H_{H_0}^i(\bar{t})} = e^{iH_0(t-t_0)} T e^{-i \int_{t_0}^t d\bar{t} H(\bar{t})} .$$

Now we introduce a closed time path which is called contour  $c_t$ . It starts at  $t_0$ , pass along the real-time axis to time  $t$  and then back to  $t_0$ . The new contour ordering operator  $T_{c_t}$  orders products of operators according to their time argument on the closed contour, whereby operators with greater time arguments, which means later on the contour, are placed to the left. To show an equivalence between the transformation of operators with real time arguments and contour times we show that the transformation between the Heisenberg pictures with respect to  $H$  and  $H_0$  can also be expressed through a transformation on the closed contour

$$O_H(t) = T_{c_t} e^{-i \int_{c_t} d\tau H_{H_0}^i(\tau)} O_{H_0}(t) . \quad (2.23)$$

To show the equivalence one expands the exponential function as a sum

$$O_H(t) = \sum_{n=0}^{\infty} \frac{(-i)^n}{n!} \int_{c_t} d\tau_1 \cdots \int_{c_t} d\tau_n T_{c_t} ,$$

splits the contour into a forward and a backward part  $c_t = \overrightarrow{c} + \overleftarrow{c}$ , expands and summarizes the terms in a new way and obtain

$$T_{c_t} e^{-i \int_{c_t} d\tau H_{H_0}^i(\tau)} O_{H_0}(t) = T_{\overleftarrow{c}} e^{-i \int_{\overleftarrow{c}} d\tau H_{H_0}^i(\tau)} O_{H_0}(t) T_{\overrightarrow{c}} e^{-i \int_{\overrightarrow{c}} d\tau H_{H_0}^i(\tau)} . \quad (2.24)$$

Now we parametrize the contour according  $\tau(t') = t'$  with  $t' \in [t_0, t]$  and connect the contour times with real times. When we consider the expressions of Eq.(2.24) with the parametrized times and compare it to Eq.(2.22) we can identify  $V(t, t_0)$ .

$$T_{\overleftarrow{c}} e^{-i \int_{\overleftarrow{c}} d\tau H_{H_0}^i(\tau)} = T e^{-i \int_{t_0}^t dt' H_{H_0}^i(t')} = V(t, t_0) \quad T_{\overrightarrow{c}} e^{-i \int_{\overrightarrow{c}} d\tau H_{H_0}^i(\tau)} = T e^{i \int_{t_0}^t dt' H_{H_0}^i(t')} = V^\dagger(t, t_0) . \quad (2.25)$$

The contour ordering operator corresponds to the normal time ordering,  $T_{\overrightarrow{c}} = T$ , and the anti-time-ordering to  $T_{\overleftarrow{c}} = \tilde{T}$ . Due to the equivalences in Eq.(2.25) one can conclude that the times in  $V(t, t_0)$  corresponds to the contour times on the forward part  $\overrightarrow{c}$  and  $V^\dagger(t, t_0)$  corresponds to contour times on the backward part  $\overleftarrow{c}$ .

### Green's Functions on a Closed Time Path

Now we use Eq.(2.23) to transform the field operators in the time-ordered Green's functions and therefore develop the contour-ordered Green's functions. The one-particle Green's function contains two field operators with two different real-time arguments  $t_1$  and  $t_{1'}$ . Again we resort to the closed time contour which starts at  $t_0$  pass along the real time axis, now through  $t_1$  and  $t_{1'}$ , then to time  $t$  and back to  $t_0$ . Since we have between  $t_0$  and  $t$  on the real time axis the two time arguments  $t_1$  and  $t_{1'}$ , each of them has two possibilities to be placed on the contour. We name the corresponding contour times  $\tau_1$  and  $\tau_{1'}$  and regard a Green's function which has its time arguments on the contour and is therefore called contour-ordered Green's function

$$G(x_1, \tau_1, x_{1'}, \tau_{1'}) = -i \frac{\text{Tr}(e^{-H/kT} T_c(\psi_H(x_1, \tau_1) \psi_H^\dagger(x_{1'}, \tau_{1'})))}{\text{Tr}(e^{-H/kT})} .$$



The contour ordering symbol orders, as said before, the field operators according to their contour time argument. Therefore we can also introduce a greater and lesser contour-ordered Green's function, whereby we used the abbreviation  $1 = x_1, \tau_1$  and  $1' = x_{1'}, \tau_{1'}$ .

$$G(1, 1') = -i \langle T_c(\psi(x_1, \tau_1)\psi^\dagger(x_{1'}, \tau_{1'})) \rangle = \begin{cases} -i \langle \psi(x_1, \tau_1)\psi^\dagger(x_{1'}, \tau_{1'}) \rangle = G^>(1, 1') & \tau_1 \stackrel{c}{>} \tau_{1'} \\ \pm i \langle \psi^\dagger(x_{1'}, \tau_{1'})\psi(x_1, \tau_1) \rangle = G^<(1, 1') & \tau_{1'} \stackrel{c}{<} \tau_1 \end{cases}$$

We apply the transformation of Eq.(2.23) to the field operators in the contour-ordered Green's function and transform them from the Heisenberg picture with respect to  $H$  to the Heisenberg picture with respect to  $H_0$ . To use the same procedure we expand the contour in such a way, that both of the two time arguments  $\tau_1$  and  $\tau_{1'}$  lay on a turning point of the contour. This can be done by introducing a contour that goes from  $t_0$  to  $\min(t_1, t_{1'})$  and back to  $t_0$  and then again from  $t_0$  to  $\max(t_1, t_{1'})$  and back to  $t_0$ . Therefore we included a closed contour part from  $t_0$  to  $\min(t_1, t_{1'})$  and back to  $t_0$ , that is equal to  $U^\dagger(\min(t_1, t_{1'}), t_0)U(\min(t_1, t_{1'}), t_0)=1$ . The complete contour is the sum of the minimal and maximal contour  $c = c_{min} + c_{max}$  and the contour-ordered Green's function becomes

$$G(1, 1') = -i \left\langle T_c \left( \psi_H(1)\psi_H^\dagger(1') \right) \right\rangle = -i \left\langle T_c \left( e^{-i \int_c d\tau H_{H_0}^i(\tau)} \psi_{H_0}(1)\psi_{H_0}^\dagger(1') \right) \right\rangle .$$

As an additional property one can include the closed contour part equal to  $U^\dagger(\max(t_1, t_{1'}), \infty)U(\max(t_1, t_{1'}), \infty)=1$  and expand the contour to infinity.

### Non-equilibrium Perturbation Theory of the Keldysh Green's Functions

Now we are able to develop the perturbation theory for the contour-ordered Green's functions. We transform the field operators in the interaction picture, using the transformation of Eq.(2.23) and obtain with  $\beta = 1/kT$

$$G(1, 1') = -i \frac{\text{Tr} \left( e^{-\beta H} T_c \left( e^{-i \int_c d\tau (H_{H_0}^{(i)}(\tau))} \psi_{H_0}(1)\psi_{H_0}^\dagger(1') \right) \right)}{\text{Tr}(e^{-\beta H})} . \quad (2.26)$$

To obtain an expression that is completely in the interaction picture we have to transform the statistical operator  $\rho$  as well. To make it work we need an imaginary time-evolution operator and therefore the contour has to be extended into to complex time plane from  $t_0$  to  $t_0 - i\beta$  [5] that we denote as  $c_a$ ,

$$e^{-\beta H} = e^{-\beta H_0} T_{c_a} e^{-i \int_{c_a} d\tau H_{H_0}^{(i)}(\tau)} . \quad (2.27)$$

We insert the transformation of Eq.(2.27) in the contour-ordered Green's function (2.26). In addition we insert the identity operator in terms of the closed contour contribution  $T_c(e^{-i \int_c d\tau (H_{H_0}^{(i)}(\tau))}) = 1$  in the denominator. The integration over the whole contour leads to the identity operator because no operators interrupts it[3]. We obtain

$$G(1, 1') = -i \frac{\text{Tr} \left( e^{-\beta H_0} \left( T_{c_a} e^{-i \int_{c_a} d\tau H_{H_0}^{(i)}(\tau)} \right) T_c \left( e^{-i \int_c d\tau H_{H_0}^{(i)}(\tau)} \psi_{H_0}(1)\psi_{H_0}^\dagger(1') \right) \right)}{\text{Tr} \left( e^{-\beta H_0} T_{c_a} e^{-i \int_{c_a} d\tau H_{H_0}^{(i)}(\tau)} T_c \left( e^{-i \int_c d\tau H_{H_0}^{(i)}(\tau)} \right) \right)} . \quad (2.28)$$

To simplify Eq.(2.28) we introduce the contour  $c_i = c+c_a$ , that consists of the general closed time contour and the additional part in the imaginary time plane and summarize the exponential functions. Since we don't consider transient phenomena we set  $t_0$  in the far past to minus infinity  $t_0 = -\infty$ . In this case we can neglect the imaginary contour part  $c_a$  compared with  $c$  and obtain the final expression

$$G(1, 1') = -i \frac{\text{Tr} \left( \rho_0 T_c \left( e^{-i \int_c d\tau H_{H_0}^{(i)}(\tau)} \psi_{H_0}(1) \psi_{H_0}^\dagger(1') \right) \right)}{\text{Tr} \left( T_c \left( e^{-i \int_c d\tau H_{H_0}^{(i)}(\tau)} \right) \right)} \quad (2.29)$$

with

$$\rho_0 = \frac{e^{-H_0/kT}}{\text{Tr} (e^{-H_0/kT})} .$$

### Wick's Theorem

If we expand the exponential function for the perturbative expansion we obtain products of the interaction Hamiltonian. Since the interaction Hamiltonian also contains field operators this leads to products of fermionic or bosonic field operators. The trace over the bosonic and fermionic operators can be separated since they are independent. To calculate the average of a long chain of field operators we use Wick's theorem, which enables to decompose a contour-ordered string of creation and annihilation operators, derived from a quadratic Hamiltonian, into a sum over all possible pairwise products

$$\langle T_C (c(\tau_n) c(\tau_{n-1}) \dots c(\tau_2) c(\tau_1)) \rangle = \sum_{a.p.p.} \prod q, q' \langle T_{c_t} (c_q(\tau) c_{q'}(\tau')) \rangle .$$

We sum over all possible ways of picking pairs (a.p.p.) of the n operators and don't take into account the ordering within a pair[3]. The coefficients "c" represent either a creation or an annihilation operator, whereby the index "q" denotes the state of the particle.

With the bosonic field operators  $\phi$  and the fermionic field operators  $\psi$  we can specify Wick's theorem for the case of a fermionic or bosonic chain of operators.

#### Wick's theorem for bosonic operators:

$$\begin{aligned} & \langle T_C (\phi(x_{2n}, \tau_{2n}) \phi(x_{2n-1}, \tau_{2n-1}) \dots \phi(x_2, \tau_2) \phi(x_1, \tau_1)) \rangle \\ &= \sum_{a.p.p.} \prod_{i \neq j} \langle T_C (\phi(x_i, \tau_i) \phi(x_j, \tau_j)) \rangle = \sum_{a.p.p.} \prod_{i \neq j} i^N D_0(x_i, \tau_i; x_j, \tau_j) \end{aligned}$$

#### Wick's theorem for fermionic operators:

$$\begin{aligned} & \langle T_C (\psi(x_{2n}, \tau_{2n}) \psi(x_{2n-1}, \tau_{2n-1}) \dots \psi(x_2, \tau_2) \psi(x_1, \tau_1)) \rangle \\ &= \sum_{a.p.p.} \prod_{i \neq j} (-1)^{\zeta_P} \langle T_C (\psi(x_i, \tau_i) \psi(x_j, \tau_j)) \rangle = \sum_{a.p.p.} \prod_{i \neq j} (-1)^{\zeta_P} i^N G_0(x_i, \tau_i; x_j, \tau_j) \end{aligned}$$

In both cases the last step is only valid if one operator is a creation operator and the other an annihilation operator. If the expression contains an odd number of creation or annihilation operators it is zero since the number of particles is not conserved.  $(-1)^{\zeta_P}$  denotes the number of transpositions of operators, since each change of two fermionic operators add a factor of  $-1$ . The denominator of Eq.(2.29) is important since it cancels all disconnected diagrams that appear due to the perturbative expansion and Wick's theorem.

## 2.3 Keldysh Green's Functions of Double-Dot Aharonov-Bohm Interferometer

So far we have introduced the time dependent Green's functions and defined the statistical operator  $\rho$ . We considered the case of an Hamiltonian containing a noninteracting and an interacting. To develop the perturbation theory of the Green's functions we have transformed the field operators to the interaction picture and replaced their real time arguments with contour times. The perturbative expansion turned out to be an expansion of an exponential function, containing an integration of the interaction and perturbation Hamiltonian over the Keldysh contour. The emerging average of a chain of field operators can be calculated by Wick's theorem with a multiplication of unperturbed Green's functions.

The time arguments of these Green's functions lay on the Keldysh contour. There are four possibilities to distribute the two arguments on the two branches. This leads in principle to four different Green's functions that are analogue to the (real-) time-ordered Green's functions of Eq.(2.18).

We denote the upper branch with  $+$  and the lower one with  $-$  and introduce the matrix Green's function  $\hat{G}_{ij}$  whereby the index  $ij$  refers to the dots 1 and 2 and the leads R and L.

The matrix Green's function is defined as [3]

$$\hat{G}_{ij} = \begin{pmatrix} G_{ij}^{++} & G_{ij}^{+-} \\ G_{ij}^{-+} & G_{ij}^{--} \end{pmatrix} \quad (2.30)$$

with

$$G_{ij}^{++} = \langle T_c(c_i(t)c_j^\dagger(t')) \rangle \quad G_{ij}^{+-} = \langle c_i(t)c_j^\dagger(t') \rangle \quad (2.31)$$

$$G_{ij}^{-+} = \langle \tilde{T}_c(c_i(t)c_j^\dagger(t')) \rangle \quad G_{ij}^{--} = \langle c_j^\dagger(t')c_i(t) \rangle. \quad (2.32)$$

### 2.3.1 Unperturbed Greater and Lesser Green's Functions

Since we will need the Keldysh Green's functions of Eq.(2.30) to calculate the covariance we determine them explicitly for the case of the parallel quantum dot coupled to the two leads.

First we calculated the unperturbed greater and lesser Green's functions  $g^{-+,+-}(E)$  based on the unperturbed retarded and advanced Green's function  $g^{r,a}(E)$  of Eq.(2.3) [4]. To calculate this dependency we consider a general noninteracting system in equilibrium, described by an

unperturbed Hamiltonian  $H_0$ . The equilibrium Green's functions depend only on a time difference. We consider the lesser Green's function which is relation to the electron distribution in equilibrium. The lesser Green's function reads

$$G_{ij}^{+-}(t-t') = i \langle c_j^\dagger(t') c_i(t) \rangle .$$

For  $t = t' = 0$  and  $i = j$  we can identify the electron distribution and we consider the Fourier transformation of  $G_{ij}^{+-}(t-t')$  at  $t = t'$ .

$$G_{ii}^{+-}(0) = i \langle c_i^\dagger(0) c_i(0) \rangle = i \langle n_i \rangle = \int \frac{dE}{2\pi} G_{ii}^{+-}(E)$$

The electron number  $\langle n_i \rangle$  is the sum over the occupation probabilities of all electrons which is the multiplication of the local density of states  $\rho_i(E)$  and the Fermi function  $f(E)$ [10]. If we replace  $\langle n_i \rangle$  with this integral representation we can identify the energy-depended lesser function  $G_{ii}^{+-}(E)$ ,

$$G_{ii}^{+-}(0) = i \langle n_i \rangle = i \int \rho_i(E) f(E) dE \quad \rightarrow \quad G_{ii}^{+-}(E) = 2\pi i \rho_i(E) f(E) .$$

We determine the greater function in an analogue way.

$$\begin{aligned} G_{ii}^{-+}(0) &= -i \langle c_i c_i^\dagger \rangle = -i \langle 1 - c_i^\dagger c_i \rangle = -i \langle 1 - n_i \rangle = -i (1 - \langle n_i \rangle) \\ &= -i \left( \int \rho_i(E) dE - \int \rho_i(E) f(E) dE \right) = \int \frac{dE}{2\pi} G_{ii}^{-+}(E) \\ G_{ii}^{-+}(E) &= -2\pi i \rho_i(E) (1 - f(E)) \end{aligned}$$

With an additional, general known relation between the Green's functions, that we will not derive here, we have three different relations for the equilibrium Green's functions:

$$G^a(E) - G^r(E) = G^{+-}(E) - G^{-+}(E) \tag{2.33}$$

$$G^{+-} = 2\pi i \rho_i(E) f(E) \quad \propto f(E) \tag{2.34}$$

$$G^{-+} = -2\pi i \rho_i(E) (1 - f(E)) \propto 1 - f(E) \tag{2.35}$$

We insert Eq.(2.34) and (2.35) in the right side of Eq.(2.33). Then we multiply each side either with the Fermi function  $f(E)$  and identify  $G^{+-}(E)$  or with  $1 - f(E)$  and identify  $G^{-+}(E)$ .

$$\begin{aligned} G^a - G^r &= G^{+-} - G^{-+} = 2\pi i \rho_i \\ (G^a - G^r) f &= 2\pi i \rho_i f = G^{+-} \\ (G^a - G^r) (1 - f) &= 2\pi i \rho_i (1 - f) = G^{-+} \end{aligned}$$

So we can express the lesser and greater Green's functions in equilibrium with the retarded and advanced Green's functions.

$$\begin{aligned} G^{+-}(E) &= [G^a(E) - G^r(E)] f(E) \\ G^{-+}(E) &= - [G^a(E) - G^r(E)] [1 - f(E)] \end{aligned}$$

The unperturbed system is defined in such a way that we don't have interactions. The unperturbed greater and lesser functions can therefore be derived from the greater and lesser Green's functions in equilibrium.

$$\begin{aligned} g_{ij}^{+-}(E) &= [g_{ij}^a(E) - g_{ij}^r(E)] f(E) \\ g_{ij}^{-+}(E) &= - [g_{ij}^a(E) - g_{ij}^r(E)] [1 - f(E)] \end{aligned}$$

### Unperturbed Greater and Lesser Green's Function of the Leads

To determine the unperturbed Green's functions of the leads we investigate what happens to the Fermi functions. We apply a bias voltage across the system such that the chemical potential of the leads differ about  $\mu_L - \mu_R = eV$ . We treated the dot-lead coupling as perturbation and include now the voltage in the unperturbed Hamiltonian by shifting the corresponding chemical potentials like

$$\mu_L = eV/2, \quad \mu_R = -eV/2$$

Due to this the shift of the chemical potential changes only the energy dependence of the unperturbed Green's functions.

The unperturbed Green's functions of the left lead read:

$$g_{LL}^{+-}(E - eV/2) = [g_{LL}^a(E - eV/2) - g_{LL}^r(E - eV/2)] f(E - eV/2) \quad (2.36)$$

$$g_{LL}^{-+}(E - eV/2) = - [g_{LL}^a(E - eV/2) - g_{LL}^r(E - eV/2)] [1 - f(E - eV/2)] \quad (2.37)$$

The unperturbed Green's functions of the right lead read:

$$g_{RR}^{+-}(E + eV/2) = [g_{RR}^a(E + eV/2) - g_{RR}^r(E + eV/2)] f(E + eV/2) \quad (2.38)$$

$$g_{RR}^{-+}(E + eV/2) = - [g_{RR}^a(E + eV/2) - g_{RR}^r(E + eV/2)] [1 - f(E + eV/2)] \quad (2.39)$$

We still use the wide-band approximation for the leads. Therefore the different energy dependences of  $g_{LL}^{a,r}$  and  $g_{RR}^{a,r}$  do not disturb. We shorten the notation with  $f_R = f(E + eV/2)$  and  $f_L = f(E - eV/2)$ .

The density of states of a quantum dot with energy level  $\varepsilon_i$  reads

$$\rho_i(E) = \delta(E - \varepsilon_i) . \quad (2.40)$$

We will see later that this fact will simplify the calculation of the full greater and lesser Green's functions and it's not necessary to determine the unperturbed ones individual.

### 2.3.2 Dyson Equation and Full Green's Functions

If we summarize all terms of the perturbative expansion of a Green's function we can also verify a Dyson equation for the Keldysh Green's functions [3]. The Dyson equation of the contour ordered Green's functions reads for each component

$$\hat{G}_{ij} = \hat{g}_{ij} + \sum_{lm} \hat{g}_{il} \hat{\Sigma}_{lm} \hat{G}_{mj} .$$

To determine the lesser and greater function we use the Langreth theroem[2].

$$\begin{aligned} G^{+-} &= g^{+-} + \left( \hat{g} \hat{\Sigma} \hat{G} \right)^{+-} \\ &= g^{+-} + g^r \Sigma^r G^{+-} + g^r \Sigma^{+-} G^a + g^{+-} \Sigma^a G^a \end{aligned} \quad (2.41)$$

$$G^{-+} = g^{-+} + g^r \Sigma^r G^{-+} + g^r \Sigma^{-+} G^a + g^{-+} \Sigma^a G^a \quad (2.42)$$

We transform Eq.(2.41).

$$\begin{aligned} (1 - g^r \Sigma^r) G^{+-} &= g^{+-} (1 + \Sigma^a G^a) + g^r \Sigma^{+-} G^a \\ G^{+-} &= g^{+-} (1 + \Sigma^a G^a) (1 - g^r \Sigma^r)^{-1} + g^r \Sigma^{+-} G^a (1 - g^r \Sigma^r)^{-1} \\ &= g^{+-} (g^r g^a)^{-1} G^r G^a + G^r \Sigma^{+-} G^a \end{aligned} \quad (2.43)$$

Since  $g^{r,a,+}$  is diagonal, the multiplication of the three unperturbed Green's functions is also a diagonal matrix. Therefore the first part of Eq.(2.43) vanishes for off-diagonal elements  $G_{ij}^{+-}$  with  $i \neq j$ . To determine the diagonal elements  $G_{ii}^{+-}$  with  $i = 1, 2, L, R$ , we consider the Green's functions of the dots and leads separately.

In the case of the dots the product  $g_i^{+-} (g_i^r g_i^a)^{-1}$  with  $i=1,2$  vanish. This is due to the fact that, according to Eq.(2.3) , the inverse of the retarded and advanced Green's functions are proportional to  $E - \varepsilon_i$ . According to Eq.(2.40) the unperturbed lesser Green's function is proportional to  $\delta(E - \varepsilon_i)$ . The product of the three unperturbed Green's functions is therefore

$$g_i^{+-} (g_i^r g_i^a)^{-1} \propto \delta(E - \varepsilon_i) (E - \varepsilon_i)^2 = 0$$

and therefore the first part of Eq.(2.43) also vanish. The same arguments hold for  $G^{-+}$ .

For the Green's functions of the leads  $G_{ii}^{+-}$  with  $i = L, R$ , one insert the expression of the unperturbed lesser function of Eq.(2.36) or (2.38) and notes the matrix multiplication of the first term. Since we will only need the greater and lesser Green's functions of the dots the one of the leads need not further be noted.

So the equation for the fermionic lesser Green's function of the dots reduces to

$$G_{ij}^{+-} = \sum_{l,m} G_{il}^r \Sigma_{lm}^{+-} G_{mj}^a , \quad (2.44)$$

with  $l, m = 1, 2, L, R$ . The retarded and advanced Green's functions have been determined in Eq.(2.14) to (2.17). In order to avoid far too complicated calculations we limit the calculation to the case of symmetric energy levels of the dots  $\varepsilon_1 = \varepsilon_2 = \varepsilon$ . The retarded and advanced fermionic Green's functions of Eq.(2.14) to (2.17) then become

$$G^{r,a} = \frac{1}{(E - \varepsilon \pm i\Gamma)^2 + \Gamma^2 \cos^2 \frac{\varphi}{2}} \begin{pmatrix} E - \varepsilon \pm i\Gamma & \mp i\Gamma \cos \frac{\varphi}{2} \\ \mp i\Gamma \cos \frac{\varphi}{2} & E - \varepsilon \pm i\Gamma \end{pmatrix} . \quad (2.45)$$

The self-energy of the system consists only of the tunneling self energy. The lesser self energy is determined by the equation [2]

$$\Sigma_{lm}^{+-} = \sum_{k\alpha=L,R} V_{k\alpha,l}^* g_{k\alpha}^{+-} V_{k\alpha,m} . \quad (2.46)$$

$V_{k\alpha,l} = t_{k\alpha,l}$  describes the coupling of the leads and the dots. Therefore  $V_{k\alpha,l} = 0$  if  $k\alpha = l = L, R$  because there is no interaction inside or via the leads. Due to this eq (2.44) of  $G_{ij}^{+-}$  reduces to a sum over  $l, m = 1, 2$ . The elements of the lead-dot coupling in the system of the two parallel quantum dots are

$$V_{L1} = V_{R2} = V_{L2}^* = V_{R1}^* = te^{i\frac{\varphi}{4}} \text{ and } V_{L1}^* = V_{R2}^* = V_{L2} = V_{R1} = te^{-i\frac{\varphi}{4}} .$$

Using these and Eq.(2.36) and (2.38) for the unperturbed lesser Green's functions, Eq.(2.46) results in the lesser self energy. The greater self energy can be easily obtained by changing  $+-$  with  $-+$ .

$$\begin{aligned} \Sigma^{+-} &= i\Gamma \begin{pmatrix} f_L + f_R & e^{-i\frac{\varphi}{2}} f_L + e^{i\frac{\varphi}{2}} f_R \\ e^{i\frac{\varphi}{2}} f_L + e^{-i\frac{\varphi}{2}} f_R & f_L + f_R \end{pmatrix} \\ \Sigma^{-+} &= i\Gamma \begin{pmatrix} f_L + f_R - 2 & e^{-i\frac{\varphi}{2}} f_L + e^{i\frac{\varphi}{2}} f_R - 2 \cos \frac{\varphi}{2} \\ e^{i\frac{\varphi}{2}} f_L + e^{-i\frac{\varphi}{2}} f_R - 2 \cos \frac{\varphi}{2} & f_L + f_R - 2 \end{pmatrix} \end{aligned}$$

Now we are able to calculate the lesser and greater Green's function. For the greater Green's function one just has to exchange the lesser self-energy with the greater self-energy. We name the common denominator of  $G^a \times G^r$

$$|\kappa|^2 := \left( (E - \varepsilon)^2 + \Gamma^2 \left( 1 + \cos^2 \frac{\varphi}{2} \right) \right)^2 - 4\Gamma^4 \cos^2 \frac{\varphi}{2} .$$

### Lesser Green's Function

$$\begin{aligned} G_{11}^{+-} &= \frac{i\Gamma}{|\kappa|^2} \left[ \left( (E - \varepsilon)^2 + \Gamma^2 \left( 1 - \cos^2 \frac{\varphi}{2} \right) \right) (f_L + f_R) + \Gamma(E - \varepsilon) \sin \varphi (f_L - f_R) \right] \\ G_{12}^{+-} &= \frac{i\Gamma}{|\kappa|^2} \left[ (E - \varepsilon)^2 \left( e^{-i\frac{\varphi}{2}} f_L + e^{i\frac{\varphi}{2}} f_R \right) - \Gamma^2 \sin^2 \frac{\varphi}{2} (f_L e^{i\frac{\varphi}{2}} + f_R e^{-i\frac{\varphi}{2}}) \right] \\ G_{21}^{+-} &= \frac{i\Gamma}{|\kappa|^2} \left[ (E - \varepsilon)^2 \left( e^{i\frac{\varphi}{2}} f_L + e^{-i\frac{\varphi}{2}} f_R \right) - \Gamma^2 \sin^2 \frac{\varphi}{2} (f_L e^{-i\frac{\varphi}{2}} + f_R e^{i\frac{\varphi}{2}}) \right] \\ G_{22}^{+-} &= \frac{i\Gamma}{|\kappa|^2} \left[ \left( (E - \varepsilon)^2 + \Gamma^2 \left( 1 - \cos^2 \frac{\varphi}{2} \right) \right) (f_L + f_R) - \Gamma(E - \varepsilon) \sin \varphi (f_L - f_R) \right] \end{aligned}$$

### Greater Green's Function

$$\begin{aligned}
 G_{11}^{-+} &= \frac{i\Gamma}{|\kappa|^2} \left[ \left( (E - \varepsilon)^2 + \Gamma^2 \left( 1 - \cos^2 \frac{\varphi}{2} \right) \right) (f_L + f_R - 2) + \Gamma(E - \varepsilon) \sin \varphi (f_L - f_R) \right] \\
 G_{12}^{-+} &= \frac{i\Gamma}{|\kappa|^2} \left[ (E - \varepsilon)^2 \left( e^{-i\frac{\varphi}{2}} f_L + e^{i\frac{\varphi}{2}} f_R - 2 \cos \frac{\varphi}{2} \right) - \Gamma^2 \sin^2 \frac{\varphi}{2} \left( f_L e^{i\frac{\varphi}{2}} + f_R e^{-i\frac{\varphi}{2}} - 2 \cos \frac{\varphi}{2} \right) \right] \\
 G_{21}^{-+} &= \frac{i\Gamma}{|\kappa|^2} \left[ (E - \varepsilon)^2 \left( e^{i\frac{\varphi}{2}} f_L + e^{-i\frac{\varphi}{2}} f_R - 2 \cos \frac{\varphi}{2} \right) - \Gamma^2 \sin^2 \frac{\varphi}{2} \left( f_L e^{-i\frac{\varphi}{2}} + f_R e^{i\frac{\varphi}{2}} - 2 \cos \frac{\varphi}{2} \right) \right] \\
 G_{22}^{-+} &= \frac{i\Gamma}{|\kappa|^2} \left[ \left( (E - \varepsilon)^2 + \Gamma^2 \left( 1 - \cos^2 \frac{\varphi}{2} \right) \right) (f_L + f_R - 2) - \Gamma(E - \varepsilon) \sin \varphi (f_L - f_R) \right]
 \end{aligned}$$

### Time-Ordered Green's Function

The time-ordered Green's function can be calculated with  $G^{++} = G^{+-} + G^r$ .

$$\begin{aligned}
 G_{11}^{++} &= \frac{i\Gamma}{|\kappa|^2} \left[ \left( (E - \varepsilon)^2 + \Gamma^2 \left( 1 - \cos^2 \frac{\varphi}{2} \right) \right) (f_L + f_R - 1) + \Gamma(E - \varepsilon) \sin \varphi (f_L - f_R) \right. \\
 &\quad \left. + (E - \varepsilon) \left( \Gamma^2 \left( 1 + \cos^2 \frac{\varphi}{2} \right) + (E - \varepsilon)^2 \right) \right] \\
 G_{12}^{++} &= \frac{i\Gamma}{|\kappa|^2} \left[ (E - \varepsilon)^2 \left( e^{-i\frac{\varphi}{2}} f_L + e^{i\frac{\varphi}{2}} f_R \right) - \Gamma^2 \sin^2 \frac{\varphi}{2} (f_L e^{i\frac{\varphi}{2}} + f_R e^{-i\frac{\varphi}{2}}) \right. \\
 &\quad \left. - \cos \frac{\varphi}{2} \left[ (E - \varepsilon - i\Gamma)^2 + \Gamma^2 \cos^2 \frac{\varphi}{2} \right] \right] \\
 G_{21}^{++} &= \frac{i\Gamma}{|\kappa|^2} \left[ (E - \varepsilon)^2 \left( e^{i\frac{\varphi}{2}} f_L + e^{-i\frac{\varphi}{2}} f_R \right) - \Gamma^2 \sin^2 \frac{\varphi}{2} (f_L e^{-i\frac{\varphi}{2}} + f_R e^{i\frac{\varphi}{2}}) \right. \\
 &\quad \left. - \cos \frac{\varphi}{2} \left[ (E - \varepsilon - i\Gamma)^2 + \Gamma^2 \cos^2 \frac{\varphi}{2} \right] \right] \\
 G_{22}^{++} &= \frac{i\Gamma}{|\kappa|^2} \left[ \left( (E - \varepsilon)^2 + \Gamma^2 \left( 1 - \cos^2 \frac{\varphi}{2} \right) \right) (f_L + f_R - 1) - \Gamma(E - \varepsilon) \sin \varphi (f_L - f_R) \right. \\
 &\quad \left. + (E - \varepsilon) \left( \Gamma^2 \left( 1 + \cos^2 \frac{\varphi}{2} \right) + (E - \varepsilon)^2 \right) \right]
 \end{aligned}$$

### Anti-Time-Ordered Green's Function

The anti-time-ordered Green's function can be calculated with  $G^{--} = G^{+-} - G^a$ .

$$\begin{aligned}
 G_{11}^{--} &= \frac{i\Gamma}{|\kappa|^2} \left[ \left( (E - \varepsilon)^2 + \Gamma^2 \left( 1 - \cos^2 \frac{\varphi}{2} \right) \right) (f_L + f_R - 1) + \Gamma(E - \varepsilon) \sin \varphi (f_L - f_R) \right. \\
 &\quad \left. - (E - \varepsilon) \left( \Gamma^2 \left( 1 + \cos^2 \frac{\varphi}{2} \right) + (E - \varepsilon)^2 \right) \right]
 \end{aligned}$$



$$\begin{aligned}
 G_{12}^{--} &= \frac{i\Gamma}{|\kappa|^2} \left[ (E - \varepsilon)^2 \left( e^{-i\frac{\varphi}{2}} f_L + e^{i\frac{\varphi}{2}} f_R \right) - \Gamma^2 \sin^2 \frac{\varphi}{2} (f_L e^{i\frac{\varphi}{2}} + f_R e^{-i\frac{\varphi}{2}}) \right. \\
 &\quad \left. - \cos \frac{\varphi}{2} \left[ (E - \varepsilon + i\Gamma)^2 + \Gamma^2 \cos^2 \frac{\varphi}{2} \right] \right] \\
 G_{21}^{--} &= \frac{i\Gamma}{|\kappa|^2} \left[ (E - \varepsilon)^2 \left( e^{i\frac{\varphi}{2}} f_L + e^{-i\frac{\varphi}{2}} f_R \right) - \Gamma^2 \sin^2 \frac{\varphi}{2} (f_L e^{-i\frac{\varphi}{2}} + f_R e^{i\frac{\varphi}{2}}) \right. \\
 &\quad \left. - \cos \frac{\varphi}{2} \left[ (E - \varepsilon + i\Gamma)^2 + \Gamma^2 \cos^2 \frac{\varphi}{2} \right] \right] \\
 G_{22}^{--} &= \frac{i\Gamma}{|\kappa|^2} \left[ \left( (E - \varepsilon)^2 + \Gamma^2 \left( 1 - \cos^2 \frac{\varphi}{2} \right) \right) (f_L + f_R - 1) - \Gamma(E - \varepsilon) \sin \varphi (f_L - f_R) \right. \\
 &\quad \left. - (E - \varepsilon) \left( \Gamma^2 \left( 1 + \cos^2 \frac{\varphi}{2} \right) + (E - \varepsilon)^2 \right) \right]
 \end{aligned}$$

### Keldysh Green's Function

To complete the contour-ordered Green's functions we calculate the Keldysh Green's function  $G^K = G^{+-} + G^{-+}$ .

$$\begin{aligned}
 G_{11}^K &= \frac{2i\Gamma}{|\kappa|^2} \left[ \left( (E - \varepsilon)^2 + \Gamma^2 \left( 1 - \cos^2 \frac{\varphi}{2} \right) \right) (f_L + f_R) + \Gamma(E - \varepsilon) \sin \varphi (f_L - f_R) \right] \\
 G_{12}^K &= \frac{2i\Gamma}{|\kappa|^2} \left[ (E - \varepsilon)^2 \left( e^{-i\frac{\varphi}{2}} f_L + e^{i\frac{\varphi}{2}} f_R - \cos \frac{\varphi}{2} \right) - \Gamma^2 \sin^2 \frac{\varphi}{2} \left( f_L e^{i\frac{\varphi}{2}} + f_R e^{-i\frac{\varphi}{2}} - \cos \frac{\varphi}{2} \right) \right] \\
 G_{21}^K &= \frac{2i\Gamma}{|\kappa|^2} \left[ (E - \varepsilon)^2 \left( e^{i\frac{\varphi}{2}} f_L + e^{-i\frac{\varphi}{2}} f_R - \cos \frac{\varphi}{2} \right) - \Gamma^2 \sin^2 \frac{\varphi}{2} \left( f_L e^{-i\frac{\varphi}{2}} + f_R e^{i\frac{\varphi}{2}} - \cos \frac{\varphi}{2} \right) \right] \\
 G_{22}^K &= \frac{2i\Gamma}{|\kappa|^2} \left[ \left( (E - \varepsilon)^2 + \Gamma^2 \left( 1 - \cos^2 \frac{\varphi}{2} \right) \right) (f_L + f_R) - \Gamma(E - \varepsilon) \sin \varphi (f_L - f_R) \right]
 \end{aligned}$$

## 2.4 Bosonic Green's Functions of a Single Microwave Cavity

For the calculation of the bosonic Green's functions we need the time evolution of the bosonic operators. The Hamiltonian for the noninteracting case of the bosonic resonator  $b$  is

$$H_0 = \hbar\omega_b b^\dagger b .$$

We insert the time-evolution of the annihilation operator in the Heisenberg picture in the equation of motion and determine the time depended creation and annihilation operators and continue again with  $\hbar = 1$ .

$$\begin{aligned}
 b(t) &= e^{iH_0 t} b e^{-iH_0 t} \\
 i\partial_t b(t) &= [b(t), H_0] = e^{iH_0 t} [b, H_0] e^{-iH_0 t} = e^{iH_0 t} \omega_b b e^{-iH_0 t} = \omega_b b(t) \\
 b(t) &= e^{-i\omega_b t} b, \quad b^\dagger(t) = e^{i\omega_b t} b^\dagger
 \end{aligned} \tag{2.47}$$

### Bosonic Green's Functions in Time Domain

Now it's easy to calculate the bosonic Green's functions in time domain. We insert the time depended bosonic operators of Eq.(2.47) in the formulas of the bosonic Green's functions which are equal to the fermionic one of Eq.(2.31) and (2.32) by replacing the fermionic with the bosonic operators.

$$\begin{aligned}
 D_b^{+-}(t, t') &= -i \langle b_t^\dagger b_{t'} \rangle_0 = -i e^{i(\omega_b t' - \omega_b t)} \langle b^\dagger b \rangle_0 = -i e^{-i\omega_b(t-t')} n_b \\
 D_b^{-+}(t, t') &= -i \langle b_t b_{t'}^\dagger \rangle_0 = -i e^{i(\omega_b t' - \omega_b t)} \langle b b^\dagger \rangle_0 = -i e^{-i\omega_b(t-t')} (n_b + 1) \\
 D_b^{++}(t, t') &= -i \langle T(b_{t'}^\dagger b_t) \rangle_0 = -\Theta(t-t') i \langle b_t b_{t'}^\dagger \rangle - \Theta(t'-t) i \langle b_{t'}^\dagger b_t \rangle \\
 &= \Theta(t-t') D_b^{-+}(t, t') + \Theta(t'-t) D_b^{+-}(t, t') \\
 D_b^{--}(t, t') &= -i \langle T(b_{t'} b_t) \rangle_0 = -\Theta(t'-t) i \langle b_t b_{t'}^\dagger \rangle - \Theta(t-t') i \langle b_{t'}^\dagger b_t \rangle \\
 &= \Theta(t'-t) D_b^{-+}(t, t') + \Theta(t-t') D_b^{+-}(t, t')
 \end{aligned}$$

### Bosonic Green's Functions in Energy Space

To obtain the bosonic Green's functions in energy space we calculate the Fourier transformations. For the greater and lesser Green's function it is easy to identify the delta function.

$$\begin{aligned}
 D_b^{+-}(E) &= -i n_b \int d(t-t') e^{i(t-t')(E-\omega_b)} = -i n_b \delta(E-\omega_b) \\
 D_b^{-+}(E) &= -i (n_b + 1) \int d(t-t') e^{i(t-t')(E-\omega_b)} = -i (n_b + 1) \delta(E-\omega_b)
 \end{aligned}$$

The time-ordered and anti-time-ordered Green's function contain Heaviside step functions that change the integration limits. Since the definite integrals would be divergent we introduce an infinitesimal imaginary part  $\pm i\eta$  to solve them. If we consider the limit of  $\eta \rightarrow 0$  after we did the integration we can identify a principle part and a delta function.

$$\begin{aligned}
 D_b^{++}(E) &= \int d(t-t') e^{i(t-t')E} \left[ -i\Theta(t-t') e^{-i\omega_b(t-t')} (n_b + 1) - i\Theta(t'-t) e^{-i\omega_b(t-t')} n_b \right] \\
 &= \lim_{\eta \rightarrow 0} \left[ -i \int_0^\infty d(t-t') e^{i(t-t')(E+i\eta-\omega_b)} (n_b + 1) + i \int_0^{-\infty} d(t-t') e^{i(t-t')(E-i\eta-\omega_b)} n_b \right] \\
 &= \lim_{\eta \rightarrow 0} \left[ \frac{E - \omega_b}{(E - \omega_b)^2 + \eta^2} - i \frac{\eta}{(E - \omega_b)^2 + \eta^2} (2n_b + 1) \right] \\
 &= P \left( \frac{1}{E - \omega_b} \right) - i\pi \delta(E - \omega_b) (2n_b + 1)
 \end{aligned}$$

$$\begin{aligned}
 D_b^{--}(E) &= \int d(t-t') e^{i(t-t')E} \left[ -i\Theta(t'-t) e^{-i\omega_b(t-t')} (n_b + 1) - i\Theta(t-t') e^{-i\omega_b(t-t')} n_b \right] \\
 &= \lim_{\eta \rightarrow 0} \left[ i \int_0^{-\infty} d(t-t') e^{i(t-t')(E-i\eta-\omega_b)} (n_b + 1) - i \int_0^{\infty} d(t-t') e^{i(t-t')(E+i\eta-\omega_b)} n_b \right] \\
 &= \lim_{\eta \rightarrow 0} \left[ -\frac{E - \omega_b}{(E - \omega_b)^2 + \eta^2} - i \frac{\eta}{(E - \omega_b)^2 + \eta^2} (2n_b + 1) \right] \\
 &= -P \left( \frac{1}{E - \omega_b} \right) - i\pi \delta(E - \omega_b) (2n_b + 1)
 \end{aligned}$$

### Bosonic Green's Funktion in Energy Space at T=0

Since we treat the system at T=0 the photon number  $n_b$  becomes zero. Therefore the bosonic Green's functions simplify again.

$$\begin{aligned}
 D_b^{++}(E) &= P \left( \frac{1}{E - \omega_b} \right) - i\pi \delta(E - \omega_b) & D_b^{+-}(E) &= 0 \\
 D_b^{--}(E) &= -P \left( \frac{1}{E - \omega_b} \right) - i\pi \delta(E - \omega_b) & D_b^{-+}(E) &= -i \delta(E - \omega_b)
 \end{aligned}$$

The bosonic Green's functions of resonator a can be simply obtained by replacing index  $b$  with  $a$ . If we assume a symmetric case with equal frequencies of the two resonators  $\omega_a = \omega_b = \omega$ , the bosonic Green's functions become equal for both resonators.

### 3 Diagrammatic Perturbative Expansion of the Covariance

To prove correlation between the mechanical oscillators we calculate the covariance  $C = \langle n_a n_b \rangle - \langle n_a \rangle \langle n_b \rangle$  using a perturbative expansion up to the fourth order of the dot-cavity coupling constant  $\lambda$ . As said before we consider the perturbation to be the dot-cavity coupling. We assume a symmetric dot-cavity coupling and so  $\lambda_a = \lambda_b = \lambda$ . Therefore the interaction Hamiltonian contained in the exponential function, that will be expanded, reads

$$H^{(i)} = \lambda(a + a^\dagger)d_1^\dagger d_1 + \lambda(b + b^\dagger)d_2^\dagger d_2 .$$

#### 3.1 Derivation of the Covariance From the Time-Ordered Expression

If the covariance is zero,  $n_a$  and  $n_b$  are uncorrelated. When the sign is positive, the variables are said to be positively correlated. When the sign is negative, the variables are said to be negatively correlated.

For the calculation of the covariance we want to make use of the perturbation theory. We have developed it for the contour-ordered Green's function. Now we show a way how to get from the full time-ordered expression to the covariance.

We first concentrate on  $\langle n_a n_b \rangle = \langle a_t^\dagger a_t b_t^\dagger b_t \rangle$  and define the function  $F$

$$F = -i \langle T_c (A_t A_{t'}^\dagger) \rangle$$

with the new operators  $A = ab = ba$  and  $A^\dagger = a^\dagger b^\dagger = b^\dagger a^\dagger$ . So we get

$$F = -i \langle T_c (A_t A_{t'}^\dagger) \rangle = -i \langle T_c (a_t b_t a_{t'}^\dagger b_{t'}^\dagger) \rangle = -i \langle T_c (a_t a_{t'}^\dagger b_t b_{t'}^\dagger) \rangle .$$

Depending on which branch the time arguments lie we obtain the four Keldysh components

$$F = \begin{pmatrix} F^{++} & F^{+-} \\ F^{-+} & F^{--} \end{pmatrix} .$$

Now we determine that  $t$  lies in the upper branch of the Keldysh contour and  $t'$  lies in the lower branch. The function  $F$  reduces to the lesser function

$$F^{+-}(t, t') = -i \langle A_{t'}^\dagger A_t \rangle = -i \langle a_{t'}^\dagger b_{t'}^\dagger a_t b_t \rangle .$$

Next we converge  $t'$  to  $t$ . Since  $a$  and  $b$  commute we obtain, after moving  $a_t$  a position forward, the expression

$$\lim_{t' \rightarrow t} iF^{+-}(t, t') = \langle a_t^\dagger b_t^\dagger a_t b_t \rangle = \langle a_t^\dagger a_t b_t^\dagger b_t \rangle = \langle n_a n_b \rangle .$$

The same applies for  $D_a(t, t') = -i \langle T_c (a_t a_{t'}^\dagger) \rangle$  and  $D_b(t, t') = -i \langle T_c (b_t b_{t'}^\dagger) \rangle$  for that follows

$$\lim_{t' \rightarrow t} iD_a^{+-}(t, t') = \langle a_t^\dagger a_t \rangle = \langle n_a \rangle ,$$

$$\lim_{t' \rightarrow t} i D_b^{+-}(t, t') = \langle b_t^\dagger b_t \rangle = \langle n_b \rangle .$$

Therefore we can express the covariance through on the full time-ordered Keldysh functions by

$$\lim_{t' \rightarrow t} i (F^{+-}(t, t') - D_a^{+-}(t, t') D_b^{+-}(t, t')) = \langle n_a n_b \rangle - \langle n_a \rangle \langle n_b \rangle$$

which is equal to

$$\lim_{t' \rightarrow t} i \left( \langle T_c (a_t a_{t'}^\dagger b_t b_{t'}^\dagger) \rangle^{+-} - \langle T_c (a_t a_{t'}^\dagger) \rangle^{+-} \langle T_c (b_t b_{t'}^\dagger) \rangle^{+-} \right) = \langle n_a n_b \rangle - \langle n_a \rangle \langle n_b \rangle . \quad (3.1)$$

## 3.2 Color Code and Legend of the Green's Functions and Feynman Diagrams

We have determined the free fermionic and free bosonic Green's functions in section (2.3.2) and (2.4) which will appear in the perturbative expansions as factors of longer products. Further we will represent the terms in Feynman diagrams. To distinguish the fermionic and bosonic Green's functions we use straight and wiggled lines. To facilitate and clarify the corresponding components of the Green's functions, in the bosonic case the belonging to the cavities a and b and in the fermionic case the components  $ij$  for  $i, j = 1, 2$ , we introduce a color code:

$D_a$ : bosonic Green's function of resonator a

$D_b$ : bosonic Green's function of resonator b


$G_{11}$ : fermionic Green's function of dot 1


$G_{22}$ : fermionic Green's function of dot 2

$G_{12}, G_{21}$ : offdiagonal elements of the fermionic Green's function corresponding to dot 1 and 2

The elements of the Feynman diagrams with the same color code like the functions are

 :  $G_{11}, G_{22}, G_{12}, G_{21}$

 :  $D_a = -i \langle T_c (a_t, a_{t'}^\dagger) \rangle, D_b = -i \langle T_c (b_t, b_{t'}^\dagger) \rangle$

 :  $\tilde{D}_a = -i \langle T_c ((a_t + a_t^\dagger)(a_{t'} + a_{t'}^\dagger)) \rangle, \tilde{D}_b = -i \langle T_c ((b_t + b_t^\dagger)(b_{t'} + b_{t'}^\dagger)) \rangle$

## 3.3 Perturbative Expansion of $\langle T_c (a_t a_{t'}^\dagger) \rangle$ and $\langle T_c (b_t b_{t'}^\dagger) \rangle$

First a comment to the notation: The free or unperturbed Green's function is generally denoted with the index "0" like  $G_0$ . For reasons of readability we neglect this index 0 and keep in mind, that the perturbative expansion and the use of Wick's theorem always leads to products of the free Green's functions.

First we are looking for the perturbative expansion of the time-ordered Green's functions of the single cavities

$$\langle T_c (a_t a_{t'}^\dagger) \rangle \text{ and } \langle T_c (b_t b_{t'}^\dagger) \rangle .$$

The first and third order term of the perturbative expansion become zero, because of the odd number of operators. We look at the perturbative expansion up to fourth order.

Notation: To use the lower index-position for the time arguments in the perturbative expansion we change the notation of the fermionic creation and annihilation operators. Dot 1 corresponds to  $d$  and  $d^\dagger$  and dot 2 corresponds to  $\tilde{d}$  and  $\tilde{d}^\dagger$ . In order to facilitate the reading, we denote the contour times with  $t_i$  instead of  $\tau_i$ . The interaction Hamiltonian becomes

$$H^{(i)} = \lambda(a + a^\dagger)d^\dagger d + \lambda(b + b^\dagger)\tilde{d}^\dagger \tilde{d}$$

and with  $\alpha = a, b$  we expand the functions

$$iD_\alpha(t, t') = \langle T_c (\alpha_t \alpha_{t'}^\dagger) \rangle = \text{Tr} \left( \rho_0 T_c \left( e^{-i \int_C d\tau H^{(i)}(\tau)} \alpha_t \alpha_{t'}^\dagger \right) \right) . \quad (3.2)$$

### Zeroth Order

The zeroth order is only the unperturbed or free Green's function

$$\langle T_c (a_t a_{t'}^\dagger) \rangle^{(0)} = \langle T_c (a_t a_{t'}^\dagger) \rangle = iD_a(t, t') .$$

### Second Order

The second order contains an integration over the two contour-time arguments  $t_1$  and  $t_2$ . The multiplication of the four terms in Eq.(3.3) reduces only to the one in Eq.(3.4), since the others would not conserve the particle number or lead to a disconnected diagram. In Eq.(3.5) we have separated the trace over the bosonic and fermionic operators. We apply Wick's theorem and neglected again terms representing disconnected diagrams or tadpoles (see chapter 3.5). The simplification of Wick's theorem results in Eq.(3.6) where we can identify the bosonic and fermionic Green's functions to obtain the final result in Eq.(3.7).

$$\langle T_c (a_t a_{t'}^\dagger) \rangle^{(2)} = \frac{(-i)^2}{2} \int_C dt_1 \int_C dt_2 \langle T_c (a_t a_{t'}^\dagger \left[ \lambda(a + a^\dagger)d^\dagger d + \lambda(b + b^\dagger)\tilde{d}^\dagger \tilde{d} \right]_{t_1} \left[ \lambda(a + a^\dagger)d^\dagger d + \lambda(b + b^\dagger)\tilde{d}^\dagger \tilde{d} \right]_{t_2} \rangle \quad (3.3)$$

$$= -\frac{1}{2} \int_C dt_1 \int_C dt_2 \langle T_c (a_t a_{t'}^\dagger \left[ \lambda(a_{t_1} + a_{t_1}^\dagger)d_{t_1}^\dagger d_{t_1} \right] \left[ \lambda(a_{t_2} + a_{t_2}^\dagger)d_{t_2}^\dagger d_{t_2} \right]) \rangle \quad (3.4)$$

$$= -\int_C dt_1 \int_C dt_2 \lambda^2 \langle T_c (a_t a_{t'}^\dagger a_{t_1} a_{t_2}^\dagger) \rangle \langle T_c (d_{t_1}^\dagger d_{t_1} d_{t_2}^\dagger d_{t_2}) \rangle \quad (3.5)$$

$$= - \int_C dt_1 \int_C dt_2 \lambda^2 \langle T_c (a_t a_{t_2}^\dagger) \rangle \langle T_c (a_{t_1} a_{t_1'}^\dagger) \rangle \langle T_c (d_{t_1}^\dagger d_{t_2}) \rangle \langle T_c (d_{t_2}^\dagger d_{t_1}) \rangle \quad (3.6)$$

$$= \int_C dt_1 \int_C dt_2 \lambda^2 D_a(t, t_2) D_a(t_1, t_1') G_{11}(t_1, t_2) G_{11}(t_2, t_1) \quad (3.7)$$

#### Fourth Order

Analogue to the second order, the fourth order term includes the integration over four contour-time arguments. In order to facilitate the reading we hide the factor of the perturbative expansion,  $\frac{1}{24} \int_C dt_1 \int_C dt_2 \int_C dt_3 \int_C dt_4 (-i)^4$ , and reintroduce it in the end.

The multiplication in Eq.(3.8) includes eight possibilities which conserve the particle number. Two terms contain only the operators  $a, a^\dagger$  or  $b, b^\dagger$ , except for the initial operators  $a_t, a_{t_1'}^\dagger$ , and six terms contain 2 operators of each type. The term containing only operators of resonator  $b$  leads to disconnected diagrams because there is no direct connection between the two resonators. Since the notation of integration variables, in this case the time arguments, can be changed the term containing only operators of resonator  $a$  leads to six contributions, Eq.(3.9). We obtain six contributions because Eq.(3.8) leads in this case to a multiplication of the four brackets containing operators  $a$ . An expansion of this leads to terms with different numbers of creation and annihilation operators. Only terms with two operators of similar type contribute. Therefore we have two out of four possibilities which corresponds to the six contributions. Due to the index notation we can summarize them into one. The other six terms, with the mixed operators, can also be combined in one term which includes four equal possibilities. For the same reason as before we have one out of two possibilities for two operator types  $a$  and  $b$ . This leads to Eq.(3.10).

$$\begin{aligned} \langle T_c (a_t a_{t_1'}^\dagger) \rangle^{(4)} &= \langle T_c (a_t a_{t_1'}^\dagger \left[ \lambda(a + a^\dagger) d^\dagger d + \lambda(b + b^\dagger) \tilde{d}^\dagger \tilde{d} \right]_{t_1} \left[ \lambda(a + a^\dagger) d^\dagger d + \lambda(b + b^\dagger) \tilde{d}^\dagger \tilde{d} \right]_{t_2} \\ &\quad \times \left[ \lambda(a + a^\dagger) d^\dagger d + \lambda(b + b^\dagger) \tilde{d}^\dagger \tilde{d} \right]_{t_3} \left[ \lambda(a + a^\dagger) d^\dagger d + \lambda(b + b^\dagger) \tilde{d}^\dagger \tilde{d} \right]_{t_4} \rangle \end{aligned} \quad (3.8)$$

$$= 6 \lambda^4 \langle T_c (a_t a_{t_1'}^\dagger a_{t_1} a_{t_2} a_{t_3}^\dagger a_{t_4}^\dagger) \rangle \langle T_c (d_{t_1}^\dagger d_{t_1} d_{t_2}^\dagger d_{t_2} d_{t_3}^\dagger d_{t_3} d_{t_4}^\dagger d_{t_4}) \rangle \quad (3.9)$$

$$+ 24 \lambda^4 \langle T_c (a_t a_{t_1'}^\dagger a_{t_1} a_{t_2}^\dagger b_{t_3} b_{t_4}^\dagger) \rangle \langle T_c (d_{t_1}^\dagger d_{t_1} d_{t_2}^\dagger d_{t_2} \tilde{d}_{t_3}^\dagger \tilde{d}_{t_3} \tilde{d}_{t_4}^\dagger \tilde{d}_{t_4}) \rangle \quad (3.10)$$

#### Application of Wick's Theorem to the Fourth Order Term

In the next step we use Wick's theorem to decompose the equations into products of free Green's functions. First we apply Wick's theorem to the bosonic parts in Eq.(3.9) and Eq.(3.10). We neglect the disconnected diagrams and obtain four different terms. Due to the arbitrary notation of the integration variable we are able to summarize them and obtain in the two cases:

$$\begin{aligned} 6 \lambda^4 \langle T_c (a_t a_{t_1'}^\dagger a_{t_1} a_{t_2} a_{t_3}^\dagger a_{t_4}^\dagger) \rangle &= 24 \lambda^4 \langle T_c (a_t a_{t_3}^\dagger) \rangle \langle T_c (a_{t_1} a_{t_1'}^\dagger) \rangle \langle T_c (a_{t_2} a_{t_4}^\dagger) \rangle \\ &= 24 \lambda^4 (-i) D_a(t, t_3) D_a(t_1, t_1') D_a(t_2, t_4) \end{aligned} \quad (3.11)$$

$$\begin{aligned}
 24 \lambda^4 \left\langle T_c \left( a_t a_{t'}^\dagger a_{t_1} a_{t_2}^\dagger b_{t_3} b_{t_4}^\dagger \right) \right\rangle &= 24 \lambda^4 \left\langle T_c \left( a_t a_{t_2}^\dagger \right) \right\rangle \left\langle T_c \left( a_{t_1} a_{t'}^\dagger \right) \right\rangle \left\langle T_c \left( b_{t_3} b_{t_4}^\dagger \right) \right\rangle \\
 &= 24 \lambda^4 (-i) D_a(t, t_2) D_a(t_1, t') D_b(t_3, t_4)
 \end{aligned} \tag{3.12}$$

We introduce the non oriented bosonic Green's function:

$$\begin{aligned}
 \tilde{D}(t_3, t_4) &= -i \left\langle T_c \left( (b_{t_3} + b_{t_3}^\dagger)(b_{t_4} + b_{t_4}^\dagger) \right) \right\rangle = -i \left\langle T_c \left( b_{t_3} b_{t_4}^\dagger + b_{t_3}^\dagger b_{t_4} + b_{t_3} b_{t_4} + b_{t_3}^\dagger b_{t_4}^\dagger \right) \right\rangle \\
 &= -i \left( \left\langle T_c \left( b_{t_3} b_{t_4}^\dagger \right) \right\rangle + \left\langle T_c \left( b_{t_4} b_{t_3}^\dagger \right) \right\rangle + \underbrace{\left\langle T_c \left( b_{t_3} b_{t_4} \right) \right\rangle}_0 + \underbrace{\left\langle T_c \left( b_{t_3}^\dagger b_{t_4}^\dagger \right) \right\rangle}_0 \right) \\
 &= D(t_4, t_3) + D(t_3, t_4)
 \end{aligned}$$

Then we apply Wick's theorem to the fermionic operators. As we applied Wick's theorem to the bosonic operators we used the possibility to interchange the time variables to combine the different addends appearing from Wick's theorem. This could also be done here but then the time arguments of the bosonic Green's functions would also change and the bosonic Green's functions couldn't be summarized in one term.

As a first step we change the time arguments  $t_2 \leftrightarrow t_3$  in Eq.(3.11) and obtain the same symmetry regarding the time arguments like in Eq.(3.12). To summarize a few terms we use the symmetric  $t_3 \leftrightarrow t_4$  of the fermionic Green's function and combine two terms by inserting  $\tilde{D}(t_3, t_4) = D(t_4, t_3) + D(t_3, t_4)$  which is the reason for the factor 2 in Eq.(3.13). The terms  $G(t_3, t_3)G(t_4, t_4)$ ,  $G(t_3, t_4)G(t_4, t_3)$ ,  $G(t_1, t_1)$  and  $G(t_2, t_2)$  lead to disconnected diagrams. We also neglect tadpoles. The fermionic part becomes:

$$\begin{aligned}
 &\left\langle T_c \left( d_{t_1} d_{t_1}^\dagger d_{t_2} d_{t_2}^\dagger d_{t_3} d_{t_3}^\dagger d_{t_4} d_{t_4}^\dagger \right) \right\rangle \\
 &= -2G(t_1, t_2)G(t_2, t_4)G(t_3, t_1)G(t_4, t_3) - 2G(t_1, t_3)G(t_2, t_1)G(t_3, t_4)G(t_4, t_2) \\
 &\quad + 2G(t_1, t_3)G(t_2, t_4)G(t_3, t_1)G(t_4, t_2) - 2G(t_1, t_3)G(t_2, t_4)G(t_3, t_2)G(t_4, t_1)
 \end{aligned} \tag{3.13}$$

To distinguish between Eq.(3.9) and Eq.(3.10) we must note, that the bosonic Green's function  $\tilde{D}(t_3, t_4)$  depends in the first equation on resonator  $a$  and in the second on resonator  $b$ . The fermionic operators of Eq.(3.9) depend all on dot 1 while Eq.(3.10) contain two operators of each dot. We add two indices to the fermionic Green's functions that indicate the belonging of each time argument to the corresponding operator. These indices are equivalent to the indices  $ij$  of Eq.(2.30). To facilitate the reading we used the color code that we have introduces in section (3.2).

### Perturbative Expansion of the Single Cavity A up to Fourth Order

The perturbative expansion up to fourth order reads:

$$\begin{aligned}
 \left\langle T_c \left( a_t a_{t'}^\dagger \right) \right\rangle &\approx \left\langle T_c \left( a_t a_{t'}^\dagger \right) \right\rangle^{(0)} + \left\langle T_c \left( a_t a_{t'}^\dagger \right) \right\rangle^{(2)} + \left\langle T_c \left( a_t a_{t'}^\dagger \right) \right\rangle^{(4)} \\
 &= iD_a(t, t')
 \end{aligned}$$



$$\begin{aligned}
 & + \int_C dt_1 \int_C dt_2 \lambda^2 D_a(t, t_2) D_a(t_1, t') G_{11}(t_1, t_2) G_{11}(t_2, t_1) \\
 & - 2i \lambda^4 \int_C dt_1 \int_C dt_2 \int_C dt_3 \int_C dt_4 \left[ \right. \\
 & \quad D_a(t, t_2) D_a(t_1, t') \tilde{D}_a(t_3, t_4) G_{11}(t_1, t_3) G_{11}(t_3, t_1) G_{11}(t_2, t_4) G_{11}(t_4, t_2) \\
 & \quad - D_a(t, t_2) D_a(t_1, t') \tilde{D}_a(t_3, t_4) G_{11}(t_1, t_3) G_{11}(t_3, t_4) G_{11}(t_2, t_1) G_{11}(t_4, t_2) \\
 & \quad - D_a(t, t_2) D_a(t_1, t') \tilde{D}_a(t_3, t_4) G_{11}(t_1, t_3) G_{11}(t_3, t_2) G_{11}(t_2, t_4) G_{11}(t_4, t_1) \\
 & \quad - D_a(t, t_2) D_a(t_1, t') \tilde{D}_a(t_3, t_4) G_{11}(t_1, t_2) G_{11}(t_3, t_1) G_{11}(t_2, t_4) G_{11}(t_4, t_3) \\
 & \quad - D_a(t, t_2) D_a(t_1, t') \tilde{D}_b(t_3, t_4) G_{11}(t_1, t_2) G_{12}(t_2, t_4) G_{21}(t_3, t_1) G_{22}(t_4, t_3) \\
 & \quad - D_a(t, t_2) D_a(t_1, t') \tilde{D}_b(t_3, t_4) G_{12}(t_1, t_3) G_{11}(t_2, t_1) G_{22}(t_3, t_4) G_{21}(t_4, t_2) \\
 & \quad + D_a(t, t_2) D_a(t_1, t') \tilde{D}_b(t_3, t_4) G_{12}(t_1, t_3) G_{12}(t_2, t_4) G_{21}(t_3, t_1) G_{21}(t_4, t_2) \\
 & \quad \left. - D_a(t, t_2) D_a(t_1, t') \tilde{D}_b(t_3, t_4) G_{12}(t_1, t_3) G_{12}(t_2, t_4) G_{21}(t_3, t_2) G_{21}(t_4, t_1) \right]
 \end{aligned}$$

### Perturbative Expansion of the Single Cavity B up to Fourth Order

The perturbative expansion of resonator  $b$  can be obtained from the one of resonator  $a$  by changing the indices  $a$  with  $b$  and 1 with 2. The interchange of 1 and 2 is necessary because the change of operator  $a$  with  $b$  induces also a change of the corresponding fermionic operator  $d$  with  $\tilde{d}$ , which correspond to dot 1 and 2.

$$\begin{aligned}
 \langle T_c (b_i b_{i'}^\dagger) \rangle & \approx \langle T_c (b_i b_{i'}^\dagger) \rangle^{(0)} + \langle T_c (b_i b_{i'}^\dagger) \rangle^{(2)} + \langle T_c (b_i b_{i'}^\dagger) \rangle^{(4)} \\
 & = i D_b(t, t') \\
 & + \lambda^2 \int_C dt_1 \int_C dt_2 D_b(t, t_2) D_b(t_1, t') G_{22}(t_1, t_2) G_{22}(t_2, t_1) \\
 & - 2i \lambda^4 \int_C dt_1 \int_C dt_2 \int_C dt_3 \int_C dt_4 \left[ \right. \\
 & \quad D_b(t, t_2) D_b(t_1, t') \tilde{D}_b(t_3, t_4) G_{22}(t_1, t_3) G_{22}(t_3, t_1) G_{22}(t_2, t_4) G_{22}(t_4, t_2) \\
 & \quad - D_b(t, t_2) D_b(t_1, t') \tilde{D}_b(t_3, t_4) G_{22}(t_1, t_3) G_{22}(t_3, t_4) G_{22}(t_2, t_1) G_{22}(t_4, t_2) \\
 & \quad - D_b(t, t_2) D_b(t_1, t') \tilde{D}_b(t_3, t_4) G_{22}(t_1, t_3) G_{22}(t_3, t_2) G_{22}(t_2, t_4) G_{22}(t_4, t_1) \\
 & \quad - D_b(t, t_2) D_b(t_1, t') \tilde{D}_b(t_3, t_4) G_{22}(t_1, t_2) G_{22}(t_3, t_1) G_{22}(t_2, t_4) G_{22}(t_4, t_3) \\
 & \quad - D_b(t, t_2) D_b(t_1, t') \tilde{D}_a(t_3, t_4) G_{22}(t_1, t_2) G_{21}(t_2, t_4) G_{12}(t_3, t_1) G_{11}(t_4, t_3) \\
 & \quad - D_b(t, t_2) D_b(t_1, t') \tilde{D}_a(t_3, t_4) G_{21}(t_1, t_3) G_{22}(t_2, t_1) G_{11}(t_3, t_4) G_{12}(t_4, t_2) \\
 & \quad + D_b(t, t_2) D_b(t_1, t') \tilde{D}_a(t_3, t_4) G_{21}(t_1, t_3) G_{21}(t_2, t_4) G_{12}(t_3, t_1) G_{12}(t_4, t_2) \\
 & \quad \left. - D_b(t, t_2) D_b(t_1, t') \tilde{D}_a(t_3, t_4) G_{21}(t_1, t_3) G_{21}(t_2, t_4) G_{12}(t_3, t_2) G_{12}(t_4, t_1) \right]
 \end{aligned}$$

### 3.4 Perturbative Expansion of $\langle T_c(a_t a_{t'}^\dagger b_t b_{t'}^\dagger) \rangle$

Now we consider the case of the combined cavities  $a$  and  $b$ . We are looking for the quantity

$$\langle T_c(A_t A_{t'}^\dagger) \rangle = \langle T_c(a_t a_{t'}^\dagger b_t b_{t'}^\dagger) \rangle .$$

The first and third order term of the perturbative expansion again become zero, because of the odd number of operators. We look at the perturbative expansion up to fourth order.

$$\begin{aligned} \langle T_c(a_t a_{t'}^\dagger b_t b_{t'}^\dagger) \rangle &\approx \langle T_c(a_t a_{t'}^\dagger b_t b_{t'}^\dagger) \rangle^{(0)} + \langle T_c(a_t a_{t'}^\dagger b_t b_{t'}^\dagger) \rangle^{(2)} + \langle T_c(a_t a_{t'}^\dagger b_t b_{t'}^\dagger) \rangle^{(4)} \\ &= \langle T_c(a_t a_{t'}^\dagger b_t b_{t'}^\dagger) \rangle \\ &\quad + \frac{1}{2} \int_C dt_1 \int_C dt_2 (-i)^2 \left\langle T_c \left( a_t a_{t'}^\dagger b_t b_{t'}^\dagger \left[ \lambda(a + a^\dagger) d^\dagger d + \lambda(b + b^\dagger) \tilde{d}^\dagger \tilde{d} \right]_{t_1} \right. \right. \\ &\quad \quad \quad \left. \left. \times \left[ \lambda(a + a^\dagger) d^\dagger d + \lambda(b + b^\dagger) \tilde{d}^\dagger \tilde{d} \right]_{t_2} \right) \right\rangle \\ &\quad + \frac{1}{24} \int_C dt_1 \int_C dt_2 \int_C dt_3 \int_C dt_4 (-i)^4 \left\langle T_c \left( a_t a_{t'}^\dagger b_t b_{t'}^\dagger \right. \right. \\ &\quad \times \left[ \lambda(a + a^\dagger) d^\dagger d + \lambda(b + b^\dagger) \tilde{d}^\dagger \tilde{d} \right]_{t_1} \left[ \lambda(a + a^\dagger) d^\dagger d + \lambda(b + b^\dagger) \tilde{d}^\dagger \tilde{d} \right]_{t_2} \\ &\quad \left. \left. \times \left[ \lambda(a + a^\dagger) d^\dagger d + \lambda(b + b^\dagger) \tilde{d}^\dagger \tilde{d} \right]_{t_3} \left[ \lambda(a + a^\dagger) d^\dagger d + \lambda(b + b^\dagger) \tilde{d}^\dagger \tilde{d} \right]_{t_4} \right) \right\rangle \end{aligned}$$

#### Zeroth Order

The application of Wick's theorem to the zeroth order term leads just to the multiplication of a bosonic Green's functions of each resonator. The mixed terms vanish since the particle number of each type (Fermions and Bosons) is not conserved.

$$\langle T_c \left( (a_t a_{t'}^\dagger b_t b_{t'}^\dagger) \right) \rangle^{(0)} = \langle T_c(a(t) a^\dagger(t')) \rangle \langle T_c(b(t) b^\dagger(t')) \rangle = -D_a(t, t') D_b(t, t')$$

#### Second Order

The second order term includes the factor  $\frac{1}{2} \int_C dt_1 \int_C dt_2 (-i)^2$ . We reintroduce it later and keep in mind that  $t_1$  and  $t_2$  are integration variables. The multiplication in Eq.(3.14) leads to two terms that conserve the particle number. Changing the name of the integration variables each line in Eq.(3.15) leads to two equal terms. We apply Wick's theorem to Eq.(3.16) and neglect both disconnected and tadpole diagrams to obtain Eq.(3.17). The sign changes from plus to

minus due to the transition changes of position of the fermionic operators. As a last step we identify the Green's functions get the expression of Eq.(3.18).

$$\left\langle T_c \left( a_t a_{t'}^\dagger b_t b_{t'}^\dagger \left[ \lambda(a + a^\dagger) d^\dagger d + \lambda(b + b^\dagger) \tilde{d}^\dagger \tilde{d} \right]_{t_1} \left[ \lambda(a + a^\dagger) d^\dagger d + \lambda(b + b^\dagger) \tilde{d}^\dagger \tilde{d} \right]_{t_2} \right) \right\rangle \quad (3.14)$$

$$\begin{aligned} &= \left\langle T_c \left( a_t a_{t'}^\dagger b_t b_{t'}^\dagger \left[ \lambda(a_{t_1} + a_{t_1}^\dagger) d_{t_1}^\dagger d_{t_1} \right] \left[ \lambda(a_{t_2} + a_{t_2}^\dagger) d_{t_2}^\dagger d_{t_2} \right] \right) \right\rangle \\ &+ \left\langle T_c \left( a_t a_{t'}^\dagger b_t b_{t'}^\dagger \left[ \lambda(b_{t_1} + b_{t_1}^\dagger) \tilde{d}_{t_1}^\dagger \tilde{d}_{t_1} \right] \left[ \lambda(b_{t_2} + b_{t_2}^\dagger) \tilde{d}_{t_2}^\dagger \tilde{d}_{t_2} \right] \right) \right\rangle \end{aligned} \quad (3.15)$$

$$\begin{aligned} &= 2\lambda^2 \left\langle T_c \left( a_t a_{t'}^\dagger b_t b_{t'}^\dagger a_{t_1} a_{t_2}^\dagger \right) \right\rangle \left\langle T_c \left( d_{t_1}^\dagger d_{t_1} d_{t_2}^\dagger d_{t_2} \right) \right\rangle \\ &+ 2\lambda^2 \left\langle T_c \left( a_t a_{t'}^\dagger b_t b_{t'}^\dagger b_{t_1} b_{t_2}^\dagger \right) \right\rangle \left\langle T_c \left( \tilde{d}_{t_1}^\dagger \tilde{d}_{t_1} \tilde{d}_{t_2}^\dagger \tilde{d}_{t_2} \right) \right\rangle \end{aligned} \quad (3.16)$$

$$\begin{aligned} &= -2\lambda^2 \left\langle T_c \left( a_t a_{t_2}^\dagger \right) \right\rangle \left\langle T_c \left( b_t b_{t'}^\dagger \right) \right\rangle \left\langle T_c \left( a_{t_1} a_{t'}^\dagger \right) \right\rangle \times \left\langle T_c \left( d_{t_1}^\dagger d_{t_2} \right) \right\rangle \left\langle T_c \left( d_{t_2}^\dagger d_{t_1} \right) \right\rangle \\ &- 2\lambda^2 \left\langle T_c \left( a_t a_{t'}^\dagger \right) \right\rangle \left\langle T_c \left( b_t b_{t_2}^\dagger \right) \right\rangle \left\langle T_c \left( b_{t_1} b_{t'}^\dagger \right) \right\rangle \times \left\langle T_c \left( \tilde{d}_{t_1}^\dagger \tilde{d}_{t_2} \right) \right\rangle \left\langle T_c \left( \tilde{d}_{t_2}^\dagger \tilde{d}_{t_1} \right) \right\rangle \end{aligned} \quad (3.17)$$

$$\begin{aligned} &= -2i\lambda^2 D_a(t, t_2) D_a(t_1, t') D_b(t, t') G_{11}(t_1, t_2) G_{11}(t_2, t_1) \\ &- 2i\lambda^2 D_a(t, t') D_b(t, t_2) D_b(t_1, t') G_{22}(t_1, t_2) G_{22}(t_2, t_1) \end{aligned} \quad (3.18)$$

#### Fourth Order

Analogue to the calculation of the fourth order perturbation term of the single resonators it includes the factor  $\frac{1}{24} \int_C dt_1 \int_C dt_2 \int_C dt_3 \int_C dt_4 (-i)^4$ . Again the multiplication in Eq.(3.19) results in eight terms with a conserved particle number. Just like for the single-resonator-calculation two terms contain only one type of bosonic or the corresponding fermionic operators. The arbitrary notation leads in this case to six equal expressions as shown in Eq.(3.20) and Eq.(3.22). The other six terms contain two operators of each type. Due to the arbitrary notation they can be combined and also include 4 equal expressions and lead to Eq.(3.21).

$$\begin{aligned} &\left\langle T_c \left( a_t a_{t'}^\dagger b_t b_{t'}^\dagger \left[ \lambda(a + a^\dagger) d^\dagger d + \lambda(b + b^\dagger) \tilde{d}^\dagger \tilde{d} \right]_{t_1} \left[ \lambda(a + a^\dagger) d^\dagger d + \lambda(b + b^\dagger) \tilde{d}^\dagger \tilde{d} \right]_{t_2} \right. \right. \\ &\quad \left. \left. \times \left[ \lambda(a + a^\dagger) d^\dagger d + \lambda(b + b^\dagger) \tilde{d}^\dagger \tilde{d} \right]_{t_3} \left[ \lambda(a + a^\dagger) d^\dagger d + \lambda(b + b^\dagger) \tilde{d}^\dagger \tilde{d} \right]_{t_4} \right) \right\rangle \end{aligned} \quad (3.19)$$

$$= 6 \lambda^4 \left\langle T_c \left( a_t a_{t'}^\dagger b_t b_{t'}^\dagger a_{t_1} a_{t_2} a_{t_3}^\dagger a_{t_4}^\dagger \right) \right\rangle \left\langle T_c \left( d_{t_1}^\dagger d_{t_1} d_{t_2}^\dagger d_{t_2} d_{t_3}^\dagger d_{t_3} d_{t_4}^\dagger d_{t_4} \right) \right\rangle \quad (3.20)$$

$$+ 24 \lambda^4 \left\langle T_c \left( a_t a_{t'}^\dagger b_t b_{t'}^\dagger a_{t_1} a_{t_2}^\dagger b_{t_3} b_{t_4}^\dagger \right) \right\rangle \left\langle T_c \left( d_{t_1}^\dagger d_{t_1} d_{t_2}^\dagger d_{t_2} \tilde{d}_{t_3}^\dagger \tilde{d}_{t_3} \tilde{d}_{t_4}^\dagger \tilde{d}_{t_4} \right) \right\rangle \quad (3.21)$$

$$+ 6 \lambda^4 \left\langle T_c \left( a_t a_{t'}^\dagger b_t b_{t'}^\dagger b_{t_1} b_{t_2} b_{t_3}^\dagger b_{t_4}^\dagger \right) \right\rangle \left\langle T_c \left( \tilde{d}_{t_1}^\dagger \tilde{d}_{t_1} \tilde{d}_{t_2}^\dagger \tilde{d}_{t_2} \tilde{d}_{t_3}^\dagger \tilde{d}_{t_3} \tilde{d}_{t_4}^\dagger \tilde{d}_{t_4} \right) \right\rangle \quad (3.22)$$

### Application of Wick's Theorem to the Fourth Order Term

First we apply Wick's theorem to the bosonic part of Eq.(3.20). We neglect again the disconnected diagrams and summarize four different pairing possibilities in one term.

$$\begin{aligned}
 & 6 \lambda^4 \left\langle T_c \left( a_t a_{t'}^\dagger b_t b_{t'}^\dagger a_{t_1} a_{t_2}^\dagger a_{t_3}^\dagger a_{t_4}^\dagger \right) \right\rangle \\
 &= 24 \lambda^4 \left\langle T_c \left( b_t b_{t'}^\dagger \right) \right\rangle \left\langle T_c \left( a_t a_{t_3}^\dagger \right) \right\rangle \left\langle T_c \left( a_{t_1} a_{t'}^\dagger \right) \right\rangle \left\langle T_c \left( a_{t_2} a_{t_4}^\dagger \right) \right\rangle \\
 &= 24 \lambda^4 D_b(t, t') D_a(t, t_3) D_a(t_1, t') D_a(t_2, t_4)
 \end{aligned}$$

The transformation of Eq.(3.22) leads analog to

$$6 \lambda^4 \left\langle T_c \left( a_t a_{t'}^\dagger b_t b_{t'}^\dagger b_{t_1} b_{t_2}^\dagger b_{t_3}^\dagger b_{t_4}^\dagger \right) \right\rangle = 24 \lambda^4 D_a(t, t') D_b(t, t_3) D_b(t_1, t') D_b(t_2, t_4) .$$

Eq. (3.21) has three possibilities to combine the operators and they cannot be summarized.

$$\begin{aligned}
 & 24 \lambda^4 \left\langle T_c \left( a_t a_{t'}^\dagger b_t b_{t'}^\dagger a_{t_1} a_{t_2}^\dagger b_{t_3} b_{t_4}^\dagger \right) \right\rangle \\
 &= 24 \lambda^4 \left[ \left\langle T_c \left( a_t a_{t'}^\dagger \right) \right\rangle \left\langle T_c \left( a_{t_1} a_{t_2}^\dagger \right) \right\rangle \left\langle T_c \left( b_t b_{t_4}^\dagger \right) \right\rangle \left\langle T_c \left( b_{t_3} b_{t'}^\dagger \right) \right\rangle \right. \\
 &\quad + \left\langle T_c \left( a_t a_{t_2}^\dagger \right) \right\rangle \left\langle T_c \left( a_{t_1} a_{t'}^\dagger \right) \right\rangle \left\langle T_c \left( b_t b_{t'}^\dagger \right) \right\rangle \left\langle T_c \left( b_{t_3} b_{t_4}^\dagger \right) \right\rangle \\
 &\quad \left. + \left\langle T_c \left( a_t a_{t_2}^\dagger \right) \right\rangle \left\langle T_c \left( a_{t_1} a_{t'}^\dagger \right) \right\rangle \left\langle T_c \left( b_t b_{t_4}^\dagger \right) \right\rangle \left\langle T_c \left( b_{t_3} b_{t'}^\dagger \right) \right\rangle \right] \\
 &= 24 \lambda^4 [D_a(t, t') D_a(t_1, t_2) D_b(t, t_4) D_b(t_3, t') + D_a(t, t_2) D_a(t_1, t') D_b(t, t') D_b(t_3, t_4) \\
 &\quad + D_a(t, t_2) D_a(t_1, t') D_b(t, t_4) D_b(t_3, t')]
 \end{aligned}$$

Next we apply Wick's theorem to the fermionic expressions. In each case we will obtain terms similar to Eq.(3.13) or longer. Therefore we waive to specify the individual sums of products from Wick's theorem and limit ourselves to indicate the used symmetries or simplifications.

In Eq.(3.20) and Eq.(3.22) we use the symmetry of  $t_2 \leftrightarrow t_4$  in the fermionic Green's functions by inserting  $\tilde{D}(t_2, t_4) = D(t_4, t_2) + D(t_2, t_4)$ . The terms  $G(t_2, t_2)G(t_4, t_4)$  and  $G(t_2, t_4)G(t_4, t_2)$  lead to disconnected diagrams.

Wick's theorem applied to the bosonic expression of Eq.(3.21) led to three different terms. For the first and second one the terms  $G(t_1, t_1)G(t_2, t_2)$  and  $G(t_1, t_2)G(t_2, t_1)$  lead to disconnected diagrams. For the first term we use the symmetry of  $t_1 \leftrightarrow t_2$  by inserting  $\tilde{D}(t_1, t_2) = D(t_2, t_1) + D(t_1, t_2)$ . For the second one we use the symmetry  $t_3 \leftrightarrow t_4$  by inserting  $\tilde{D}(t_3, t_4) = D(t_4, t_3) + D(t_3, t_4)$ . At the third term  $G(t_1, t_1)G(t_3, t_3)$  and  $G(t_1, t_3)G(t_3, t_1)$  leads to a disconnected diagram and it implies no symmetry.

By the application of Wick's theorem we obtain in the case of Eq.(3.20), the first and second addend of Eq.(3.21) and Eq.(3.22) ten different addends for each term. In each case six terms represent a disconnected diagrams so only four terms per equation remain. For the third addend of Eq.(3.21) Wick's theorem leads to twenty terms of which twelve terms drop out and eight remain. Combined with the zeroth and second order term we obtain the perturbative expansion of the combined cavities up to fourth order.

## Perturbative Expansion of the Combined Cavities A and B up to Fourth Order

$$\begin{aligned}
 & \left\langle T_c \left( a_t b_t a_t^\dagger b_t^\dagger \right) \right\rangle \approx \left\langle T_c \left( a_t a_t b_t^\dagger b_t^\dagger \right) \right\rangle^{(0)} + \left\langle T_c \left( a_t a_t b_t^\dagger b_t^\dagger \right) \right\rangle^{(2)} + \left\langle T_c \left( a_t a_t b_t^\dagger b_t^\dagger \right) \right\rangle^{(4)} \\
 & = -D_a(t, t') D_b(t, t') \\
 & + i\lambda^2 \int_C dt_1 \int_C dt_2 D_a(t, t_2) D_a(t_1, t') D_b(t, t') G_{11}(t_1, t_2) G_{11}(t_2, t_1) \\
 & + i\lambda^2 \int_C dt_1 \int_C dt_2 D_a(t, t') D_b(t, t_2) D_b(t_1, t') G_{22}(t_1, t_2) G_{22}(t_2, t_1) \\
 & + \lambda^4 \int_C dt_1 \int_C dt_2 \int_C dt_3 \int_C dt_4 \left[ \right. \\
 & \quad 2D_b(t, t') D_a(t, t_2) D_a(t_1, t') \tilde{D}_a(t_3, t_4) G_{11}(t_1, t_3) G_{11}(t_3, t_1) G_{11}(t_2, t_4) G_{11}(t_4, t_2) \\
 & \quad - 2D_b(t, t') D_a(t, t_2) D_a(t_1, t') \tilde{D}_a(t_3, t_4) G_{11}(t_1, t_3) G_{11}(t_3, t_4) G_{11}(t_2, t_1) G_{11}(t_4, t_2) \\
 & \quad - 2D_b(t, t') D_a(t, t_2) D_a(t_1, t') \tilde{D}_a(t_3, t_4) G_{11}(t_1, t_3) G_{11}(t_3, t_2) G_{11}(t_2, t_4) G_{11}(t_4, t_1) \\
 & \quad - 2D_b(t, t') D_a(t, t_2) D_a(t_1, t') \tilde{D}_a(t_3, t_4) G_{11}(t_1, t_2) G_{11}(t_3, t_1) G_{11}(t_2, t_4) G_{11}(t_4, t_3) \\
 & \quad + 2D_a(t, t') D_b(t, t_2) D_b(t_1, t') \tilde{D}_b(t_3, t_4) G_{22}(t_1, t_3) G_{22}(t_3, t_1) G_{22}(t_2, t_4) G_{22}(t_4, t_2) \\
 & \quad - 2D_a(t, t') D_b(t, t_2) D_b(t_1, t') \tilde{D}_b(t_3, t_4) G_{22}(t_1, t_3) G_{22}(t_3, t_4) G_{22}(t_2, t_1) G_{22}(t_4, t_2) \\
 & \quad - 2D_a(t, t') D_b(t, t_2) D_b(t_1, t') \tilde{D}_b(t_3, t_4) G_{22}(t_1, t_3) G_{22}(t_3, t_2) G_{22}(t_2, t_4) G_{22}(t_4, t_1) \\
 & \quad - 2D_a(t, t') D_b(t, t_2) D_b(t_1, t') \tilde{D}_b(t_3, t_4) G_{22}(t_1, t_2) G_{22}(t_3, t_1) G_{22}(t_2, t_4) G_{22}(t_4, t_3) \\
 & \quad - 2D_a(t, t') \tilde{D}_a(t_3, t_4) D_b(t, t_2) D_b(t_1, t') G_{11}(t_3, t_4) G_{12}(t_4, t_2) G_{21}(t_1, t_3) G_{22}(t_2, t_1) \\
 & \quad - 2D_a(t, t') \tilde{D}_a(t_3, t_4) D_b(t, t_2) D_b(t_1, t') G_{11}(t_3, t_4) G_{12}(t_4, t_1) G_{22}(t_1, t_2) G_{21}(t_2, t_3) \\
 & \quad + 2D_a(t, t') \tilde{D}_a(t_3, t_4) D_b(t, t_2) D_b(t_1, t') G_{12}(t_3, t_1) G_{12}(t_4, t_2) G_{21}(t_1, t_3) G_{21}(t_2, t_4) \\
 & \quad - 2D_a(t, t') \tilde{D}_a(t_3, t_4) D_b(t, t_2) D_b(t_1, t') G_{12}(t_3, t_1) G_{12}(t_4, t_2) G_{21}(t_1, t_4) G_{21}(t_2, t_3) \\
 & \quad - 2D_a(t, t_2) D_a(t_1, t') D_b(t, t') \tilde{D}_b(t_3, t_4) G_{11}(t_1, t_2) G_{12}(t_2, t_4) G_{21}(t_3, t_1) G_{22}(t_4, t_3) \\
 & \quad - 2D_a(t, t_2) D_a(t_1, t') D_b(t, t') \tilde{D}_b(t_3, t_4) G_{12}(t_1, t_3) G_{11}(t_2, t_1) G_{22}(t_3, t_4) G_{21}(t_4, t_2) \\
 & \quad + 2D_a(t, t_2) D_a(t_1, t') D_b(t, t') \tilde{D}_b(t_3, t_4) G_{12}(t_1, t_3) G_{12}(t_2, t_4) G_{21}(t_3, t_1) G_{21}(t_4, t_2) \\
 & \quad - 2D_a(t, t_2) D_a(t_1, t') D_b(t, t') \tilde{D}_b(t_3, t_4) G_{12}(t_1, t_3) G_{12}(t_2, t_4) G_{21}(t_3, t_2) G_{21}(t_4, t_1) \\
 & \quad + D_a(t, t_2) D_a(t_1, t') D_b(t, t_4) D_b(t_3, t') G_{11}(t_1, t_2) G_{11}(t_2, t_1) G_{22}(t_3, t_4) G_{22}(t_4, t_3) \\
 & \quad - D_a(t, t_2) D_a(t_1, t') D_b(t, t_4) D_b(t_3, t') G_{11}(t_1, t_2) G_{12}(t_2, t_4) G_{21}(t_3, t_1) G_{22}(t_4, t_3) \\
 & \quad - D_a(t, t_2) D_a(t_1, t') D_b(t, t_4) D_b(t_3, t') G_{11}(t_1, t_2) G_{12}(t_2, t_3) G_{22}(t_3, t_4) G_{21}(t_4, t_1) \\
 & \quad - D_a(t, t_2) D_a(t_1, t') D_b(t, t_4) D_b(t_3, t') G_{12}(t_1, t_3) G_{11}(t_2, t_1) G_{22}(t_3, t_4) G_{21}(t_4, t_2) \\
 & \quad - D_a(t, t_2) D_a(t_1, t') D_b(t, t_4) D_b(t_3, t') G_{12}(t_1, t_3) G_{12}(t_2, t_4) G_{21}(t_3, t_2) G_{21}(t_4, t_1)
 \end{aligned}$$

$$\begin{aligned}
 & - D_a(t, t_2)D_a(t_1, t')D_b(t, t_4)D_b(t_3, t')G_{12}(t_1, t_4)G_{11}(t_2, t_1)G_{21}(t_3, t_2)G_{22}(t_4, t_3) \\
 & - D_a(t, t_2)D_a(t_1, t')D_b(t, t_4)D_b(t_3, t')G_{12}(t_1, t_4)G_{12}(t_2, t_3)G_{21}(t_3, t_1)G_{21}(t_4, t_2) \\
 & + D_a(t, t_2)D_a(t_3, t')D_b(t, t_4)D_b(t_1, t')G_{12}(t_3, t_4)G_{12}(t_2, t_1)G_{21}(t_1, t_2)G_{21}(t_4, t_3)
 \end{aligned}
 \Big]$$

### 3.5 Neglect of Tadpole Diagrams

All terms of the perturbative expansion but in particular the fourth order term contained many so-called tadpole diagrams. This is an effect due to a shift of the two resonators because of an average, non zero force acting on them. In the case of a system without a shift of the resonator this tadpole diagrams wouldn't appear. To neglect the terms containing tadpoles we redefine the bosonic operator concerning this shift like

$$b' = b - \langle b \rangle .$$

We have a detailed look on the first order perturbative expansion of  $\langle b \rangle$  with the interaction Hamiltonian  $H^{(i)} = \lambda(a + a^\dagger)d^\dagger d + \lambda(b + b^\dagger)\tilde{d}^\dagger \tilde{d}$

$$\begin{aligned}
 \langle b \rangle & \approx \underbrace{\langle b \rangle_0}_0 + \left\langle \lambda \int_C dt_1 (-i)b_t \left( (a_{t_1} + a_{t_1}^\dagger)d_{t_1}^\dagger d_{t_1} + (b_{t_1} + b_{t_1}^\dagger)\tilde{d}_{t_1}^\dagger \tilde{d}_{t_1} \right) \right\rangle \\
 & = -i\lambda \int_C dt_1 \langle b_t b_{t_1} \rangle \langle \tilde{d}_{t_1}^\dagger \tilde{d}_{t_1} \rangle \\
 & = i\lambda \int_C dt_1 D(t, t_1)G_{22}(t_1, t_1)
 \end{aligned}$$

and it's corresponding Feynman diagram.

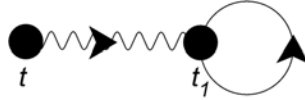


Figure 9: Tadpole diagram of order of  $\lambda$  as integrand of the first order perturbative expansion of  $\langle b \rangle$

The first order term represents exactly the first order tadpole diagram. Regarding this first order perturbative expansion we redefine the bosonic operator like

$$b' = b - \langle b \rangle_\lambda$$

And obtain

$$\langle b' \rangle = \langle b \rangle - \langle b \rangle_\lambda = \underbrace{\langle b \rangle_0}_0 + \underbrace{\langle b \rangle_\lambda}_0 + \underbrace{\langle b \rangle_{\lambda^2}}_0 + \langle b \rangle_{\lambda^3} + \dots - \langle b \rangle_\lambda .$$

Since  $\langle b \rangle_\lambda$  is canceled it means that diagrams containing tadpoles of the first order would vanish with the new bosonic operators  $b' = b - \langle b \rangle$  and only a tadpole diagram of third order remain. If we proceed in this way and define the bosonic operator like

$$b' = b - \langle b \rangle$$

while  $\langle b \rangle = \langle b \rangle_\lambda + \langle b \rangle_{\lambda^2} + \dots$ , it cancel every tadpole-like diagram and result in a  $\langle b' \rangle$  without tadpoles. Therefore the diagrams containing tadpoles doesn't contribute to the result.

Since we consider the perturbative expansion up to fourth order only tadpole diagrams of first and third order appear. These tadpole diagrams are depicted in Fig. (10).

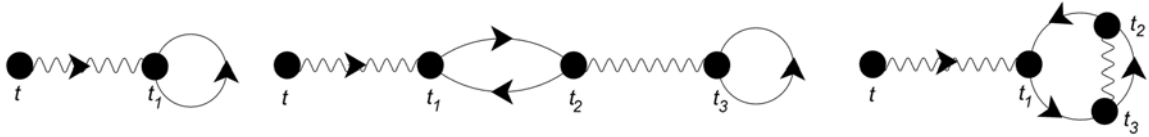


Figure 10: Integrand of the perturbative expansion of  $\langle b \rangle$  up to third order

### 3.6 Perturbative Expansion represented as Feynman Diagrams

A more pleasant way to consider the perturbative expansion and to compare the different terms for the calculation of the covariance is the representation in Feynman diagrams.

#### Perturbative Expansion of the Zeroth Order

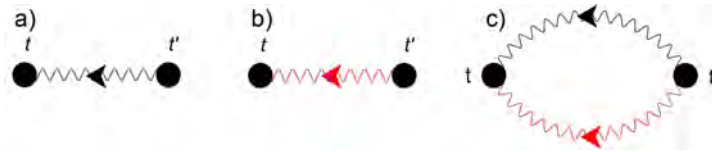


Figure 11: Feynman diagrams of the zeroth order perturbative expansion.

a)  $\langle T_c(a_t a_{t'}^\dagger) \rangle^{(0)}$ , b)  $\langle T_c(b_t b_{t'}^\dagger) \rangle^{(0)}$  and c)  $\langle T_c(a_t a_{t'}^\dagger b_t b_{t'}^\dagger) \rangle^{(0)}$

#### Perturbative Expansion of the Second Order

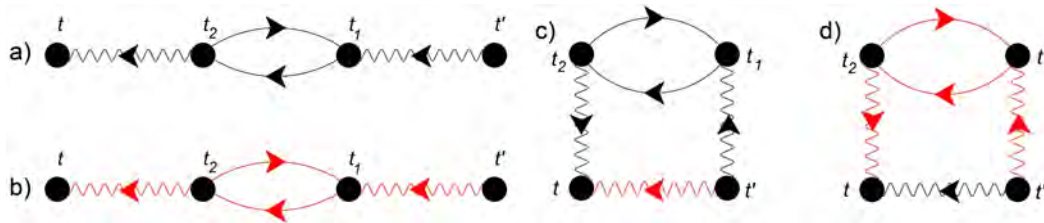


Figure 12: Feynman diagrams of the second order perturbative expansion.

a)  $\langle T_c(a_t a_{t'}^\dagger) \rangle^{(2)}$ , b)  $\langle T_c(b_t b_{t'}^\dagger) \rangle^{(2)}$  and c), d)  $\langle T_c(a_t a_{t'}^\dagger b_t b_{t'}^\dagger) \rangle^{(2)}$

#### Perturbative Expansion of the Fourth Order of $\langle T_c(a_t a_{t'}^\dagger) \rangle$ and $\langle T_c(b_t b_{t'}^\dagger) \rangle$

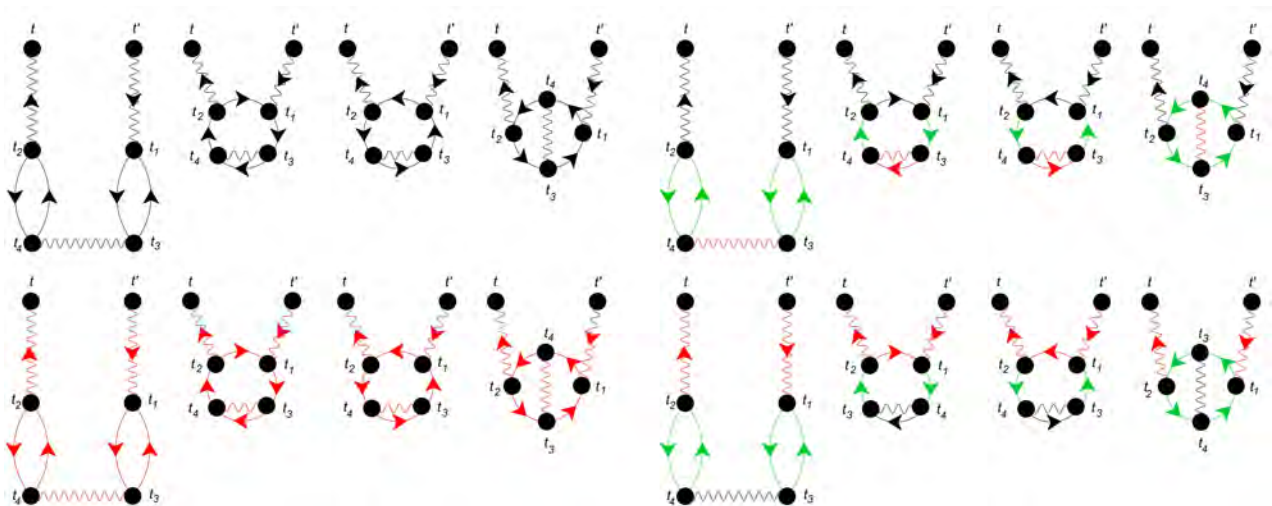


Figure 13: Feynman diagrams of the perturbative expansion of the fourth order of the single cavities. First row belongs to  $\langle T_c(a_t a_{t'}^\dagger) \rangle^{(4)}$  and the second row belongs to  $\langle T_c(b_t b_{t'}^\dagger) \rangle^{(4)}$ .



**Perturbative Expansion of the Fourth Order of  $\langle T_c(a_t a_{t'}^\dagger b_t b_{t'}^\dagger) \rangle$**

The lower eight diagrams of Fig. (14) shows the last eight terms of the perturbative expansion of  $\langle T_c(a_t a_{t'}^\dagger b_t b_{t'}^\dagger) \rangle$ . All other terms of the fourth order are shown in the upper two lines.

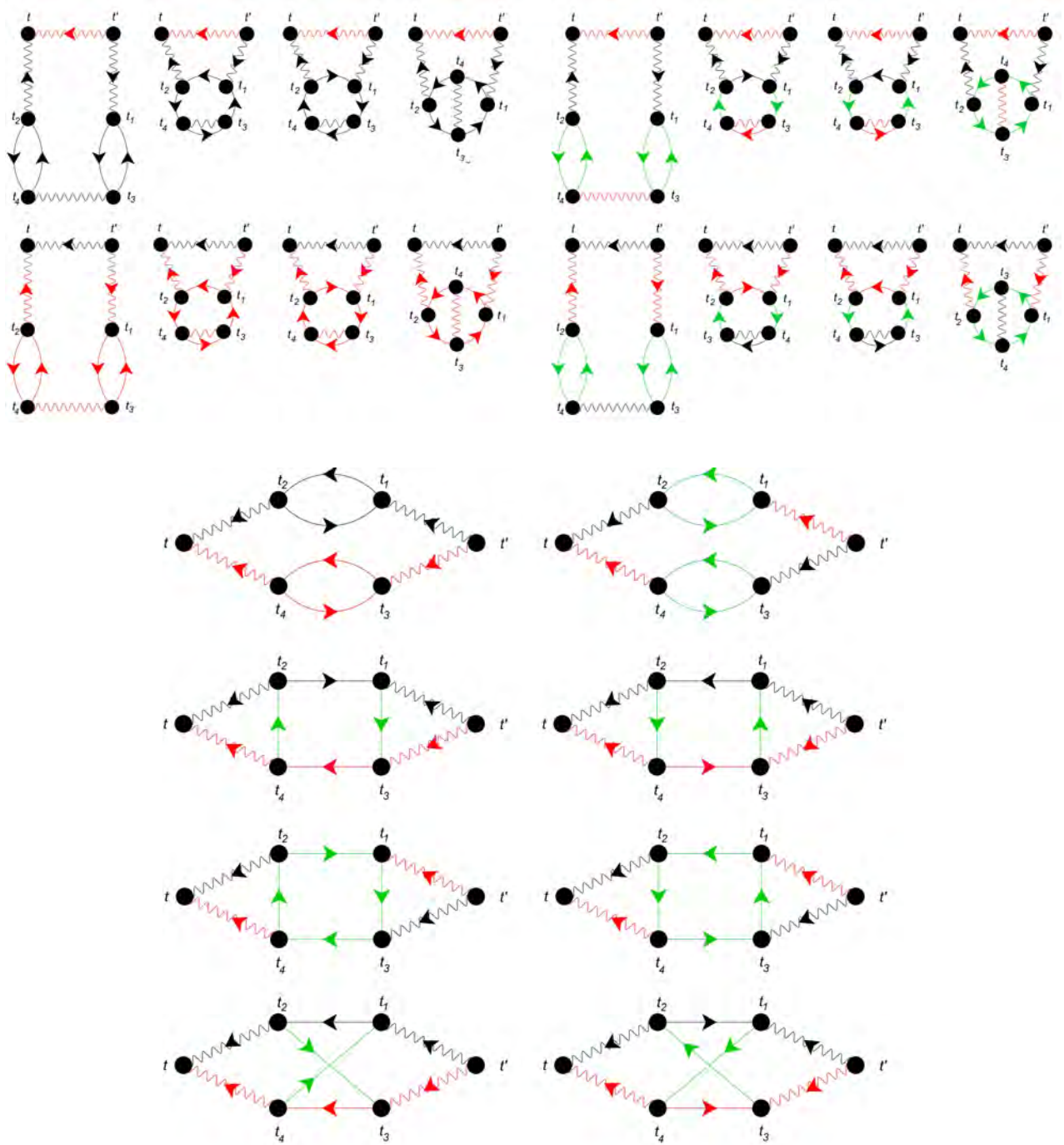


Figure 14: Feynman diagrams of the fourth order perturbative expansion of the combined cavities  $\langle T_c(a_t a_{t'}^\dagger b_t b_{t'}^\dagger) \rangle^{(4)}$ .

### 3.7 Specification of the Covariance in Terms of the Perturbative Expansion

To determine the covariance we started with the time-ordered expression

$$\lim_{t' \rightarrow t} i \left( \left\langle T_c \left( a_t a_{t'}^\dagger b_t b_{t'}^\dagger \right) \right\rangle^{+-} - \left\langle T_c \left( a_t a_{t'}^\dagger \right) \right\rangle^{+-} \left\langle T_c \left( b_t b_{t'}^\dagger \right) \right\rangle^{+-} \right) = \langle n_a n_b \rangle - \langle n_a \rangle \langle n_b \rangle . \quad (3.23)$$

We expanded each of the three terms up to the fourth order. From the expansion we will get terms with increasing order of the dot-cavity coupling constant  $\lambda$ . To calculate the covariance we compare those parts of  $\langle T_c(a_t a_{t'}^\dagger b_t b_{t'}^\dagger) \rangle$  with  $\langle T_c(a_t a_{t'}^\dagger) \rangle \langle T_c(b_t b_{t'}^\dagger) \rangle$  that are proportional to the same order of  $\lambda$ . Since  $\lambda$  is linear in the perturbation Hamiltonian the order of  $\lambda$  is direct proportional to the order of the perturbation term. For the first part of Eq.(3.23) we obtain

$$\left\langle T_c \left( a_t a_{t'}^\dagger b_t b_{t'}^\dagger \right) \right\rangle \approx \left\langle T_c \left( a_t a_{t'}^\dagger b_t b_{t'}^\dagger \right) \right\rangle^{(0)} + \left\langle T_c \left( a_t a_{t'}^\dagger b_t b_{t'}^\dagger \right) \right\rangle^{(2)} + \left\langle T_c \left( a_t a_{t'}^\dagger b_t b_{t'}^\dagger \right) \right\rangle^{(4)} .$$

And therefore the belonging to the different orders of  $\lambda$  is

$$\lambda^0 : \left\langle T_c \left( a_t a_{t'}^\dagger b_t b_{t'}^\dagger \right) \right\rangle^{(0)} , \quad \lambda^2 : \left\langle T_c \left( a_t a_{t'}^\dagger b_t b_{t'}^\dagger \right) \right\rangle^{(2)} , \quad \lambda^4 : \left\langle T_c \left( a_t a_{t'}^\dagger b_t b_{t'}^\dagger \right) \right\rangle^{(4)} .$$

We expand each factor of  $\langle T_c(a_t a_{t'}^\dagger) \rangle \langle T_c(b_t b_{t'}^\dagger) \rangle$  up to fourth order and multiply them. Since the perturbative expansion of the first and third order is zero, we multiply in each case three terms and sort them according to their order in  $\lambda$ .

$$\begin{aligned} \left\langle T_c \left( a_t a_{t'}^\dagger \right) \right\rangle \left\langle T_c \left( b_t b_{t'}^\dagger \right) \right\rangle &\approx \left( \left\langle T_c \left( a_t a_{t'}^\dagger \right) \right\rangle^{(0)} + \left\langle T_c \left( a_t a_{t'}^\dagger \right) \right\rangle^{(2)} + \left\langle T_c \left( a_t a_{t'}^\dagger \right) \right\rangle^{(4)} \right) \\ &\cdot \left( \left\langle T_c \left( b_t b_{t'}^\dagger \right) \right\rangle^{(0)} + \left\langle T_c \left( b_t b_{t'}^\dagger \right) \right\rangle^{(2)} + \left\langle T_c \left( b_t b_{t'}^\dagger \right) \right\rangle^{(4)} \right) \end{aligned}$$

$$\lambda^0 : \left\langle T_c \left( a_t a_{t'}^\dagger \right) \right\rangle^{(0)} \left\langle T_c \left( b_t b_{t'}^\dagger \right) \right\rangle^{(0)} \quad (3.24)$$

$$\lambda^2 : \left\langle T_c \left( a_t a_{t'}^\dagger \right) \right\rangle^{(0)} \left\langle T_c \left( b_t b_{t'}^\dagger \right) \right\rangle^{(2)} + \left\langle T_c \left( a_t a_{t'}^\dagger \right) \right\rangle^{(2)} \left\langle T_c \left( b_t b_{t'}^\dagger \right) \right\rangle^{(0)} \quad (3.25)$$

$$\lambda^4 : \left\langle T_c \left( a_t a_{t'}^\dagger \right) \right\rangle^{(0)} \left\langle T_c \left( b_t b_{t'}^\dagger \right) \right\rangle^{(4)} + \left\langle T_c \left( a_t a_{t'}^\dagger \right) \right\rangle^{(2)} \left\langle T_c \left( b_t b_{t'}^\dagger \right) \right\rangle^{(2)} + \left\langle T_c \left( a_t a_{t'}^\dagger \right) \right\rangle^{(4)} \left\langle T_c \left( b_t b_{t'}^\dagger \right) \right\rangle^{(0)} \quad (3.26)$$

#### Remaining Diagrams of the Covariance up to Fourth Order

Now we compare the equations or the corresponding Feynman diagrams of the perturbative expansion of parts within terms of equal orders of  $\lambda$ .

In Fig. (11) one can see plainly that the multiplication of the two zeroth order terms of the single resonators, corresponding to Eq.(3.24), is equal to the zeroth order of the combined resonators.

Regarding Fig. (11) and Fig. (12) it seems clear, that the multiplications of the zeroth order term of a single resonator with a second order term of the complementary resonator, corresponding to Eq.(3.25) are equal to the second order terms of the combined cavities.

To compare the terms or diagrams of the fourth order we beginn with the outer terms of Eq.(3.26). We multiply the zeroth order of the single resonators, see Fig. (11), with the fourth order terms of the complementary single resonator, see Fig. (13). These diagrams comply with those of the upper two lines in Fig. (14). The center term of Eq.(3.26) corresponds to the two diagrams a) and b) of Fig. (12). The multiplication of these two is equal to the first of the lower eight diagrams in Fig. (14).

Since the terms of the multiplied single-resonator-terms are subtracted from the combined expression only seven equations or corresponding Feynman diagrams remain and contribute to the covariance. The equation of the covariance reduces to

$$\begin{aligned}
 C = \lambda^4 \int_C dt_1 \int_C dt_2 \int_C dt_3 \int_C dt_4 [ & \\
 + D_a(t, t_1) D_a(t_2, t') D_b(t, t_3) D_b(t_4, t') G_{12}(t_4, t_3) G_{12}(t_1, t_2) G_{21}(t_2, t_1) G_{21}(t_3, t_4) & \\
 - D_a(t, t_1) D_a(t_2, t') D_b(t, t_3) D_b(t_4, t') G_{11}(t_2, t_1) G_{12}(t_1, t_3) G_{21}(t_4, t_2) G_{22}(t_3, t_4) & \\
 - D_a(t, t_1) D_a(t_2, t') D_b(t, t_3) D_b(t_4, t') G_{12}(t_2, t_4) G_{11}(t_1, t_2) G_{22}(t_4, t_3) G_{21}(t_3, t_1) & \\
 - D_a(t, t_1) D_a(t_2, t') D_b(t, t_3) D_b(t_4, t') G_{12}(t_4, t_2) G_{12}(t_1, t_3) G_{21}(t_2, t_1) G_{21}(t_3, t_4) & \\
 - D_a(t, t_1) D_a(t_2, t') D_b(t, t_3) D_b(t_4, t') G_{12}(t_4, t_3) G_{12}(t_1, t_2) G_{21}(t_2, t_4) G_{21}(t_3, t_1) & \\
 - D_a(t, t_1) D_a(t_2, t') D_b(t, t_3) D_b(t_4, t') G_{12}(t_2, t_3) G_{11}(t_1, t_2) G_{21}(t_4, t_1) G_{22}(t_3, t_4) & \\
 - D_a(t, t_1) D_a(t_2, t') D_b(t, t_3) D_b(t_4, t') G_{11}(t_2, t_1) G_{12}(t_1, t_4) G_{22}(t_4, t_3) G_{21}(t_3, t_2) & ]
 \end{aligned}$$

The corresponding Feynman diagrams are shown in Fig(15).

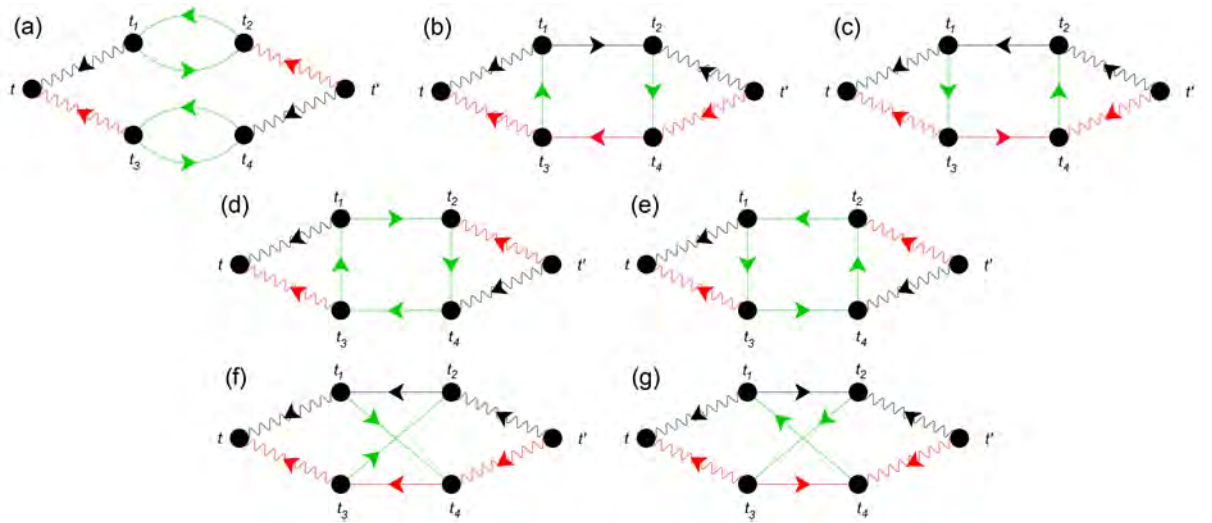


Figure 15: Feynman diagrams representing the Covariance



## 4 Results: Analytic Formula for the Covariance

We reduced the calculation of the covariance in terms of the perturbative expansion up to fourth order to the integration of seven terms that can be represented in the seven Feynman diagrams of Fig. (15). Since the Green's functions of these diagrams correspond to contour time arguments we have to transform them to real time and do the integration.

### 4.1 Real Time and Frequency Representation

The seven diagrams reduce in principle to three different types. The *square-shaped* diagrams have some counterparts where the inner fermionic Green's functions go the other way round as well different components of the Green's functions.

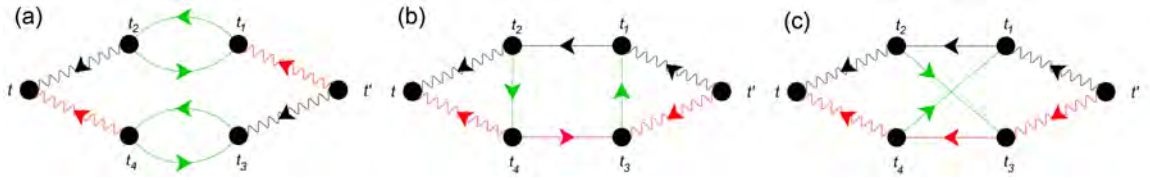


Figure 16: Three different types of diagrams that are contained in the covariance C.

The first diagram Fig. (16)(a) is just the multiplication of two bubble-diagrams. The second and third diagram consists of the same outer bosonic Green's functions and different inner fermionic. At first glance, the third diagram might be a twisted version of the second diagram. But if we open the outer time arguments, twist the lower line and close the time arguments again we obtain the same structure of diagrams with identical fermionic arrows but the direction of the arrows of the lower bosonic Green's functions are reversed. Therefore we have to consider each type individual.

### Transformation to Real Time Space

The Green's function of the diagrams Fig. (16) read in a short notation

$$\oint_C dt_1 \oint_C dt_2 \oint_C dt_3 \oint_C dt_4 D(t, t_1) D(t, t_3) P(t_1, t_2, t_3, t_4) D(t_2, t') D(t_4, t') .$$

We parametrize the contour according [3]

$$\int_C d\tau_i = \int_{-\infty}^{\infty} dt_i + \int_{\infty}^{-\infty} dt_i = \int_{-\infty}^{\infty} dt_i - \int_{-\infty}^{\infty} dt_i .$$

If we introduce the notation  $s_i$  that corresponds to the position of the time argument  $t_i$ , the Green's function in real time space reads

$$\sum_{s_1, s_2, s_3, s_4 = \pm} s_1 s_2 s_3 s_4 \int_{-\infty}^{\infty} dt_1^{s_1} \int_{-\infty}^{\infty} dt_2^{s_2} \int_{-\infty}^{\infty} dt_3^{s_3} \int_{-\infty}^{\infty} dt_4^{s_4} D^{s_t s_1}(t, t_1) D^{s_t s_3}(t, t_3) P^{s_1 s_2 s_3 s_4}(t_1, t_2, t_3, t_4)$$

$$\cdot D^{s_2 s_{t'}}(t_2, t') D^{s_4 s_{t'}}(t_4, t')$$

whereby we have summed up all possible distributions of the time arguments on the contour. Since we are looking for the limit of the lesser function  $\lim_{t' \rightarrow t} iF^<(t, t')$ , it holds that  $t < t'$  and therefore  $t'$  lies always on the lower branch and  $t$  on the upper branch. Hence  $s_t = +$  and  $s_{t'} = -$ .

#### 4.1.1 Transformation of the Bubble Diagram

We consider the basic diagram of the bubble diagram like in Fig. (16)(a).

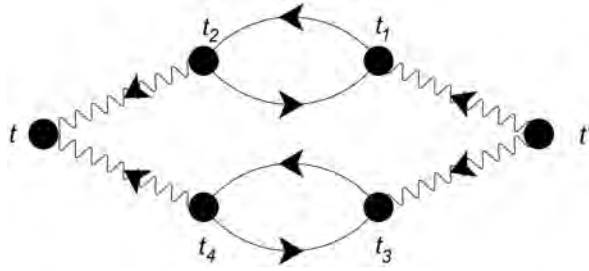


Figure 17: Basic diagram of the bubble diagram.

We introduce

$$P^{s_1 s_2 s_3 s_4}(t_1, t_2, t_3, t_4) = G^{s_1 s_2}(t_1, t_2) G^{s_2 s_1}(t_2, t_1) G^{s_3 s_4}(t_3, t_4) G^{s_4 s_3}(t_4, t_3)$$

and a simpler notation. We sort the Green's functions according to the upper and lower branch in Fig. (17).

$$\sum_{\substack{s_1, s_2 \\ s_3, s_4 = \pm}} s_1 s_2 s_3 s_4 \iiint \int dt_1^{s_1} dt_2^{s_2} dt_3^{s_3} dt_4^{s_4} (D^{+1} G^{12} G^{21} D^{2-}) (D^{+3} G^{34} G^{43} D^{4-})$$

Since we have calculated the bosonic and fermionic Green's functions depending on the energy insert the Fourier transformation of the Green's functions and transform them to the frequency domain.

$$\begin{aligned} & \sum_{\substack{s_1, s_2 \\ s_3, s_4 = \pm}} s_1 s_2 s_3 s_4 \iiint \int dt_1 dt_2 dt_3 dt_4 \iiint \int \int \int d\omega_1 d\omega_2 d\omega_3 d\omega_4 d\omega_5 d\omega_6 \\ & D^{+1}(\omega_1) e^{-i\omega_1(t-t_1)} G^{12}(\omega_2) e^{-i\omega_2(t_1-t_2)} G^{21}(-\omega_2) e^{-i\omega_2(t_2-t_1)} D^{2-}(\omega_3) e^{-i\omega_3(t_2-t')} \\ & \cdot D^{+3}(\omega_4) e^{-i\omega_4(t-t_3)} G^{34}(-\omega_5) e^{-i\omega_5(t_3-t_4)} G^{43}(\omega_5) e^{-i\omega_5(t_4-t_3)} D^{4-}(\omega_6) e^{-i\omega_6(t_4-t')} \end{aligned}$$

This expression includes the time integrations

$$\begin{aligned} \int dt_1 e^{it_1(\omega_1 - \omega_2 + \omega_2)} &= \delta(\omega_1), & \int dt_2 e^{it_2(\omega_2 - \omega_2 - \omega_3)} &= \delta(-\omega_3), \\ \int dt_3 e^{it_3(\omega_4 - \omega_5 + \omega_5)} &= \delta(\omega_4), & \int dt_4 e^{it_4(\omega_5 - \omega_5 - \omega_6)} &= \delta(-\omega_6). \end{aligned}$$

If we perform the time integrations the equation becomes

$$\sum_{\substack{s_1, s_2 \\ s_3, s_4 = \pm}} s_1 s_2 s_3 s_4 \iiint \iiint \iiint d\omega_1 d\omega_2 d\omega_3 d\omega_4 d\omega_5 d\omega_6 \cdot e^{-i\omega_1 t} e^{i\omega_3 t'} e^{-i\omega_4 t} e^{i\omega_6 t'}$$

$$\delta(\omega_1) \delta(-\omega_3) \delta(-\omega_4) \delta(-\omega_6)$$

$$D^{+1}(\omega_1) G^{12}(\omega_2) G^{21}(-\omega_2) D^{2-}(\omega_3) D^{+3}(\omega_4) G^{34}(-\omega_5) G^{43}(\omega_5) D^{4-}(\omega_6) .$$

We perform four integrations over the frequencies which are arguments of the delta functions.

$$\sum_{\substack{s_1, s_2 \\ s_3, s_4 = \pm}} s_1 s_2 s_3 s_4 \iint d\omega_2 d\omega_5 (D^{+1}(0) G^{12}(\omega_2) G^{21}(-\omega_2) D^{2-}(0)) (D^{+3}(0) G^{34}(-\omega_5) G^{43}(\omega_5) D^{4-}(0))$$

#### 4.1.2 Transformation of a Square-shaped Diagram

We consider the basic diagram of the square-shaped diagrams like the type of Fig. (16)(b).

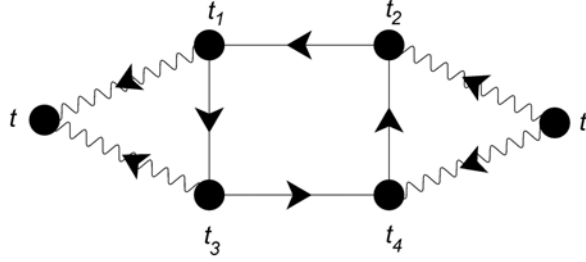


Figure 18: Basic diagram of the square-shaped diagrams.

We introduce

$$P^{s_1 s_2 s_3 s_4}(t_1, t_2, t_3, t_4) = G^{s_4 s_3}(t_4, t_3) G^{s_3 s_1}(t_3, t_1) G^{s_1 s_2}(t_1, t_2) G^{s_2 s_4}(t_2, t_4)$$

and the simpler notation. We sort the Green's functions according to the upper and lower branch in Fig. (18) and the two vertical connections.

$$\sum_{\substack{s_1, s_2 \\ s_3, s_4 = \pm}} s_1 s_2 s_3 s_4 \iiint \iiint dt_1^{s_1} dt_2^{s_2} dt_3^{s_3} dt_4^{s_4} D^{+1} G^{12} D^{2-} G^{31} G^{24} D^{+3} G^{43} D^{4-}$$

We insert the Fourier transformation of the Green's functions

$$\sum_{\substack{s_1, s_2 \\ s_3, s_4 = \pm}} s_1 s_2 s_3 s_4 \iiint \iiint dt_1 dt_2 dt_3 dt_4 \iiint \iiint \iiint d\omega_1 d\omega_2 d\omega_3 d\omega_4 d\omega_5 d\omega_6 d\omega_x d\omega_y$$

$$D^{+1}(\omega_1) e^{-i\omega_1(t-t_1)} G^{12}(\omega_2) e^{-i\omega_2(t_1-t_2)} D^{2-}(\omega_3) e^{-i\omega_3(t_2-t')} G^{31}(\omega_x) e^{-i\omega_x(t_3-t_1)}$$

$$\cdot G^{24}(\omega_y) e^{-i\omega_y(t_2-t_4)} D^{+3}(\omega_4) e^{-i\omega_4(t-t_3)} G^{43}(\omega_5) e^{-i\omega_5(t_4-t_3)} D^{4-}(\omega_6) e^{-i\omega_6(t_4-t')}$$

Which includes the time integrations

$$\int dt_1 e^{it_1(\omega_1 - \omega_2 + \omega_x)} = \delta(\omega_1 - \omega_2 + \omega_x), \quad \int dt_2 e^{it_2(\omega_2 - \omega_3 - \omega_y)} = \delta(\omega_2 - \omega_3 - \omega_y),$$

$$\int dt_3 e^{it_3(-\omega_x + \omega_4 + \omega_5)} = \delta(-\omega_x + \omega_4 + \omega_5), \quad \int dt_4 e^{it_4(\omega_y - \omega_5 - \omega_6)} = \delta(\omega_y - \omega_5 - \omega_6).$$

We perform the integration over the time arguments, four frequencies that are arguments in the delta functions and consider the case  $t = t'$ .

$$\sum_{\substack{s_1, s_2 \\ s_3, s_4 = \pm}} s_1 s_2 s_3 s_4 \iiint \iiint \iiint \iiint d\omega_1 d\omega_2 d\omega_3 d\omega_4 d\omega_5 d\omega_6 d\omega_x d\omega_y \cdot e^{-i\omega_1 t} e^{i\omega_3 t'} e^{-i\omega_4 t} e^{i\omega_6 t'}$$

$$\delta(\omega_1 - \omega_2 + \omega_x) \delta(\omega_2 - \omega_3 - \omega_y) \delta(-\omega_x + \omega_4 + \omega_5) \delta(\omega_y - \omega_5 - \omega_6)$$

$$D^{+1}(\omega_1) G^{12}(\omega_2) D^{2-}(\omega_3) G^{31}(\omega_x) G^{24}(\omega_y) D^{+3}(\omega_4) G^{43}(\omega_5) D^{4-}(\omega_6)$$

$$= \sum_{\substack{s_1, s_2 \\ s_3, s_4 = \pm}} s_1 s_2 s_3 s_4 \iiint \iiint d\omega_2 d\omega_5 d\omega_x d\omega_y \cdot e^{i(t-t')(\omega_5 - \omega_2)}$$

$$D^{+1}(\omega_2 - \omega_x) G^{12}(\omega_2) D^{2-}(\omega_2 - \omega_y) G^{31}(\omega_x) G^{24}(\omega_y)$$

$$D^{+3}(\omega_x - \omega_5) G^{43}(\omega_5) D^{4-}(\omega_y - \omega_5)$$

$$\stackrel{t=t'}{=} \sum_{\substack{s_1, s_2 \\ s_3, s_4 = \pm}} s_1 s_2 s_3 s_4 \iiint \iiint d\omega_2 d\omega_5 d\omega_x d\omega_y$$

$$D^{+1}(\omega_2 - \omega_x) G^{12}(\omega_2) D^{2-}(\omega_2 - \omega_y) G^{31}(\omega_x) G^{24}(\omega_y)$$

$$D^{+3}(\omega_x - \omega_5) G^{43}(\omega_5) D^{4-}(\omega_y - \omega_5)$$

### 4.1.3 Transformation of a Twisted-shaped Diagram

We consider the basic diagram of the twisted-shaped diagrams like the type of Fig. (16)(c).

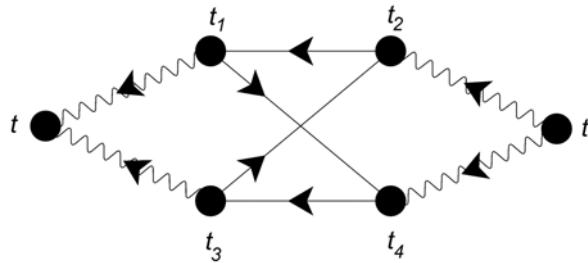


Figure 19: Basic diagram of the twisted-shaped diagrams.

Here  $P$  takes the form

$$P^{s_1 s_2 s_3 s_4}(t_1, t_2, t_3, t_4) = G^{s_4 s_1}(t_4, t_1) G^{s_1 s_2}(t_1, t_2) G^{s_2 s_3}(t_2, t_3) G^{s_3 s_4}(t_3, t_4)$$



and we use again the short notation. We also sort the Green's functions according to the upper and lower branch in Fig. (19) and the two vertical connections.

$$\sum_{\substack{s_1, s_2 \\ s_3, s_4 = \pm}} s_1 s_2 s_3 s_4 \iiint dt_1^{s_1} dt_2^{s_2} dt_3^{s_3} dt_4^{s_4} D^{+1} G^{12} D^{2-} G^{23} G^{41} D^{+3} G^{34} D^{4-}$$

We insert the Fourier transformation of the Green's functions

$$\begin{aligned} & \sum_{\substack{s_1, s_2 \\ s_3, s_4 = \pm}} s_1 s_2 s_3 s_4 \iiint dt_1 dt_2 dt_3 dt_4 \iiint \iiint \iiint d\omega_1 d\omega_2 d\omega_3 d\omega_4 d\omega_5 d\omega_6 d\omega_v d\omega_z \\ & D^{+1}(\omega_1) e^{-i\omega_1(t-t_1)} G^{12}(\omega_2) e^{-i\omega_2(t_1-t_2)} D^{2-}(\omega_3) e^{-i\omega_3(t_2-t')} G^{23}(\omega_v) e^{-i\omega_v(t_2-t_3)} \\ & \cdot G^{41}(\omega_z) e^{-i\omega_z(t_4-t_1)} D^{+3}(\omega_4) e^{-i\omega_4(t-t_3)} G^{34}(-\omega_5) e^{-i\omega_5(t_3-t_4)} D^{4-}(\omega_6) e^{-i\omega_6(t_4-t')} \end{aligned}$$

Which includes the time integrations

$$\begin{aligned} \int dt_1 e^{it_1(\omega_1 - \omega_2 + \omega_z)} &= \delta(\omega_1 - \omega_2 + \omega_z) , & \int dt_2 e^{it_2(\omega_2 - \omega_3 - \omega_v)} &= \delta(\omega_2 - \omega_3 - \omega_v) , \\ \int dt_3 e^{it_3(\omega_v + \omega_4 - \omega_5)} &= \delta(\omega_v + \omega_4 - \omega_5) , & \int dt_4 e^{it_4(-\omega_z + \omega_5 - \omega_6)} &= \delta(-\omega_z + \omega_5 - \omega_6) . \end{aligned}$$

An analog calculation leads to

$$\begin{aligned} & \sum_{\substack{s_1, s_2 \\ s_3, s_4 = \pm}} s_1 s_2 s_3 s_4 \iiint \iiint \iiint \iiint d\omega_1 d\omega_2 d\omega_3 d\omega_4 d\omega_5 d\omega_6 d\omega_v d\omega_z e^{-i\omega_1 t} e^{i\omega_3 t'} e^{-i\omega_4 t} e^{i\omega_6 t'} \\ & \delta(\omega_1 - \omega_2 + \omega_z) \delta(\omega_2 - \omega_3 - \omega_v) \delta(\omega_v + \omega_4 - \omega_5) \delta(-\omega_z + \omega_5 - \omega_6) \\ & D^{+1}(\omega_1) G^{12}(\omega_2) D^{2-}(\omega_3) G^{23}(\omega_v) G^{41}(\omega_z) D^{+3}(\omega_4) G^{34}(-\omega_5) D^{4-}(\omega_6) \\ = & \sum_{s_1, s_2, s_3, s_4 = \pm} s_1 s_2 s_3 s_4 \iiint \iiint d\omega_2 d\omega_5 d\omega_v d\omega_z e^{-i(\omega_2 - \omega_z + \omega_5 - \omega_v)(t-t')} \\ & D^{+1}(\omega_2 - \omega_z) G^{12}(\omega_2) D^{2-}(\omega_2 - \omega_v) G^{23}(\omega_v) G^{41}(\omega_z) \\ & D^{+3}(\omega_5 - \omega_v) G^{34}(-\omega_5) D^{4-}(\omega_5 - \omega_z) \\ \stackrel{t=t'}{=} & \sum_{s_1, s_2, s_3, s_4 = \pm} s_1 s_2 s_3 s_4 \iiint \iiint d\omega_2 d\omega_5 d\omega_v d\omega_z \\ & D^{+1}(\omega_2 - \omega_z) G^{12}(\omega_2) D^{2-}(\omega_2 - \omega_v) G^{23}(\omega_v) G^{41}(\omega_z) \\ & D^{+3}(\omega_5 - \omega_v) G^{34}(-\omega_5) D^{4-}(\omega_5 - \omega_z) \end{aligned}$$

### Summation Over Inner Time Arguments

The summation of  $s_1$  to  $s_4$  leads to 16 different combinations. So we first look for some simplifications. Since we consider the whole system at zero temperature the bosonic lesser Green's function becomes zero.

$$D_{a,b}^{+-}(\omega_i) = -in_{a,b}\delta(\omega_i - \omega_{a,b}) \underset{T=0}{=} 0$$

This simplify the calculations a lot. The integral for all types of diagrams includes the multiplication of the four bosonic functions  $D^{+1}D^{2-}D^{+3}D^{4-}$ . The expression  $D^{+-} = 0$  occurs in the case of  $1 = -, 2 = +, 3 = -$  or  $4 = +$ . Hence the only remaining combination is  $1 = +, 2 = -, 3 = +$  and  $4 = -$ . This determines the four bosonic Green's functions to  $D^{++}D^{--}D^{++}D^{--}$ . The distribution of the indices of the fermionic Green's functions depends on each diagram.

Until now, we have done the perturbative expansion using the Keldysh nonequilibrium Green's function technique which ended up in an integration of Keldysh Green's functions over several contour time arguments. We transformed these equations to an integration in the real time space by parameterizing the contour. We replaced the Green's functions in the integration with their Fourier transformations and receive now an integral in the frequency domain. We determine the integrals in the frequency domain of all diagrams in the same way as before. The only varying part is the direction of the fermionic Green's function and their components. After we determined these terms we insert the indices  $1 = +, 2 = -, 3 = +$  and  $4 = -$  and sort the integral according to the different dependencies on  $\omega_i$ .

The seven remaining diagrams are shown in Fig. (20).

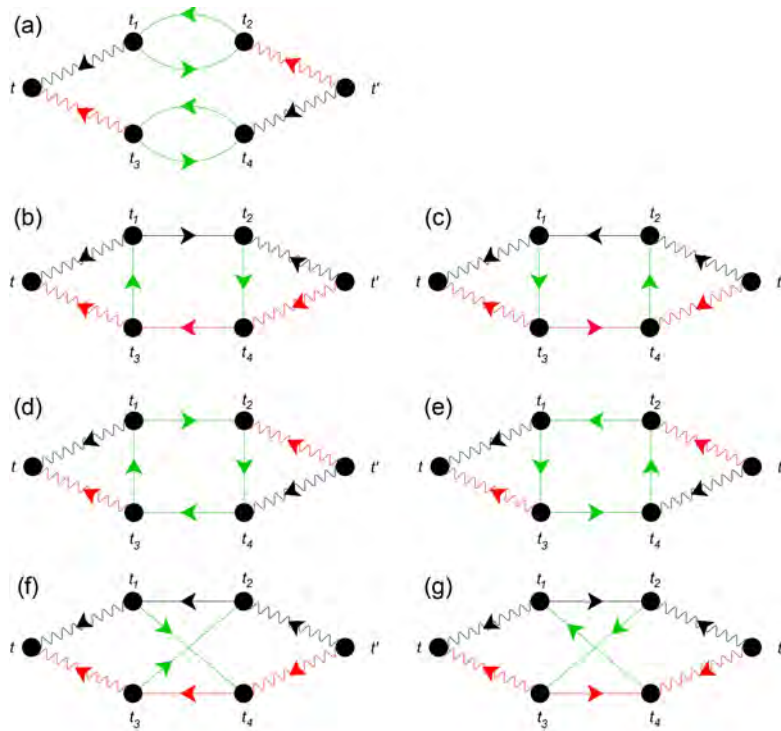


Figure 20: All diagrams for the calculation of the covariance

The integrals in the frequency domain of the seven diagrams read:

Diagram Fig. (20)(a)

$$\iint d\omega_2 d\omega_5 D_a^{++}(0)D_a^{--}(0)D_b^{++}(0)D_b^{--}(0) \\ G_{12}^{+-}(\omega_2)G_{21}^{-+}(-\omega_2)G_{21}^{+-}(-\omega_5)G_{12}^{-+}(\omega_5)$$

Diagram Fig. (20)(b)

$$\iint d\omega_x d\omega_y G_{12}^{++}(-\omega_x)G_{21}^{--}(-\omega_y) \\ \int d\omega_2 D_a^{++}(\omega_2 - \omega_x)G_{11}^{-+}(-\omega_2)D_a^{--}(\omega_2 - \omega_y) \\ \int d\omega_5 D_b^{++}(\omega_x - \omega_5)G_{22}^{+-}(-\omega_5)D_b^{--}(\omega_y - \omega_5)$$

Diagram Fig. (20)(c)

$$\iint d\omega_x d\omega_y G_{21}^{++}(\omega_x)G_{12}^{--}(\omega_y) \\ \int d\omega_2 D_a^{++}(\omega_2 - \omega_x)G_{11}^{+-}(\omega_2)D_a^{--}(\omega_2 - \omega_y) \\ \int d\omega_5 D_b^{++}(\omega_x - \omega_5)G_{22}^{+-}(\omega_5)D_b^{--}(\omega_y - \omega_5)$$

Diagram Fig. (20)(d)

$$\iint d\omega_x d\omega_y G_{12}^{++}(-\omega_x)G_{12}^{--}(-\omega_y) \\ \int d\omega_2 D_a^{++}(\omega_2 - \omega_x)G_{21}^{-+}(-\omega_2)D_b^{--}(\omega_2 - \omega_y) \\ \int d\omega_5 D_b^{++}(\omega_x - \omega_5)G_{21}^{+-}(-\omega_5)D_a^{--}(\omega_y - \omega_5)$$

Diagram Fig. (20)(e)

$$\iint d\omega_x d\omega_y G_{21}^{++}(\omega_x)G_{21}^{--}(\omega_y) \\ \int d\omega_2 D_a^{++}(\omega_2 - \omega_x)G_{12}^{+-}(\omega_2)D_b^{--}(\omega_2 - \omega_y) \\ \int d\omega_5 D_b^{++}(\omega_x - \omega_5)G_{12}^{-+}(\omega_5)D_a^{--}(\omega_y - \omega_5)$$

Diagram Fig. (20)(f)

$$\iint d\omega_v d\omega_z G_{12}^{-+}(\omega_v)G_{21}^{-+}(\omega_z) \\ \int d\omega_2 D_a^{++}(\omega_2 - \omega_z)G_{11}^{+-}(\omega_2)D_a^{--}(\omega_2 - \omega_v) \\ \int d\omega_5 D_b^{++}(\omega_5 - \omega_v)G_{22}^{+-}(-\omega_5)D_b^{--}(\omega_5 - \omega_z)$$

Diagram Fig. (20)(g)

$$\iint d\omega_v d\omega_z G_{21}^{+-}(-\omega_v)G_{12}^{-+}(-\omega_z) \\ \int d\omega_2 D_a^{++}(\omega_2 - \omega_z)G_{11}^{-+}(-\omega_2)D_a^{--}(\omega_2 - \omega_v) \\ \int d\omega_5 D_b^{++}(\omega_5 - \omega_v)G_{22}^{+-}(\omega_5)D_b^{--}(\omega_5 - \omega_z)$$

## 4.2 Integration at the Example of a Square-Shaped Diagram

Exemplary for all diagrams, except for the first bubble-diagram, we do the integration for the diagram 20 (c). We sorted the Green's functions according to the different integration variables. As a first step we do the integration over  $\omega_5$  analytically. Afterwards we transfer the calculation to the integration over  $\omega_2$ .

$$\begin{aligned} & \iint d\omega_x d\omega_y G_{21}^{++}(\omega_x) G_{12}^{--}(\omega_y) \\ & \int d\omega_2 D_a^{++}(\omega_2 - \omega_x) G_{11}^{+-}(\omega_2) D_a^{--}(\omega_2 - \omega_y) \\ & \int d\omega_5 D_b^{++}(\omega_x - \omega_5) G_{22}^{+-}(\omega_5) D_b^{--}(\omega_y - \omega_5) \end{aligned}$$

### Integration over $\omega_5$

We start with the integration over  $\omega_5$ . We insert the bosonic Green's functions, consisting of a principle part and a delta function, and the fermionic Green's function. The expression can be divided in four parts. Three of these parts contain a delta function which makes the integration really easy. The complicated part is the integration of the two principle parts multiplied with the fermionic Green's function.

$$\begin{aligned} I_5(\omega_x, \omega_y) &= \int d\omega_5 D_b^{++}(\omega_x - \omega_5) G_{22}^{+-}(\omega_5) D_b^{--}(\omega_y - \omega_5) \\ &= \int d\omega_5 \frac{i\Gamma \left[ ((\omega_5 - \varepsilon)^2 + \Gamma^2 (1 - \cos^2 \frac{\varphi}{2})) (f_L + f_R - 2) - \Gamma(\omega_5 - \varepsilon) \sin \varphi (f_L - f_R) \right]}{\left( (\omega_5 - \varepsilon)^2 + \Gamma^2 (1 + \cos^2 \frac{\varphi}{2}) \right)^2 - 4\Gamma^4 \cos^2 \frac{\varphi}{2}} \\ & \quad \cdot \left[ P \left( \frac{1}{\omega_x - \omega_5 - \omega_b} \right) - i\pi\delta(\omega_x - \omega_5 - \omega_b) \right] \cdot \left[ -P \left( \frac{1}{\omega_y - \omega_5 - \omega_b} \right) - i\pi\delta(\omega_y - \omega_5 - \omega_b) \right] \\ &= \int d\omega_5 \frac{i\Gamma \left[ ((\omega_5 - \varepsilon)^2 + \Gamma^2 (1 - \cos^2 \frac{\varphi}{2})) (f_L + f_R - 2) - \Gamma(\omega_5 - \varepsilon) \sin \varphi (f_L - f_R) \right]}{\left( (\omega_5 - \varepsilon)^2 + \Gamma^2 (1 + \cos^2 \frac{\varphi}{2}) \right)^2 - 4\Gamma^4 \cos^2 \frac{\varphi}{2}} \\ & \quad \left[ -P \left( \frac{1}{\omega_x - \omega_5 - \omega_b} \right) P \left( \frac{1}{\omega_y - \omega_5 - \omega_b} \right) - P \left( \frac{1}{\omega_x - \omega_5 - \omega_b} \right) i\pi\delta(\omega_y - \omega_5 - \omega_b) \right. \\ & \quad \left. + P \left( \frac{1}{\omega_y - \omega_5 - \omega_b} \right) i\pi\delta(\omega_x - \omega_5 - \omega_b) + i\pi\delta(\omega_x - \omega_5 - \omega_b) i\pi\delta(\omega_y - \omega_5 - \omega_b) \right] \end{aligned}$$

### 4.2.1 Integral Containing Two Principal Values

Since the integration of the delta functions is quiet easy we focus first on the complicated part containing the two principle values.

$$I_5(\omega_x, \omega_y) = - \int d\omega_5 P \left( \frac{1}{\omega_x - \omega_5 - \omega_b} \right) P \left( \frac{1}{\omega_y - \omega_5 - \omega_b} \right) \cdot \frac{i\Gamma \left[ ((\omega_5 - \varepsilon)^2 + \Gamma^2 (1 - \cos^2 \frac{\varphi}{2})) (f_L + f_R - 2) - \Gamma(\omega_5 - \varepsilon) \sin \varphi (f_L - f_R) \right]}{\left( (\omega_5 - \varepsilon)^2 + \Gamma^2 (1 + \cos^2 \frac{\varphi}{2}) \right)^2 - 4\Gamma^4 \cos^2 \frac{\varphi}{2}}$$

To solve the integral we express the principle value as

$$P \left( \frac{1}{x} \right) = \lim_{\Delta \rightarrow 0} \frac{x}{x^2 + \Delta^2} .$$

Furthermore we transform the denominator

$$\begin{aligned} & \left( (\omega_5 - \varepsilon)^2 + \Gamma^2 \left( 1 + \cos^2 \frac{\varphi}{2} \right) \right)^2 - 4\Gamma^4 \cos^2 \frac{\varphi}{2} \\ &= \left( (\omega_5 - \varepsilon)^2 + \Gamma^2 \left( 1 - \cos^2 \frac{\varphi}{2} \right) \right)^2 \cdot \left( (\omega_5 - \varepsilon)^2 + \Gamma^2 \left( 1 + \cos^2 \frac{\varphi}{2} \right) \right)^2 . \end{aligned}$$

So the integration becomes

$$\begin{aligned} I_5(\omega_x, \omega_y) &= \\ & \lim_{\Delta \rightarrow 0} - \int d\omega_5 \frac{i\Gamma \left[ ((\omega_5 - \varepsilon)^2 + \Gamma^2 (1 - \cos^2 \frac{\varphi}{2})) (f_L + f_R - 2) - \Gamma(\omega_5 - \varepsilon) \sin \varphi (f_L - f_R) \right]}{\left( (\omega_5 - \varepsilon)^2 + \Gamma^2 (1 - \cos^2 \frac{\varphi}{2}) \right)^2 \cdot \left( (\omega_5 - \varepsilon)^2 + \Gamma^2 (1 + \cos^2 \frac{\varphi}{2}) \right)^2} \\ & \cdot \frac{\omega_x - \omega_5 - \omega_b}{(\omega_x - \omega_5 - \omega_b)^2 + \Delta^2} \cdot \frac{\omega_y - \omega_5 - \omega_b}{(\omega_y - \omega_5 - \omega_b)^2 + \Delta^2} . \end{aligned}$$

We define new variables to simplify the expression

$$\Omega_x^\pm = \omega_x \pm \omega_b, \quad \Omega_y^\pm = \omega_y \pm \omega_b \quad \text{and} \quad \Lambda_\pm = \Gamma \left( 1 \pm \cos^2 \frac{\varphi}{2} \right) .$$

The nominator of the fermionic Green's function can be splitted in three parts, whereby each of them depends on a different order of  $(\omega_5 - \varepsilon)$ . Since we want to perform a partial fraction decomposition in  $\omega_5$ , we consider each of these parts individually. If the integrand contains the Fermi-function, the upper integration limit will be changed. In the case of  $f_{L,R}$  to  $\pm eV/2$ . We will see later that the part that contains the factor "-2" but no Fermi function cancels, so we ignore it at the moment and come back to it later. The integration over  $\omega_5$  contains now three different integrals  $I_1$ ,  $I_2$  and  $I_3$  with different factors. Each  $I_i$  will be determined through a partial fraction decomposition.

$$\begin{aligned} I_5(\omega_x, \omega_y) &= -i\Gamma \left[ I_1 \mp \Gamma \sin \varphi \cdot I_2 + \Gamma^2 \sin^2 \frac{\varphi}{2} \cdot I_3 \right] \\ I_1 &= \lim_{\Delta \rightarrow 0} \int_{-\infty}^{\pm eV/2} d\omega_5 \frac{\Omega_x^- - \omega_5}{(\Omega_x^- - \omega_5)^2 + \Delta^2} \cdot \frac{\Omega_y^- - \omega_5}{(\Omega_y^- - \omega_5)^2 + \Delta^2} \cdot \frac{(\omega_5 - \varepsilon)}{((\omega_5 - \varepsilon)^2 + \Lambda_-^2)} \cdot \frac{(\omega_5 - \varepsilon)}{((\omega_5 - \varepsilon)^2 + \Lambda_+^2)} \end{aligned}$$

$$I_2 = \lim_{\Delta \rightarrow 0} \int_{-\infty}^{\pm eV/2} d\omega_5 \frac{\Omega_x^- - \omega_5}{(\Omega_x^- - \omega_5)^2 + \Delta^2} \cdot \frac{\Omega_y^- - \omega_5}{(\Omega_y^- - \omega_5)^2 + \Delta^2} \cdot \frac{(\omega_5 - \varepsilon)}{((\omega_5 - \varepsilon)^2 + \Lambda_-^2)} \cdot \frac{1}{((\omega_5 - \varepsilon)^2 + \Lambda_+^2)}$$

$$I_3 = \lim_{\Delta \rightarrow 0} \int_{-\infty}^{\pm eV/2} d\omega_5 \frac{\Omega_x^- - \omega_5}{(\Omega_x^- - \omega_5)^2 + \Delta^2} \cdot \frac{\Omega_y^- - \omega_5}{(\Omega_y^- - \omega_5)^2 + \Delta^2} \cdot \frac{1}{((\omega_5 - \varepsilon)^2 + \Lambda_-^2)} \cdot \frac{1}{((\omega_5 - \varepsilon)^2 + \Lambda_+^2)}$$

We perform this partial fraction decomposition for each of the four factors inside each  $I_i$ , multiply them and repeat the partial fraction decomposition until we have decomposed the complete expression. The partial fraction decomposition of  $I_1$  to  $I_3$  differ only in the coefficients of the decomposition. Therefore the integration of the decomposition is equal in all three cases except for the coefficients. We label the coefficients of the decomposition of the different integrals with

$$a_i \rightarrow I_1, b_i \rightarrow I_2 \text{ and } c_i \rightarrow I_3 .$$

We calculate the partial fraction decomposition exemplary for  $I_1$ .

$$\begin{aligned} & \frac{\omega_5 - \Omega_{\omega_5}^-}{(\omega_5 - \Omega_{\omega_5}^-)^2 + \Delta^2} \cdot \frac{\omega_5 - \Omega_{\Delta}^-}{(\omega_5 - \Omega_{\Delta}^-)^2 + \Delta^2} \cdot \frac{\omega_5 - \varepsilon}{(\omega_5 - \varepsilon)^2 + \Lambda_+^2} \cdot \frac{\omega_5 - \varepsilon}{(\omega_5 - \varepsilon)^2 + \Lambda_-^2} \\ &= \frac{a_1}{\omega_5 - (\Omega_{\omega_5}^- + i\Delta)} + \frac{a_2}{\omega_5 - (\Omega_{\omega_5}^- - i\Delta)} + \frac{a_3}{\omega_5 - (\Omega_{\Delta}^- + i\Delta)} + \frac{a_4}{\omega_5 - (\Omega_{\Delta}^- - i\Delta)} \\ &+ \frac{a_5}{\omega_5 - (\varepsilon + i\Lambda_+)} + \frac{a_6}{\omega_5 - (\varepsilon - i\Lambda_+)} + \frac{a_7}{\omega_5 - (\varepsilon + i\Lambda_-)} + \frac{a_8}{\omega_5 - (\varepsilon - i\Lambda_-)} \\ &= \frac{\omega_5(a_1 + a_2) - \Omega_{\omega_5}^-(a_1 + a_2) + i\Delta(a_1 - a_2)}{(\omega_5 - \Omega_{\omega_5}^-)^2 + \Delta^2} + \frac{\omega_5(a_3 + a_4) - \Omega_{\Delta}^-(a_3 + a_4) + i\Delta(a_3 - a_4)}{(\omega_5 - \Omega_{\Delta}^-)^2 + \Delta^2} \\ &+ \frac{\omega_5(a_5 + a_6) - \varepsilon(a_5 + a_6) + i\Lambda_+(a_5 - a_6)}{(\omega_5 - \varepsilon)^2 + \Lambda_+^2} + \frac{\omega_5(a_7 + a_8) - \varepsilon(a_7 + a_8) + i\Lambda_-(a_7 - a_8)}{(\omega_5 - \varepsilon)^2 + \Lambda_-^2} \end{aligned}$$

With the indefinite integrals

$$\boxed{\begin{aligned} \int dx \frac{x}{(x - x_i)^2 + y^2} &= \frac{x_i}{y} \arctan\left(\frac{x - x_i}{y}\right) + \frac{1}{2} \log((x - x_i)^2 + y^2) , \\ \int dx \frac{1}{(x - x_i)^2 + y^2} &= \frac{1}{y} \arctan\left(\frac{x - x_i}{y}\right) , \end{aligned}}$$

we obtain for the integration for example of the first addend:

$$\lim_{\Delta \rightarrow 0} \int_{-\infty}^{\pm eV/2} d\omega_5 \frac{\omega_5(a_1 + a_2) - \Omega_{\omega_5}^-(a_1 + a_2) + i\Delta(a_1 - a_2)}{(\omega_5 - \Omega_{\omega_5}^-)^2 + \Delta^2}$$

$$\begin{aligned}
 &= \lim_{\Delta \rightarrow 0} \left[ (a_1 + a_2) \left( \frac{\Omega_x^-}{\Delta} \arctan \left( \frac{\omega_5 - \Omega_x^-}{\Delta} \right) + \frac{1}{2} \log \left( (\omega_5 - \Omega_x^-)^2 + \Delta^2 \right) - \frac{\Omega_x^-}{\Delta} \arctan \left( \frac{\omega_5 - \Omega_x^-}{\Delta} \right) \right) \right. \\
 &\quad \left. + i(a_1 - a_2) \arctan \frac{\omega_5 - \Omega_x^-}{\Delta} \right]_{-\infty}^{\pm eV/2} \\
 &= \lim_{\Delta \rightarrow 0} (a_1 + a_2) \frac{1}{2} \log \left( (\omega_5 - \Omega_x^-)^2 + \Delta^2 \right) \Big|_{-\infty}^{\pm eV/2}
 \end{aligned}$$

The first and second arctan-term cancel each other and since the factor  $a_1 - a_2$  is zero it cancels the third arctan-term. The difference of the corresponding coefficients of the other three addends is also zero. The identical calculation for the other addends with different coefficients  $a_i$  leads to complete expression of  $I_1$

$$\begin{aligned}
 I_1 = \lim_{\Delta \rightarrow 0} -\frac{i\Gamma}{2} \Big[ &(a_1 + a_2) \log \left( (x - \Omega_x^-)^2 + \Delta^2 \right) + (a_3 + a_4) \log \left( (x - \Omega_\Delta^-)^2 + \Delta^2 \right) \\
 &+ (a_5 + a_6) \log \left( (x - \varepsilon)^2 + \Lambda_+^2 \right) + (a_7 + a_8) \log \left( (x - \varepsilon)^2 + \Lambda_-^2 \right) \Big]_{-\infty}^{\pm eV/2}
 \end{aligned}$$

Since  $\Omega_x^- = \omega_x - \omega_b$ ,  $\Omega_y^- = \omega_y - \omega_b$ ,  $\varepsilon$  and  $\Lambda_\pm = \Gamma(1 \pm \cos \frac{\varphi}{2})$  are small compared to  $\infty$  we can summarize all logarithmic terms with the upper integration limit as its argument.

$$\begin{aligned}
 &(a_1 + a_2) \log \left( (-\infty - x_1)^2 + y^2 \right) + (a_3 + a_4) \log \left( (-\infty - x_2)^2 + y^2 \right) \\
 &+ (a_5 + a_6) \log \left( (-\infty - x_3)^2 + \lambda^2 \right) + (a_7 + a_8) \log \left( (-\infty - x_3)^2 + \bar{\lambda}^2 \right)
 \end{aligned}$$

In the limit  $y \rightarrow 0$  the sum of all factors is zero and the logarithmic term evaluated at the upper integration limit cancels. Now we remember that the initial integral also contained a part without a Fermi function. In this case both integration limits would be infinity and therefore both terms would be canceled because the sum of coefficients is zero. This also applies for the coefficients of  $I_2$  and  $I_3$ .

$$\sum_{i=1}^8 a_i = \sum_{i=1}^8 b_i = \sum_{i=1}^8 c_i = 0$$

Furthermore the differences such as  $a_1 - a_2$  are also zero for the coefficients  $b_i$  and  $c_i$ .

The complete integration then reads

$$\begin{aligned}
 I_5(\omega_x, \omega_y) &= -i\Gamma \left[ I_1 \mp \Gamma \sin \varphi \cdot I_2 + \Gamma^2 \sin^2 \frac{\varphi}{2} \cdot I_3 \right] \\
 &= -\frac{1}{2} i\Gamma \left[ \left( a_1 + a_1 \mp \Gamma \sin \varphi (b_1 + b_2) + \Gamma^2 \left( 1 - \cos^2 \frac{\varphi}{2} \right) (c_1 + c_2) \right) \log \left( (\pm eV/2 - \Omega_x^-)^2 \right) \right. \\
 &\quad + \left( a_3 + a_4 \mp \Gamma \sin \varphi (b_3 + b_4) + \Gamma^2 \left( 1 - \cos^2 \frac{\varphi}{2} \right) (c_3 + c_4) \right) \log \left( (\pm eV/2 - \Omega_y^-)^2 \right) \\
 &\quad + \left( a_5 + a_6 \mp \Gamma \sin \varphi (b_5 + b_6) + \Gamma^2 \left( 1 - \cos^2 \frac{\varphi}{2} \right) (c_5 + c_6) \right) \log \left( (\pm eV/2 - \varepsilon)^2 + \Lambda_-^2 \right) \\
 &\quad \left. + \left( a_7 + a_8 \mp \Gamma \sin \varphi (b_7 + b_8) + \Gamma^2 \left( 1 - \cos^2 \frac{\varphi}{2} \right) (c_7 + c_8) \right) \log \left( (\pm eV/2 - \varepsilon)^2 + \Lambda_+^2 \right) \right], \tag{4.1}
 \end{aligned}$$

whereby we still have to sum up the parts with the upper and lower sign.

### 4.2.2 Integration of Components Containing Delta Functions

The full integration over  $\omega_5$  contains four integrands from which three contain a delta function. Additionally, they contain a Fermi function which changes the integration limits. Therefore the integration of the delta function will give additional Heaviside functions. Using the indefinite integral

$$\int_a^b f(x)\delta(x-c) = f(c)\Theta(c-a)\Theta(b-c), \text{ the fact that } \Theta(c-(-\infty)) = 1 ,$$

the previously introduced variables  $\Omega_{x,y}^- = \omega_{x,y} - \omega_b$  and  $\Lambda_{\pm} = \Gamma(1 \pm \cos^2 \frac{\varphi}{2})$  the integration of one of these diagrams becomes

$$\begin{aligned} & \int d\omega_5 P \left( \frac{1}{\omega_y - \omega_5 - \omega_b} \right) i\pi \delta(\omega_x - \omega_5 - \omega_b) \\ & \cdot \frac{i\Gamma \left[ ((\omega_5 - \varepsilon)^2 + \Gamma^2 (1 - \cos^2 \frac{\varphi}{2})) (f_L + f_R - 2) - \Gamma(\omega_5 - \varepsilon) \sin \varphi (f_L - f_R) \right]}{((\omega_5 - \varepsilon)^2 + \Gamma^2 (1 + \cos^2 \frac{\varphi}{2}))^2 - 4\Gamma^4 \cos^2 \frac{\varphi}{2}} \\ & = -P \left( \frac{1}{\Omega_y^- - \Omega_x^-} \right) \cdot \frac{\Gamma\pi}{((\Omega_x^- - \varepsilon)^2 + \Lambda_+^2) ((\Omega_x^- - \varepsilon)^2 + \Lambda_-^2)} \\ & \cdot \left[ (\Theta(eV/2 - \Omega_x^-) + \Theta(-eV/2 - \Omega_x^-) - 2) \left( (\Omega_x^- - \varepsilon)^2 + \Gamma^2 \left( 1 - \cos^2 \frac{\varphi}{2} \right) \right) \right. \\ & \left. - (\Theta(eV/2 - \Omega_x^-) - \Theta(-eV/2 - \Omega_x^-)) \Gamma(\Omega_x^- - \varepsilon) \sin \varphi \right] \end{aligned} \quad (4.2)$$

A similar calculation solves the integration of the other two components.

### Integration over $\omega_2$

Since the integrands of the integration over  $\omega_5$  and  $\omega_2$  are similar, it is easy to use the definite integral that we just have calculated and change only some variables and factors. For this purpose we compare in each case the bosonic and fermionic Green's functions. The two integrals read

$$\begin{aligned} I_5(\omega_x, \omega_y) &= \int d\omega_5 D_b^{++}(\omega_x - \omega_5) G_{22}^{-+}(\omega_5) D_b^{--}(\omega_y - \omega_5) \\ I_2(\omega_x, \omega_y) &= \int d\omega_2 D_a^{++}(\omega_2 - \omega_x) G_{11}^{+-}(\omega_2) D_a^{--}(\omega_2 - \omega_y) \end{aligned}$$

The bosonic Green's functions consists of a principle part and a delta function. Their argument at  $D_b^{++}(\omega_x - \omega_5)$  and  $D_b^{--}(\omega_y - \omega_5)$  is  $\Omega_{x,y}^- - \omega_5$ .

In the case of  $D_a^{++}(\omega_2 - \omega_x)$  and  $D_a^{--}(\omega_2 - \omega_y)$  it changes to  $\omega_2 - \Omega_{x,y}^+$ . The delta function is symmetric about the y-axis and the principle part is symmetric about the zero point which means

$$\delta(x) = \delta(-x), \text{ and } P \left( \frac{1}{x} \right) = -P \left( \frac{1}{-x} \right) .$$



The two fermionic Green's functions read

$$G_{22}^{-+}(\omega_5) = i\Gamma \frac{[(\omega_5 - \varepsilon)^2 + \Gamma^2 (1 - \cos^2 \frac{\varphi}{2})] (f_L + f_R - 2) - \Gamma(\omega_5 - \varepsilon) \sin \varphi (f_L - f_R)}{((\omega_5 - \varepsilon)^2 + \Gamma^2 (1 + \cos^2 \frac{\varphi}{2}))^2 - 4\Gamma^4 \cos^2 \frac{\varphi}{2}}$$

$$G_{11}^{+-}(\omega_2) = i\Gamma \frac{[(\omega_2 - \varepsilon)^2 + \Gamma^2 (1 - \cos^2 \frac{\varphi}{2})] (f_L + f_R) + \Gamma(\omega_2 - \varepsilon) \sin \varphi (f_L - f_R)}{((\omega_2 - \varepsilon)^2 + \Gamma^2 (1 + \cos^2 \frac{\varphi}{2}))^2 - 4\Gamma^4 \cos^2 \frac{\varphi}{2}}$$

The only difference is an additional factor "-2" in  $G_{22}^{-+}(\omega_5)$ , which drops out at the integration, and the sign of the last term proportional to  $f_L - f_R$  changes.

Therefore we are able to use the definite integral of the integration over  $\omega_5$  and change the variables  $\Omega_{x,y}^- \rightarrow \Omega_{x,y}^+$  and the sign of the principle values as well as the sign of the latter part of the fermionic Green's function. It should be kept in mind that, due to the different resonance frequencies of the cavities, the originally defined variable  $\Omega_{x,y}^\pm = \omega_{x,y} \pm \omega_b$  changes to  $\Omega_{x,y}^\pm = \omega_{x,y} \pm \omega_a$ . To keep things simple we don't observe this fact hereinafter but it is easy to reintroduce if it's required.

### 4.2.3 Full Analytical Integral

Now we recompose the expression of the integration over  $\omega_5$  and  $\omega_2$ . For this we insert all coefficients of the partial fraction decomposition in equation (4.1) and summarize the integrations containing a delta function similar to equation (4.2). Then we add the same parts again and apply the modifications that we have developed in the chapter before. To obtain the full expression we add the integral over  $\omega_x$  and  $\omega_y$  and the two remaining fermionic Green's functions. It should be noted that the following equations contain several  $\pm$ , or  $\mp$ . To obtain the full expression the equations with the upper sign have to be added to the one with the lower sign.

$$\iint d\omega_x d\omega_y G_{21}^{++}(\omega_x) G_{12}^{--}(\omega_y)$$

$$\int d\omega_2 D_a^{++}(\omega_2 - \omega_x) G_{11}^{+-}(\omega_2) D_a^{--}(\omega_2 - \omega_y)$$

$$\int d\omega_5 D_b^{++}(\omega_x - \omega_5) G_{22}^{-+}(\omega_5) D_b^{--}(\omega_y - \omega_5)$$

$$\begin{aligned}
 &= \iint d\omega_x d\omega_y \frac{i\Gamma}{((\omega_x - \varepsilon)^2 + \Lambda_+^2) ((\omega_x - \varepsilon)^2 + \Lambda_-^2) ((\omega_y - \varepsilon)^2 + \Lambda_+^2) ((\omega_y - \varepsilon)^2 + \Lambda_-^2)} \\
 &\cdot \left[ (\omega_x - \varepsilon)^2 \left( e^{-i\frac{\varphi}{2}} f_L + e^{i\frac{\varphi}{2}} f_R \right) - \Gamma^2 \sin^2 \frac{\varphi}{2} (f_L e^{-i\frac{\varphi}{2}} + f_R e^{i\frac{\varphi}{2}}) - \cos \frac{\varphi}{2} \left[ (\omega_x - \varphi - i\Gamma)^2 + \Gamma^2 \cos^2 \frac{\varphi}{2} \right] \right] \\
 &\cdot \left[ (\omega_y - \varepsilon)^2 \left( e^{i\frac{\varphi}{2}} f_L + e^{-i\frac{\varphi}{2}} f_R \right) - \Gamma^2 \sin^2 \frac{\varphi}{2} (f_L e^{i\frac{\varphi}{2}} + f_R e^{-i\frac{\varphi}{2}}) - \cos \frac{\varphi}{2} \left[ (\omega_y - \varphi + i\Gamma)^2 + \Gamma^2 \cos^2 \frac{\varphi}{2} \right] \right] \\
 &\left[ -\frac{1}{2} \log((\pm eV/2 - \Omega_x^+)^2) \frac{(\Omega_x^+ - \varepsilon)^2 \mp i\Gamma \sin \varphi \frac{(\Lambda_+ \Lambda_- - (\Omega_x^+ - \varepsilon)^2)}{\Lambda_+ + \Lambda_-} + \Gamma^2 \sin^2 \frac{\varphi}{2}}{(\Omega_x^+ - \Omega_y^+) ((\Omega_x^+ - \varepsilon)^2 + \Lambda_+^2) \cdot ((\Omega_x^+ - \varepsilon)^2 + \Lambda_-^2)} \right. \\
 &+ \frac{1}{2} \log((\pm eV/2 - \Omega_y^+)^2) \frac{(\Omega_y^+ - \varepsilon)^2 \mp i\Gamma \sin \varphi \frac{(\Lambda_+ \Lambda_- - (\Omega_y^+ - \varepsilon)^2)}{\Lambda_+ + \Lambda_-} + \Gamma^2 \sin^2 \frac{\varphi}{2}}{(\Omega_x^+ - \Omega_y^+) ((\Omega_y^+ - \varepsilon)^2 + \Lambda_+^2) \cdot ((\Omega_y^+ - \varepsilon)^2 + \Lambda_-^2)} \\
 &+ \frac{1}{2} \log((\pm eV/2 - \varepsilon)^2 + \Lambda_-^2) \frac{[(\Omega_y^+ - \varepsilon)^2 - (\Omega_x^+ - \varepsilon)^2] \cdot [\Lambda_+^2 \pm i\Gamma \sin \varphi \Lambda_+ + \Gamma^2 \sin^2 \frac{\varphi}{2}]}{(\Omega_x^+ - \Omega_y^+) (\Lambda_+^2 - \Lambda_-^2) ((\Omega_x^+ - \varepsilon)^2 + \Lambda_+^2) \cdot ((\Omega_y^+ - \varepsilon)^2 + \Lambda_+^2)} \\
 &- \frac{1}{2} \log((\pm eV/2 - \varepsilon)^2 + \Lambda_+^2) \frac{[(\Omega_y^+ - \varepsilon)^2 - (\Omega_x^+ - \varepsilon)^2] \cdot [\Lambda_-^2 \pm i\Gamma \sin \varphi \Lambda_- + \Gamma^2 \sin^2 \frac{\varphi}{2}]}{(\Omega_x^+ - \Omega_y^+) (\Lambda_+^2 - \Lambda_-^2) ((\Omega_x^+ - \varepsilon)^2 + \Lambda_-^2) \cdot ((\Omega_y^+ - \varepsilon)^2 + \Lambda_-^2)} \\
 &- \frac{1}{2} \log((\pm eV/2 - \Omega_x^-)^2) \frac{(\Omega_x^- - \varepsilon)^2 \pm i\Gamma \sin \varphi \frac{(\Lambda_+ \Lambda_- - (\Omega_x^- - \varepsilon)^2)}{\Lambda_+ + \Lambda_-} + \Gamma^2 \sin^2 \frac{\varphi}{2}}{(\Omega_x^- - \Omega_y^-) ((\Omega_x^- - \varepsilon)^2 + \Lambda_+^2) \cdot ((\Omega_x^- - \varepsilon)^2 + \Lambda_-^2)} \\
 &+ \frac{1}{2} \log((\pm eV/2 - \Omega_y^-)^2) \frac{(\Omega_y^- - \varepsilon)^2 \pm i\Gamma \sin \varphi \frac{(\Lambda_+ \Lambda_- - (\Omega_y^- - \varepsilon)^2)}{\Lambda_+ + \Lambda_-} + \Gamma^2 \sin^2 \frac{\varphi}{2}}{(\Omega_x^- - \Omega_y^-) ((\Omega_y^- - \varepsilon)^2 + \Lambda_+^2) \cdot ((\Omega_y^- - \varepsilon)^2 + \Lambda_-^2)} \\
 &+ \frac{1}{2} \log((\pm eV/2 - \varepsilon)^2 + \Lambda_-^2) \frac{[(\Omega_y^- - \varepsilon)^2 - (\Omega_x^- - \varepsilon)^2] \cdot [\Lambda_+^2 \mp i\Gamma \sin \varphi \Lambda_+ + \Gamma^2 \sin^2 \frac{\varphi}{2}]}{(\Omega_x^- - \Omega_y^-) (\Lambda_+^2 - \Lambda_-^2) ((\Omega_x^- - \varepsilon)^2 + \Lambda_+^2) \cdot ((\Omega_y^- - \varepsilon)^2 + \Lambda_+^2)} \\
 &- \frac{1}{2} \log((\pm eV/2 - \varepsilon)^2 + \Lambda_+^2) \frac{[(\Omega_y^- - \varepsilon)^2 - (\Omega_x^- - \varepsilon)^2] \cdot [\Lambda_-^2 \mp i\Gamma \sin \varphi \Lambda_- + \Gamma^2 \sin^2 \frac{\varphi}{2}]}{(\Omega_x^- - \Omega_y^-) (\Lambda_+^2 - \Lambda_-^2) ((\Omega_x^- - \varepsilon)^2 + \Lambda_-^2) \cdot ((\Omega_y^- - \varepsilon)^2 + \Lambda_-^2)} \\
 &\pm iP \left( \frac{1}{\Omega_y^\pm - \Omega_x^\pm} \right) \cdot \frac{\pi}{((\Omega_y^\pm - \varepsilon)^2 + \Lambda_+^2) ((\Omega_y^\pm - \varepsilon)^2 + \Lambda_-^2)} \\
 &\cdot \left[ (\Theta(eV/2 - \Omega_y^\pm) + \Theta(-eV/2 - \Omega_y^\pm - 2)) \left( (\Omega_y^\pm - \varepsilon)^2 + \Gamma^2 \left( 1 - \cos^2 \frac{\varphi}{2} \right) \right) \right. \\
 &\quad \left. \pm (\Theta(eV/2 - \Omega_y^\pm) - \Theta(-eV/2 - \Omega_y^\pm)) \Gamma (\Omega_y^\pm - \varepsilon) \sin \varphi \right] \\
 &+ i \left( \mp P \left( \frac{1}{\Omega_y^\pm - \Omega_x^\pm} \right) + i\pi \delta(\Omega_x^\pm - \Omega_y^\pm) \right) \cdot \frac{\pi}{((\Omega_x^\pm - \varepsilon)^2 + \Lambda_+^2) ((\Omega_x^\pm - \varepsilon)^2 + \Lambda_-^2)} \\
 &\cdot \left[ (\Theta(eV/2 - \Omega_x^\pm) + \Theta(-eV/2 - \Omega_x^\pm - 2)) \left( (\Omega_x^\pm - \varepsilon)^2 + \Gamma^2 \left( 1 - \cos^2 \frac{\varphi}{2} \right) \right) \right. \\
 &\quad \left. \pm (\Theta(eV/2 - \Omega_x^\pm) - \Theta(-eV/2 - \Omega_x^\pm)) \Gamma (\Omega_x^\pm - \varepsilon) \sin \varphi \right] \Big]
 \end{aligned}$$

### 4.3 Extension of the Integration to the Remaining Diagrams

We have done the integration for the diagram (c).

Since the integrals of the other diagrams are quiet similar we check how to apply the formalism to the integration of the other diagrams. The main structure of all integrals is equal.

One sort the Green's functions regarding the integration variable and obtain three parts: An integration over  $\omega_5$  and  $\omega_2$ , containing two bosonic and a single fermionic Green's function which also depends on  $\omega_x, \omega_y, \omega_v$  or  $\omega_z$ .

And an integration over  $\omega_x$  and  $\omega_y$  or  $\omega_v$  and  $\omega_z$ , containing the four bosonic and two fermionic Green's functions from before and two additional fermionic Green's functions which depend only on  $\omega_x, \omega_y, \omega_v$  or  $\omega_z$ .

Exactly as in the previous calculation of the integral over  $\omega_2$  we compare 2 bosonic and the single fermionic Green's function with those of an integral that we have finished to apply these results to the new diagram.

#### Determination of Diagram (b)

We start with diagram (b) using the integration of diagram (c). We compare the Green's functions of the two diagrams and shift the frequencies  $\omega_2$  and  $\omega_5$  to  $-\omega_2$  and  $-\omega_5$  to obtain fermionic Green's functions with equal dependencies of  $\omega_i$  like in the integral of diagram (c). In order to obtain that the bosonic Green's functions depend on a difference of two frequencies we also shift  $\omega_x$  and  $\omega_y$  to the negative.

Diagram fig.(20)(b)

$$\begin{aligned} & \iint d\omega_x d\omega_y G_{12}^{++}(-\omega_x) G_{21}^{--}(-\omega_y) \\ & \int d\omega_2 D_a^{++}(\omega_2 - \omega_x) G_{11}^{-+}(-\omega_2) D_a^{--}(\omega_2 - \omega_y) \\ & \int d\omega_5 D_b^{++}(\omega_x - \omega_5) G_{22}^{+-}(-\omega_5) D_b^{--}(\omega_y - \omega_5) \end{aligned}$$

Diagram fig.(20)(c)

$$\begin{aligned} & \iint d\omega_x d\omega_y G_{21}^{++}(\omega_x) G_{12}^{--}(\omega_y) \\ & \int d\omega_2 D_a^{++}(\omega_2 - \omega_x) G_{11}^{+-}(\omega_2) D_a^{--}(\omega_2 - \omega_y) \\ & \int d\omega_5 D_b^{++}(\omega_x - \omega_5) G_{22}^{+-}(\omega_5) D_b^{--}(\omega_y - \omega_5) \end{aligned}$$

Diagram fig.(20)(b) with shifted frequencies

$$\begin{aligned} & \iint d\omega_x d\omega_y G_{12}^{++}(\omega_x) G_{21}^{--}(\omega_y) \\ & \int d\omega_2 D_a^{++}(-\omega_2 + \omega_x) G_{11}^{-+}(\omega_2) D_a^{--}(-\omega_2 + \omega_y) \\ & \int d\omega_5 D_b^{++}(-\omega_x + \omega_5) G_{22}^{+-}(\omega_5) D_b^{--}(-\omega_y + \omega_5) \end{aligned}$$

Now we can argue in the same manner as before. The fermionic Green's functions are equivalent to those of diagram (c). The argument of the bosonic Green's functions changed the sign compared to diagram (c). They contain a principle part which is symmetric to the zero point and a delta function which is symmetric to the y-axis. Therefore we obtain the same definite integral as before but change the sign of the principle parts and replace  $\Omega_{x,y}^-$  with  $\Omega_{x,y}^+$ .

### Determination of Diagram (g)

In the next step we consider diagram (g) using the integration of diagram (c). In the first step we compare the integrands of the integration over  $\omega_5$ . The fermionic Green's function is equal. The argument of the bosonic Green's function of (g) depends again on the negative argument of diagram (c). The indices changed from  $x$  and  $y$  to  $v$  and  $z$ . As before the integration leads to the equal definite integral as in (c) and we change the sign of the principle part and the variable  $\Omega_{x,y}^-$  to  $\Omega_{v,z}^+$ . In a next step we consider the integration over  $\omega_2$ . We shift the frequencies  $\omega_2$ ,  $\omega_v$  and  $\omega_z$  to negative values and obtain again the same structure of the fermionic and bosonic Green's functions with negative arguments that we know how to solve. It is important to note that the second shift of the frequencies  $\omega_v$  and  $\omega_z$  also shifted the frequencies in the definite integral of  $\omega_5$ . Therefore the variables  $\Omega_{v,z}^+$  are shifted to  $-\Omega_{v,z}^-$ .

Diagram fig.(20)(g)

$$\begin{aligned} & \iint d\omega_v d\omega_z G_{21}^{+-}(-\omega_v) G_{12}^{+-}(-\omega_z) \\ & \int d\omega_2 D_a^{++}(\omega_2 - \omega_z) G_{11}^{-+}(-\omega_2) D_a^{--}(\omega_2 - \omega_v) \\ & \int d\omega_5 D_b^{++}(\omega_5 - \omega_v) G_{22}^{-+}(\omega_5) D_b^{--}(\omega_5 - \omega_z) \end{aligned}$$

Diagram fig.(20)(c)

$$\begin{aligned} & \iint d\omega_x d\omega_y G_{21}^{++}(\omega_x) G_{12}^{--}(\omega_y) \\ & \int d\omega_2 D_a^{++}(\omega_2 - \omega_x) G_{11}^{+-}(\omega_2) D_a^{--}(\omega_2 - \omega_y) \\ & \int d\omega_5 D_b^{++}(\omega_x - \omega_5) G_{22}^{-+}(\omega_5) D_b^{--}(\omega_y - \omega_5) \end{aligned}$$

### Determination of Diagram (f)

We consider diagram (f) using again the integration of diagram (c). The integration over  $\omega_2$  is completely equal to the one of diagram (c) paying attention to the changed indices from  $x$  and  $y$  to  $v$  and  $z$ . After we did this integration we shift the frequencies  $\omega_5$ ,  $\omega_v$  and  $\omega_z$  to negative values and obtain again the structure of an equal fermionic Green's function and bosonic Green's functions with negative arguments. Du to the second shift of the frequencies  $\omega_v$  and  $\omega_z$  we shift again the frequencies in the definite integral of  $\omega_2$ . Therefore the variables change from  $\Omega_{v,z}^+$  to  $-\Omega_{v,z}^-$ .

Diagram fig.(20)(f)

$$\begin{aligned} & \iint d\omega_v d\omega_z G_{12}^{-+}(\omega_v) G_{21}^{-+}(\omega_z) \\ & \int d\omega_2 D_a^{++}(\omega_2 - \omega_z) G_{11}^{+-}(\omega_2) D_a^{--}(\omega_2 - \omega_v) \\ & \int d\omega_5 D_b^{++}(\omega_5 - \omega_v) G_{22}^{-+}(-\omega_5) D_b^{--}(\omega_5 - \omega_z) \end{aligned}$$

Diagram fig.(20)(c)

$$\begin{aligned} & \iint d\omega_x d\omega_y G_{21}^{++}(\omega_x) G_{12}^{--}(\omega_y) \\ & \int d\omega_2 D_a^{++}(\omega_2 - \omega_x) G_{11}^{+-}(\omega_2) D_a^{--}(\omega_2 - \omega_y) \\ & \int d\omega_5 D_b^{++}(\omega_x - \omega_5) G_{22}^{-+}(\omega_5) D_b^{--}(\omega_y - \omega_5) \end{aligned}$$

### Determination of Diagram (e)

Now we focus on diagram (e) by use of the integration of diagram (c). The arguments of the diagrams are equal. The only difference is the used component of the fermionic Green's function.

Diagram fig.(20)(e)

$$\begin{aligned} & \iint d\omega_x d\omega_y G_{21}^{+++}(\omega_x) G_{21}^{---}(\omega_y) \\ & \int d\omega_2 D_a^{++}(\omega_2 - \omega_x) G_{12}^{+-}(\omega_2) D_b^{--}(\omega_2 - \omega_y) \\ & \int d\omega_5 D_b^{++}(\omega_x - \omega_5) G_{12}^{+-}(\omega_5) D_a^{--}(\omega_y - \omega_5) \end{aligned}$$

Diagram fig.(20)(c)

$$\begin{aligned} & \iint d\omega_x d\omega_y G_{21}^{+++}(\omega_x) G_{12}^{---}(\omega_y) \\ & \int d\omega_2 D_a^{++}(\omega_2 - \omega_x) G_{11}^{+-}(\omega_2) D_a^{--}(\omega_2 - \omega_y) \\ & \int d\omega_5 D_b^{++}(\omega_x - \omega_5) G_{22}^{+-}(\omega_5) D_b^{--}(\omega_y - \omega_5) \end{aligned}$$

Therefore we compare the two fermionic Green's functions  $G_{12}^{+-}(\omega_5)$  and  $G_{22}^{+-}(\omega_5)$ .

$$\begin{aligned} G_{12}^{+-}(\omega_5) &= \frac{i\Gamma}{|\Omega|^2} \left[ (\omega_5 - \varepsilon)^2 \left( e^{-i\frac{\varphi}{2}} f_L + e^{i\frac{\varphi}{2}} f_R - 2 \cos \frac{\varphi}{2} \right) - \Gamma^2 \sin^2 \frac{\varphi}{2} \left( f_L e^{i\frac{\varphi}{2}} + f_R e^{-i\frac{\varphi}{2}} - 2 \cos \frac{\varphi}{2} \right) \right] \\ G_{22}^{+-}(\omega_5) &= \frac{i\Gamma}{|\Omega|^2} \left[ \left( (\omega_5 - \varepsilon)^2 + \Gamma^2 \sin^2 \frac{\varphi}{2} \right) (f_L + f_R - 2) - \Gamma(\omega_5 - \varepsilon) \sin \varphi (f_L - f_R) \right] \end{aligned}$$

The two parts in  $G_{12}^{+-}(\omega_5)$  containing "  $- 2 \cos \frac{\varphi}{2}$ " are not combined with a Fermi function and will therefore drop out at the integration. The same happens for the factor "  $- 2$ " in  $G_{22}^{+-}(\omega_5)$ . The exponential functions are just additional factors that are multiplied after the integration. The main difference is that  $G_{12}^{+-}(\omega_5)$  doesn't contain a part proportional to  $\omega_5 - \varepsilon$ . Therefore the coefficients  $b_i$  become all zero. To solve the integral we can use the definite integral that we obtained from diagram (c), cross out the terms according to the coefficients  $b_i$  and multiply the exponential functions. Since the difference between the greater and lesser Green's function is only the constant factor without the Fermi function, the integration over  $\omega_2$  works in the same way.

### Determination of Diagram (d)

We obtain diagram (d) by use of diagram (b). If we compare the two integrals we recognize the same similarities as between diagram (c) and (e). So we can use the definite integral of diagram (b) with the same modifications that we discussed before.

Diagram fig.(20)(b)

$$\begin{aligned} & \iint d\omega_x d\omega_y G_{12}^{+++}(-\omega_x) G_{21}^{---}(-\omega_y) \\ & \int d\omega_2 D_a^{++}(\omega_2 - \omega_x) G_{11}^{+-}(-\omega_2) D_a^{--}(\omega_2 - \omega_y) \\ & \int d\omega_5 D_b^{++}(\omega_x - \omega_5) G_{22}^{+-}(-\omega_5) D_b^{--}(\omega_y - \omega_5) \end{aligned}$$

Diagram fig.(20)(d)

$$\begin{aligned} & \iint d\omega_x d\omega_y G_{12}^{+++}(-\omega_x) G_{12}^{---}(-\omega_y) \\ & \int d\omega_2 D_a^{++}(\omega_2 - \omega_x) G_{21}^{+-}(-\omega_2) D_b^{--}(\omega_2 - \omega_y) \\ & \int d\omega_5 D_b^{++}(\omega_x - \omega_5) G_{21}^{+-}(-\omega_5) D_a^{--}(\omega_y - \omega_5) \end{aligned}$$

## 5 Conclusion

Motivated by several experiments in system formed by quantum dots microwave cavities, we studied a system of two parallel quantum dots in an Aharonov-Bohm set up interferometer (ABI) coupled to two electrodes, with each dot coupled to a microwave cavity.

Our goal was to explore correlation and entanglement between the two cavity fields generated by the coherent transport of a single electron traveling in two different paths of the ABI.

In this thesis we focused on the calculation of a correlation between the two microwave cavities by calculate the covariance. For this we rely on the diagrammatic perturbative expansion, using the Keldysh Greens functions, to the fourth order in the dot-cavity coupling constant. According to the non-equilibrium perturbation theory on the Keldysh contour we calculated the terms of the perturbative expansion by Wick's theorem. This leads to a sum of multiplications of Green's functions that could have been represented as Feynman diagrams. We were able to determine that the covariance is selected only to to seven diagrams.

To calculate these diagrams we identified three different types of diagrams and transformed each of them from contour times to the real times by parameterizing the Keldysh contour.

Generally this leads to a large expression because each contour time arguments has two possible positions on the contour. We discussed the zero temperature limit such that all possible orders of time arguments reduce to one.

We used the Fourier transformations of the free Green's functions. We did the time integration and obtained an integration of four bosonic and four fermionic Green's functions over four frequencies. Using a partial fraction decomposition we did the integration over two frequencies. We obtained an analytic formula that includes only two integrations over the frequencies.

To summarize, we derived an analytic formula for the covariance that is now ready to be computed numerically. Therefore the next step would be the numerical evaluation and to investigate the behavior of the system for different regimes of the parameters, for example by varying the magnetic flux or the bias voltage.

Subsequently, we will explore if the states of the cavities are not only correlated but also entangled. We will calculate the second-order coherence function, entering in the Cauchy-Schwarz inequality, using again the diagrammatic perturbative expansion in a similar way as done in this thesis.

---

## References

- [1] S. Datta, *Electronic Transport in Mesoscopic Systems*. (2001), Cambridge University Press
- [2] H. Haug, A.-P. Jauho, *Quantum Kinetics in Transport and Optics*. (2008), Springer-Verlag Berlin Heidelberg 2nd edition
- [3] J. Rammer, *Quantum field theory of non-equilibrium states*. (2007), Cambridge University Press
- [4] J. Cuevas, E Scheer *MOLECULAR ELECTRONICS An Introduction to Theory and Experiment*. (2010), World Scientific Publishing Co. Pte. Ltd.
- [5] M. Pourfath, *Numerical Study of Quantum Transport in Carbon Nanotube Based Transistors*. (2007) (Doctoral dissertation). Retrieved from <http://www.iue.tuwien.ac.at/phd>
- [6] W. Martienssen, H. Warlimont. *Springer Handbook of Condensed Matter and Materials Data*. (2005) Springer-Verlag Berlin Heidelberg
- [7] T. Ihn, *Semiconductor Nanostructures*. (2010) Oxford University Press
- [8] R. Landauer, Spatial variation of currents and fields due to localized scatterers in metallic conduction. (1957) *IBM J. Res. Dev.* 1, 223-231
- [9] E. Weig. *Lecture slides of Solid-state Nanostructures: Mechanical, electronical and optical properties* (2014) University Konstanz
- [10] R. Gross, A. Marx, *Festkörperphysik*. (2012) Oldenbourg Wissenschaftsverlag
- [11] Y. Aharonov, D. Bohm, *Phys. Rev.* 115, 485 (1959)
- [12] J. Koenig, Y. Gefen, *Phys. Rev. Lett.* 86, 3855 (2001)
- [13] H. Akera, *Phys. Rev. B* 47, 6835 (1993)
- [14] J. Koenig, Y. Gefen, *Phys. Rev. B* 65, 045316 (2002)
- [15] A. Yacoby, et al. *Phys. Rev. Lett.* 74, 4047 (1995)
- [16] R. Schuster et al. *Nature* 385, 417 (1997)
- [17] W.G. van der Wiel et al. *Science* 289, 2105 (2000)
- [18] A.W. Holleitner et al. *Phys. Rev. Lett.* 89, 256802 (2001)
- [19] B. Kubala, *Aharonov-Bohm Interferometrie mit Quantenpunkten*. (2002) (diploma thesis). Retrieved from [http://www.thp2.nat.uni-erlangen.de/index.php/Homepage\\_Bjoern\\_Kubala](http://www.thp2.nat.uni-erlangen.de/index.php/Homepage_Bjoern_Kubala)
- [20] A. Wallraff et al. *Nature* 431, 162 (2004)
- [21] Matthieu Delbecq. *Coupling quantum dot circuits to microwave cavities*. *Quantum Physics [quant-ph]*. Universit"ae Pierre et Marie Curie - Paris VI, 2012. English. <NNT :2012PAO66491>. <tel-00828147>
- [22] M. R. Delbecq et al. *Phys. Rev. Lett.* 107, 256804
- [23] M. R. Delbecq et al. *Nat. Commun.* 4, 1400 (2013)
- [24] A. L. Yeyati et al. *Phys. Rev. B* 55, R6137(R) (1997)
- [25] C.W.J. Beenakker, *Phys Rev. B*. 44, 1646 (1991)
- [26] H. Yi and C. L. Kane, *Phys. Rev. B* 53, 12956 (1996)

- [27] M. Pustilnik and L. Glazman, *J. Phys.: Condens. Matter* 16 (2004) R513?R537
- [28] R.I.A. Davis et al. *J. Phys. A: Math. Gen.* 33 1895 (2000)
- [29] J. S. Bell, *Physics* 1, 195 (1964)
- [30] A. Einstein, B. Podolsky, and N. Rosen, *Phys. Rev.* 47, 777 (1935)
- [31] M. Hillery and M. S. Zubairy, *Phys. Rev. Lett.* 96, 050503 (2006)
- [32] L.-M. Duan et al., *Phys. Rev. Lett.* 84, 2722 (2000).
- [33] S. Mancini et al., *Phys. Rev. Lett.* 88, 120401 (2002).
- [34] V. Giovannetti et al., *Phys. Rev. A* 67, 022320 (2003).
- [35] M. G. Raymer et al., *Phys. Rev. A* 67, 052104 (2003).
- [36] S. Wlk et al, *Phys. Rev. A* 90, 022315 (2014)
- [37] S. Sapmaz and C. Meyer, International Society for Optical Engineering (SPIE), doi: 10.1117/2.1200609.0403 (2006)
- [38] A. Wallraff et al. arXiv:cond-mat/0407325 (2004)
- [39] A. Wallraff et al. *Nature (London)* 431, 162-167 (2004)
- [38] D.F. Walls and G.J. Milburn, *Quantum Optics.* (2008) Springer-Verlag Berlin-Heidelberg